

Studies on Crystal Structural Change of Molecule-based Materials under Pressure

Kota Sasamori

Department of Chemistry
Graduate School of Science and Engineering
Tokyo Metropolitan University

2013

CONTENTS

I.	General Introduction	1
II.	Development of the Method for Single Crystal X-ray Structural Analysis under Pressure Using DAC	
2-1.	Introduction	5
2-2.	Experimental & Results	
2-2-1.	General Details & Procedures	11
2-2-2.	Sample Centering & Measurement Condition	13
2-2-3.	Indexing	16
2-2-4.	Absorption Correction	20
2-3.	Discussion	27
2-4.	Conclusion	36
2-5.	References	37
2-6.	Appendix	38
III.	Crystal Structural Study of Pressure-Induced Molecule-based Superconductor β-(BDA-TTP)₂FeCl₄ at Low Temperature and under High Pressure	
3-1.	Introduction	53
3-2.	Experimental Details	57
3-3.	Results & Discussion	
3-3-1.	Low-Temperature Crystal and Electric Structures	59
3-3-2.	Crystal Structure under Pressure	71
3-4.	Conclusion	79
3-5.	References	80
3-6.	Appendix	82

IV. Crystal Structural Study in [Cr(CN)₆][Mn((<i>R</i>)-pnH)(H₂O)](H₂O) under Pressure	
4-1. Introduction	103
4-2. Experimental Details	110
4-3. Results & Discussion	
4-3-1. High-Pressure Form	112
4-3-2. Structures under Pressure	118
4-4. Conclusion	122
4-5. References	124
4-6. Appendix	125
 V. Preparation, Crystal Structure and Magnetic Properties of a New Dithiolene Ligand, 1,3,2-Dithiazole-4-thione-5-thiolate, and its Metal Complex	
5-1. Introduction	129
5-2. Experimental Details	132
5-3. Results & Discussion	
5-3-1. Crystal Structure and Physical Properties of TBA·dttt (1)	136
5-3-2. Crystal Structure and Magnetic Properties of Cr(dttd) ₃ ·CS ₂ (2)	141
5-4. Conclusion	147
5-5. References	148
5-6. Appendix	152
 VI. Summary	163
 List of Publications	165
 Acknowledgement	166

Chapter I. General Introduction

The development of the molecule-based materials with useful and fascinating properties such as conductivity, magnetism, photoreactivity and optical properties has been currently much challenging target. One feature of molecule-based materials is that their properties can be controlled by the chemical modification of molecules as building block. Another feature is that molecule-based materials are sensitive to pressure: low pressure sometimes brings about the change of the physical properties as well as crystal structure following the change of their ground state [1-5]. On the other hand, higher pressure, by an order of magnitude, is required to change the structures and physical properties for inorganic crystals such as popular semiconductors, ordinary metals, and copper oxide superconductors. Therefore, intermolecular or interatomic distances in molecule-based materials can be largely modified by moderate pressures to show dramatic change in electric properties. In order to develop new molecule-based materials, it is necessary to clarify relationship between the physical property and crystal structure. Therefore the crystal structural analysis under pressure is important for the development of new molecule-materials. Structural studies for inorganic materials under pressure had been many reported, however, these are performed by X-ray structural analysis using powder sample. Since a number of independent atoms exist in a molecule-based material more than in a inorganic solid and the atomic coordinates of them have to be determined precisely, it is necessary to carry out the X-ray structural analysis for molecule-based materials under pressure using single crystal. However, in order to perform the X-ray diffraction measurements with enclosing a single crystal in a pressure cell, the angle range of measurement is restricted. For this reason, the X-ray structural analysis for molecule-based materials under pressure is more complicated and only few studies were reported [6-8].

In this work, the method of single crystal X-ray structural analysis under pressure using diamond anvil cell (DAC) is developed. The structural studies under pressure for pressure-induced molecule-based superconductor, β -(BDA-TTP)₂FeCl₄ [BDA-TTP = 2,5-bis(1,3-dithian-2-ylidene)-1,3,4,6-tetrathiapentalene] that its ground-state is changed with pressure, and molecule-based chiral ferrimagnet [Cr(CN₆)] [Mn(R)-pnH(H₂O)](H₂O) ((R)-pn = (R)-1,2-diamonopropane), termed as Green Needle (GN), that is expected for the structural change with pressure, were carried out using the method developed in this studies. The X-ray structural analysis for the new metal dithiolene complex Cr(dttt)₃·CS₂ (dttt = 1,3,2-dithiazole-4-thione-5-thiolate) that its magnetic properties are expected to change under pressure are also performed.

Overview of This Thesis

In chapter II, development of the method for the X-ray structural analysis under pressure using single crystal encapsulated in the Diamond anvil cell (DAC) are described. The author succeeded in analyzing the crystal structure under pressure by programming the absorption correction of DAC. Here the measurement data of β -(BDA-TTP)₂FeCl₄ and (R)-GN is used for explanation of the experiments. The validity of this method is discussed comparing the results from no-loading sample in the DAC with ones from the naked crystal under ambient pressure.

In Chapter III, the relationship between the structure and the physical property for pressure induced molecule-based superconductor, β -(BDA-TTP)₂FeCl₄ are described. X-ray crystal structural analysis at low temperature and under pressure is performed. The author succeeded in providing structural evidence for the 2-fold structure and charge separation causing the metal-insulator (MI) transition in β -(BDA-TTP)₂FeCl₄ by X-ray structure analysis below $T_{MI} = 113$ K. The author also found that the application of pressures causes variations in the conformation of donor molecule and the donor arrangement, which are responsible for almost uniform interaction in

the donor stacking and for an increase in bandwidth (W) as a result, the suppression of MI transition and subsequent occurrence of superconductivity would be observed in β -(BDA-TTP) $_2$ FeCl $_4$ increasing pressure.

In Chapter IV, the structural change of the molecule-based magnet, [Cr(CN) $_6$][Mn(R)-pnH(H $_2$ O)](H $_2$ O) ((R)-pn = (R)-1,2-diaminopropane), termed as Green Needle, under pressure are described. The novel structure that cannot be obtained under ambient pressure, High-Pressure Form, was found out by applying pressure.

In Chapter V, the preparation, crystal structure, and magnetic properties of new dithiolene ligand dttt $^-$ and its chromium tris(dithiolene) complex, Cr(dttt) $_3$ ·CS $_2$ are described.

References

- [1] T. Ishiguro, K. Yamaji, G. Saito, *Organic Superconductors*, Springer, Berlin, Germany (1998).
- [2] H. Kino, H. Fukuyama, *J. Phys. Soc. Jpn.* 64 (1995) 1877.
- [3] K. Kanoda, *Physica C* 282-287 (1997) 299.
- [4] K. Kanoda, *Hyperfine Int.* 104 (1997) 235.
- [5] H. Seo, C. Hotta, H. Fukuyama, *Chem. Rev.* 104 (2004) 5005.
- [6] S. Kagoshima and R. Kondo: *Chem. Rev.* 104 (2004) 5593.
- [7] J. Yamaura, A. Nakao, and R. Kato: *J. Phys. Soc. Jpn.* 73 (2004) 976.
- [8] A. Dawson, D. R. Allan, S. Parsons, and M. Ruf: *J. Appl. Cryst.* 37 (2004) 410.

Chapter II. Development of the Method for Single Crystal X-ray Structural Analysis under Pressure Using DAC.

2-1. INTRODUCTION

Single Crystal Diffraction Studies under Pressure

Although two-dimensional area detector, such as charge coupled device (CCD) and imaging plate (IP) are now widely used in single crystal diffraction, they have not been employed so extensively in crystallographic studies at high pressure. The single-crystal diffraction studies at high pressure have been performed using four-circle diffractometers with point detector [1]. However, data collection times may run into weeks, especially for relatively weakly diffracting organic samples with low-symmetry crystal systems in the measurement with point detector, and high intensity X-ray source, such as synchrotron radiation, is required in these cases. It is important to realize the high-pressure measurement in the laboratory-system.

In high-pressure measurement, centering the sample may be difficult because of the restrictions on viewing by the body of the pressure cell. Diffraction images contain not only sample spots but also powder lines from the gasket and backing-disk materials and very intense spots from the diamond anvils. The results are high and variable background, which can present problems during indexing and unit-cell determination. Shading of the detector by the body of the pressure cell means that only a restricted volume of reciprocal space can be sampled. As a result, observed reflections decrease in high-pressure measurement. The high background and shading also introduce problems during integration. After integration, the absorption correction needs to take into account not only sample anisotropy but also absorption by the diamonds and backing disks.

Piston Cylinder Clamp-type Pressure Cell

A piston cylinder clamp-type pressure cell (clamp cell) and a diamond anvil cell [2] are widely used high-pressure devices. These compact size means that it can be mounted on a standard goniometer head. A schematic view of clamp cell is shown in Fig. 2-1. It is mainly made of CuBe cell and Be pipe that transmits an X-ray. CuBe cell have X-ray window and the angle range in the X-ray diffraction measurement depends on its open angles. A crystal is encapsulated in the Teflon pipe with pressure transmitting medium. The Teflon pipe is pressurized through gauges and the pressure are kept by clamping screws. One feature of the clamp cell is also applicable to the measurements under uniaxial strain. The schematic drawing of them are shown in Fig. 2-2. The hydrostatic pressure is that the sample is pressurized isotropically using liquid medium such as Daphne oil. On the other hand, the uniaxial strain is that the sample is mounted in the substance that has compressibility comparable as sample, such as an epoxy resin in the case of molecule-based conductors, and it is pressurized to only one direction. Spread of the sample to the directions perpendicular to pressed one (Poisson effect) is suppressed with these substances. In this work, all experiments are performed under hydrostatic pressure and in the following, "pressure" means "hydrostatic" one unless otherwise noted.

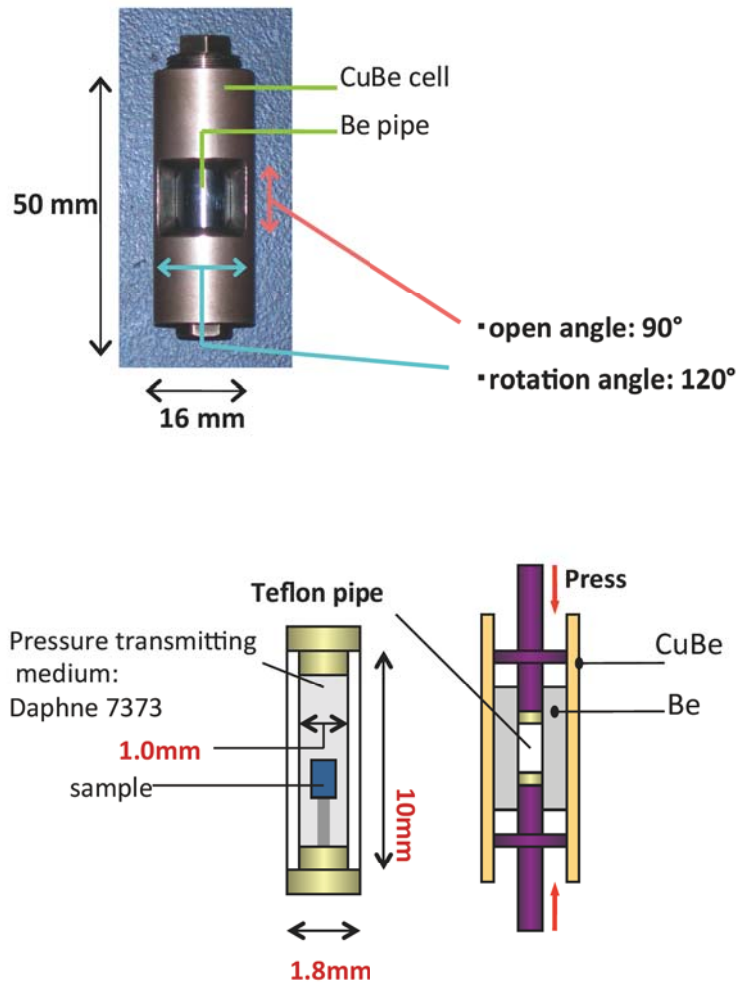


FIGURE 2-1. Schematic view of piston-cylinder clamp type pressure cell.

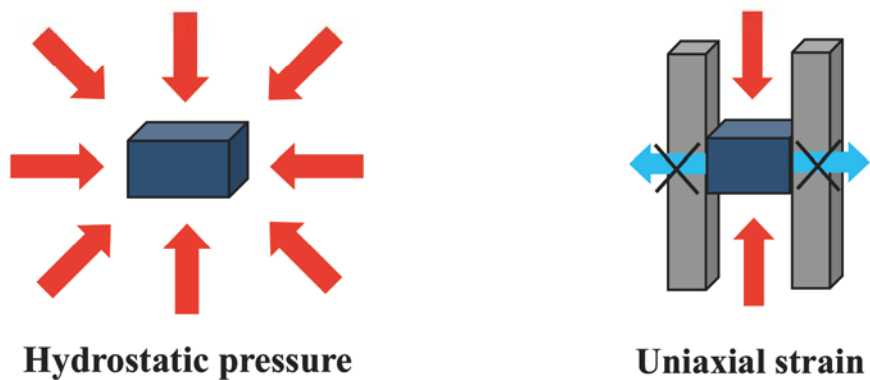


FIGURE 2-2. Schematic views of hydrostatic pressure and uniaxial strain.

In author's laboratory, the method of the single crystal X-ray structure analysis under pressure, using the clamp cell and Bruker SMART APEX diffractometer, was established and it was applied for studies on some molecule-based conductors, such as β -(BDA-TTP)₂I₃ [3] and β -(BDA-TTP)₂FeCl₄ [4]. Under hydrostatic pressure, the sample crystal was encapsulated in the Teflon pipe and Daphne 7373 was used as pressure transmitting medium. The X-ray diffraction measurements under uniaxial strain can be also performed using the clamp cell. Instead of Teflon pipe, the rod that encloses the single crystal in Stycast 1266 was made and it was pressurized. The method of analysis under uniaxial strain is the same as the one under hydrostatic pressure. However, since the treatment of a sample crystal is difficult under uniaxial strain, the structural analysis with precise refinement has not yet realized in author's laboratory. It has succeeded in determining atomic coordinates roughly by preliminary research using β -(BDA-TTP)₂I₃ under uniaxial strain [5]. Clamp cell has some disadvantage. The sample doesn't be observed optically under pressure since the crystal is fully enclosed in Be pipe. Although it is dependent on the diameter of the Be pipe, it can be pressurized only to about 1 GPa by clamp cell used in author's laboratory. Moreover, since the sample space is generally also small, it is difficult to place a substance for estimating the applied pressure precisely with sample crystal.

Diamond Anvil Cell (DAC)

The schematic drawing of the DAC is shown in Fig. 2-3 (§2-2) and the detailed explanation of the DAC is described in §2-2. The advantage and fault of the DAC in comparison with a clamp cell are described here. The optical measurements through diamonds are possible as advantages of DAC. A ruby fragment is contained with the crystal in the sample space and the applied pressure can be estimated precisely by measuring the wavelength of the fluorescence of a ruby [6]. Moreover, the maximum pressure is dependent on the diameter of diamond culet and the DAC used in author's laboratory can be applied to 10 GPa. On the other hand, detailed modulation of pressure is difficult using the DAC in low-pressure region. Furthermore it is necessary to use a smaller crystal than one used in the clamp cell measurement since the sample space become smaller with increasing pressure. Higher intensity of X-ray source and longer exposure time than measurement using clamp cell are also needed in the diffraction measurement using DAC. In author's laboratory, although the measurement using the clamp cell has been performed by Bruker APEX SMART System with CCD detector, the measurement using DAC is performed by MACScience DIP320V imaging plate (IP) detector which has high-power X-ray source and long time exposure is possible. Since the method of structure analysis also differs in these measurement systems, the method that already established using the clamp cell could not be applied for the analysis using DAC. It is necessary to develop the method of structural analysis for the measurement using DAC on MACScience system.

This Work

In this Chapter, the development of the method for the X-ray structural analysis under pressure using the single crystal encapsulated in the diamond anvil cell (DAC) is described. It is explained comparing between the usual X-ray diffraction measurement using naked crystal under ambient pressure and at room temperature, and measurement using DAC.

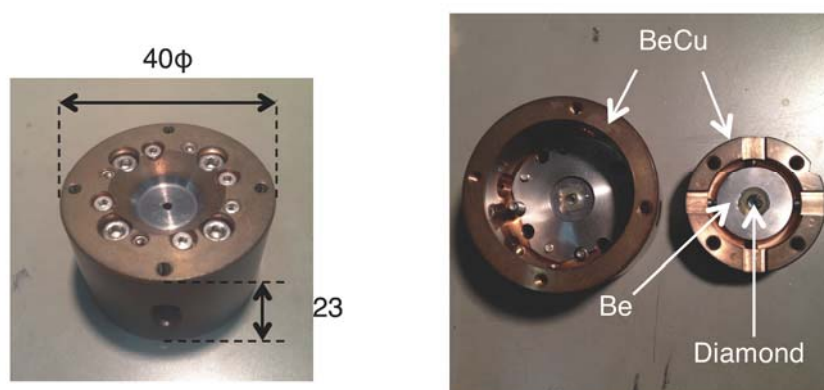
2-2. EXPERIMENTAL & RESULTS

2-2-1. General Details & Procedures

The pressure was generated by diamond anvil cell (DAC) made of BeCu frames, Be backing disks, diamonds, and SUS301 gasket (Fig. 2-3). 40φ × 23 mm BeCu frames, which is minimized so that it can be mounted on a standard goniometer head of the laboratory system, are cylinder-type and the pressure was maintained by clamped. X-ray can enter and exit in a cone of 45° half-angle through the Be backing disks in order that X-ray cannot be transmitted to BeCu. The Be backing disks have a hole and optical measurement is also be possible. 1.0φ diamond culet can be pressurized up to 10 GPa. The sample crystal was placed at the 0.4φ × 0.2 mm gasket hole, which filled with the transmitting medium. In this work, the pressure-transmitting medium was Daphne 7373 (Idemitsu Co. Ltd.), which maintained the hydrostatic pressure up to 2 GPa. The ruby fragment was also placed in the hole and the pressure was determined by the ruby fluorescence method [6].

The single crystal of β -(BDA-TTP)₂FeCl₄ [BDA-TTP = 2,5-bis(1,3-dithian-2-ylidene)-1,3,4,6-tetrathiapentalene] was used as a test sample for this measurement. The crystal size is 0.25 × 0.20 × 0.10 mm. The detailed physical properties of the β -(BDA-TTP)₂FeCl₄ are described in Chapter III. All intensity data for the crystal structure analysis were collected at room temperature. A curved imaging plate MACScience DIP320V was used for data collection. The measurements were performed using a 6 kW rotating-anode X-ray generator with a graphite monochromated MoK α radiation (λ = 0.71073 Å). Cell refinements and data reduction were performed using the *Denzo* and *Scalepack* programs [7]. The structure was solved by direct method and refined by least-squares method on F^2 using the SHELXS-97 program [8].

(a)



(b)

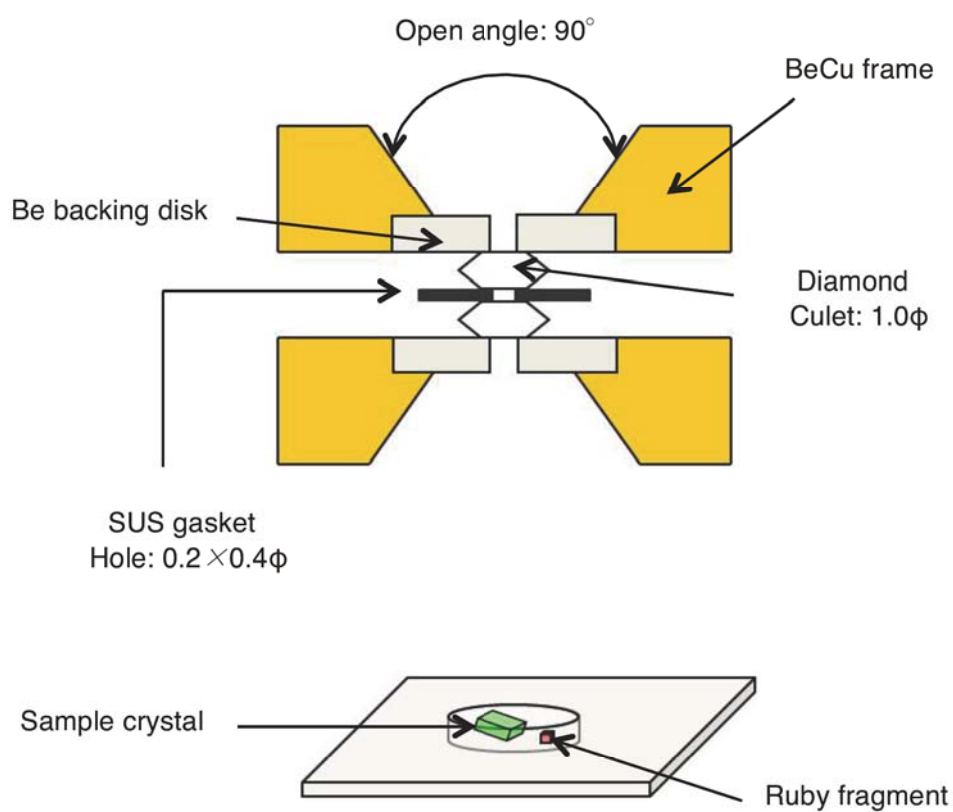


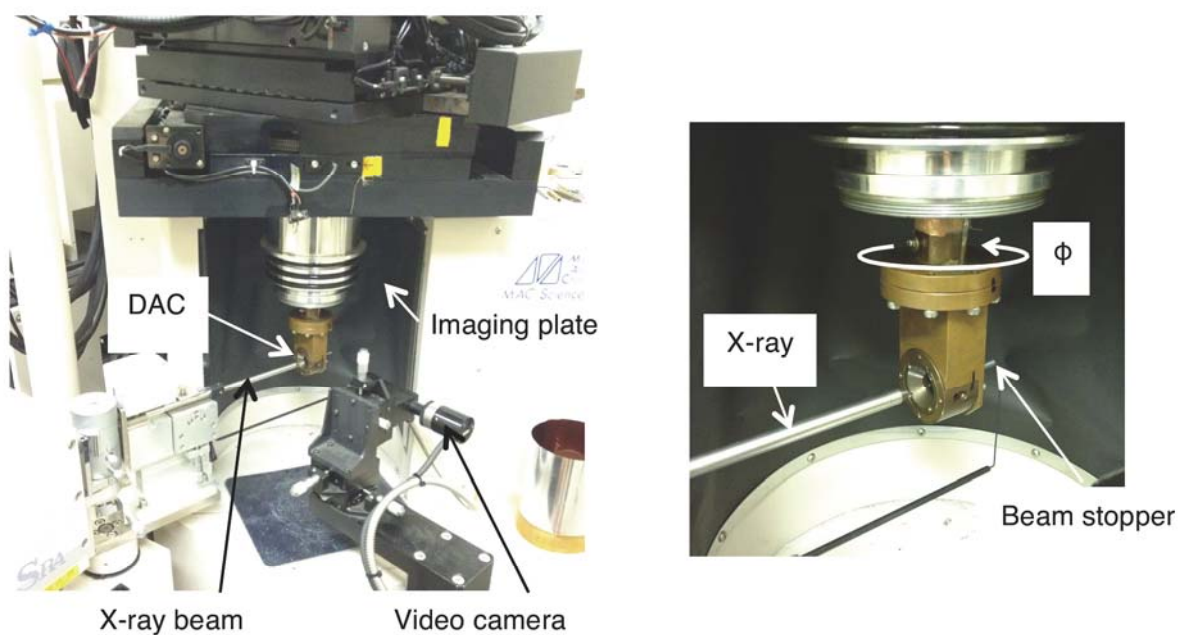
FIGURE 2-3. (a) The photograph and **(b)** schematic drawing of the diamond anvil cell (DAC).

2-2-2. Sample Centering & Measurement Condition

Centering

In usual measurements, a sample crystal can be viewed by video camera from all directions, so the centering of the crystal is straightforward. On the other hand, when the sample crystal contained in the DAC, it can only be viewed along the direction parallel to the cell axis through the diamond anvils (Fig. 2-4). The two-step centering of the crystal in the DAC was performed. First, optical centering of the crystal in the two orthogonal directions perpendicular to cell axis were roughly performed by video camera. Accurate optical centering along the cell axis is not possible because the gasket obscured the sample crystal. Centering in this direction is roughly achieved by the edge of the gasket as center of the sample approximately. Second, accurate centering based on diffractometric measurements was performed. The oscillation photograph was taken for each exposure of 1 min, whenever the crystal position was moved with about 0.1 mm for each orthogonal direction. In the observed photograph, the position dependence of the diffraction intensity for a certain spot was investigated, and the center of the sample was the position where the maximum intensity was observed. Actual diffraction measurement for structural analysis was performed rotating the crystal. As a result of the centering by the method described above, the diffraction spot was observed in every rotation angle. This suggests that the centering method is accurate.

(a)



(b)

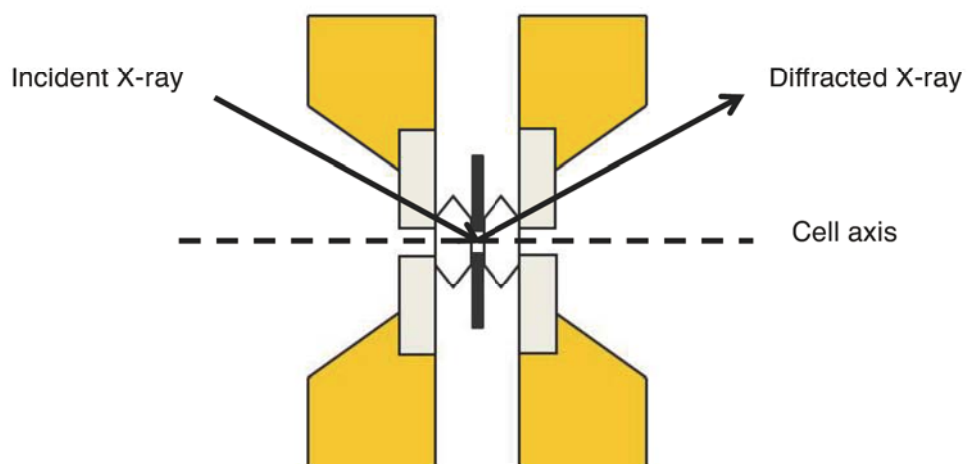


FIGURE 2-4. (a) The photograph of MACScience DIP320V. **(b)** A schematic representation of the relationship between X-ray and DAC, showing the definition of the cell axis.

Measurement Condition

The photograph of DIP320V when DAC was set is shown in Fig. 2-4. The oscillation photographs were taken with the oscillation angle ϕ , which was rotate around the rotation axis shown in Fig. 2-4. In usual measurement of this experiment, the X-ray tube voltage was 50 kV and current was 40 mA, the oscillation angle ϕ were 5° with 1° overlaps and exposure time were 10 min for each photograph. All of the measurement angle range was 180° . While in the measurements using the DAC, the voltage was 50 kV and the current was 100 mA, which is the maximum value in this X-ray generator, because of the attenuation of the X-ray intensity thorough the DAC. Oscillation photographs were taken with the angle of 3° with 0.5° overlaps for each exposure of 60 min. All of the measurement angle range was about 90° for the restriction by the open angle of DAC.

2-2-3. Indexing

The `osc###.ipf` file as an oscillation photograph was created by the measurement. The `###` means the frame number of the measurement. For example, the initial oscillation photograph file was named `osc001.ipf`. The diffraction photograph in usual measurement and the measurement using DAC were shown in Fig. 2-5. In usual measurement, only strong diffractions from the sample crystal were observed up to wide-angle side. While in the measurement using DAC, not only spots from the sample crystal but also strong spots from diamond were observed. The halo pattern that was the diffraction from the Be backing disks and gasket were also observed. These halo appear so strongly that the angle between the incident X-ray and cell axis becomes large. Moreover, because spots at the wide-angle side cannot be observed for the restriction by the open angle of the DAC, the shielding region also appears in the diffraction photograph. The first step in structure analysis is peak search for an oscillation photograph by *Denzo* program. In usual measurement, any photograph can be use for peak search. While in the measurement using DAC, the peak search was performed to the oscillation photograph measured near the direction along the cell axis, because the diffraction from DAC is weakest at this photograph. After the peak search, the indexing is performed to all diffraction spots in an oscillation photograph based on the spots from the peak search using *Denzo*. In usual measurement, the indexing to diffraction spots observed where the 2θ was 60° were performed. While because of the open angle of DAC, if the same indexing is performed in the measurement using DAC, indexing with the spots that are not observed will be performed. In order to avoid this, the value of the function `resolution limits`, which corresponds to the distance between crystal faces in the Bragg's equation, in *Denzo* was changed.

$$2d \sin \theta = n\lambda$$

The value of the resolution limits is 0.75 ($2\theta \approx 60^\circ$) in usual measurement, while this value was changed into 0.95 ($2\theta \approx 45^\circ$) in the measurement with DAC. The diffraction photographs with indexing were also shown in Fig. 2-3. Circles denote the predicted positions of the diffraction spots from the calculation of *Denzo* program. Green, yellow and red circles mean full, partial and reject spots, respectively. All the observed reflections were good agreed with the predicted spot in both usual measurement and one using DAC. This suggests that the indexing was succeeded. In the measurement with DAC, diffraction spots on the halo or strong spots from the diamond were included in the structural analysis using the parameter in the usual measurement. However, since the intensity of these spots were incorrect, it is better not to include in the analysis. In order to perform this, the value of the function `reject` which deletes diffraction spots in *Denzo* was changed. In usual measurement, the value of `reject slope` and `systematic` were 300 and 0.4 respectively, while in the measurement with DAC, these value change to 50 and 0.01, respectively. The diffraction photographs with indexing using various `reject` values were shown in Fig. 2-6. It succeeded in rejecting the diffraction spot on the halo or the spots from diamond by changing the value of `reject`. Accurate indexing was performed with the procedure described above to the first oscillation photograph. The unit cell parameters were also refined, the crystal system was determined, and the intensity of the diffraction spots were integrated in this step. The indexing after the second frame was performed based on the results of the first photograph. The results of these calculations were outputted to the `osc###.x` file for every oscillation photograph. The information of each diffraction spot such as index of *hkl* and integrated intensity, and measurement conditions for each oscillation photograph were summarized in the `.x` file.

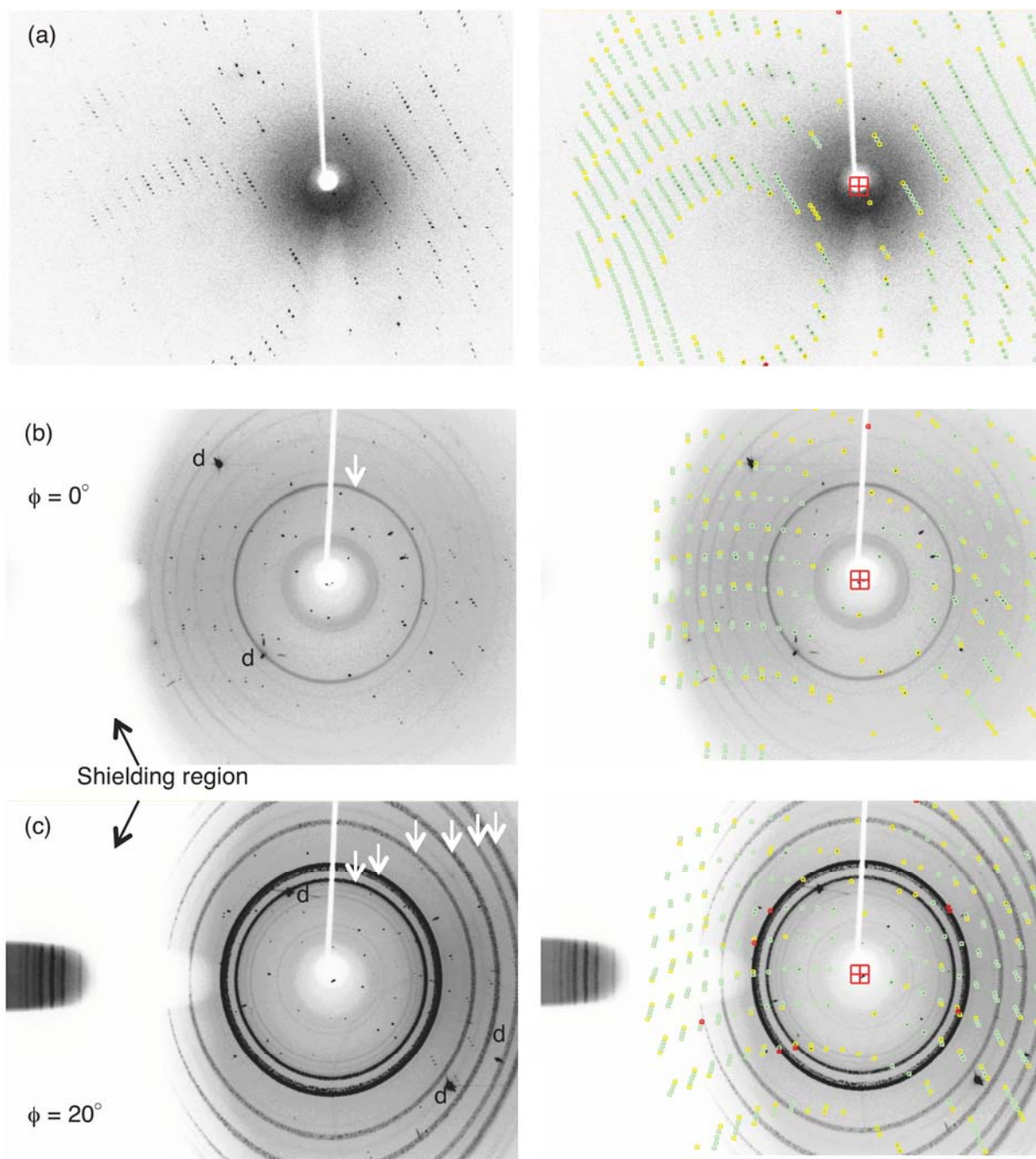


FIGURE 2-5. Diffraction photographs (**left**) with indexing (**right**) in usual measurement (**a**) and measurement using DAC measurement at $\phi = 0^\circ$ (**b**) and 20° (**c**). White arrows and “d” denotes halo pattern from DAC and the spots from diamond, respectively.

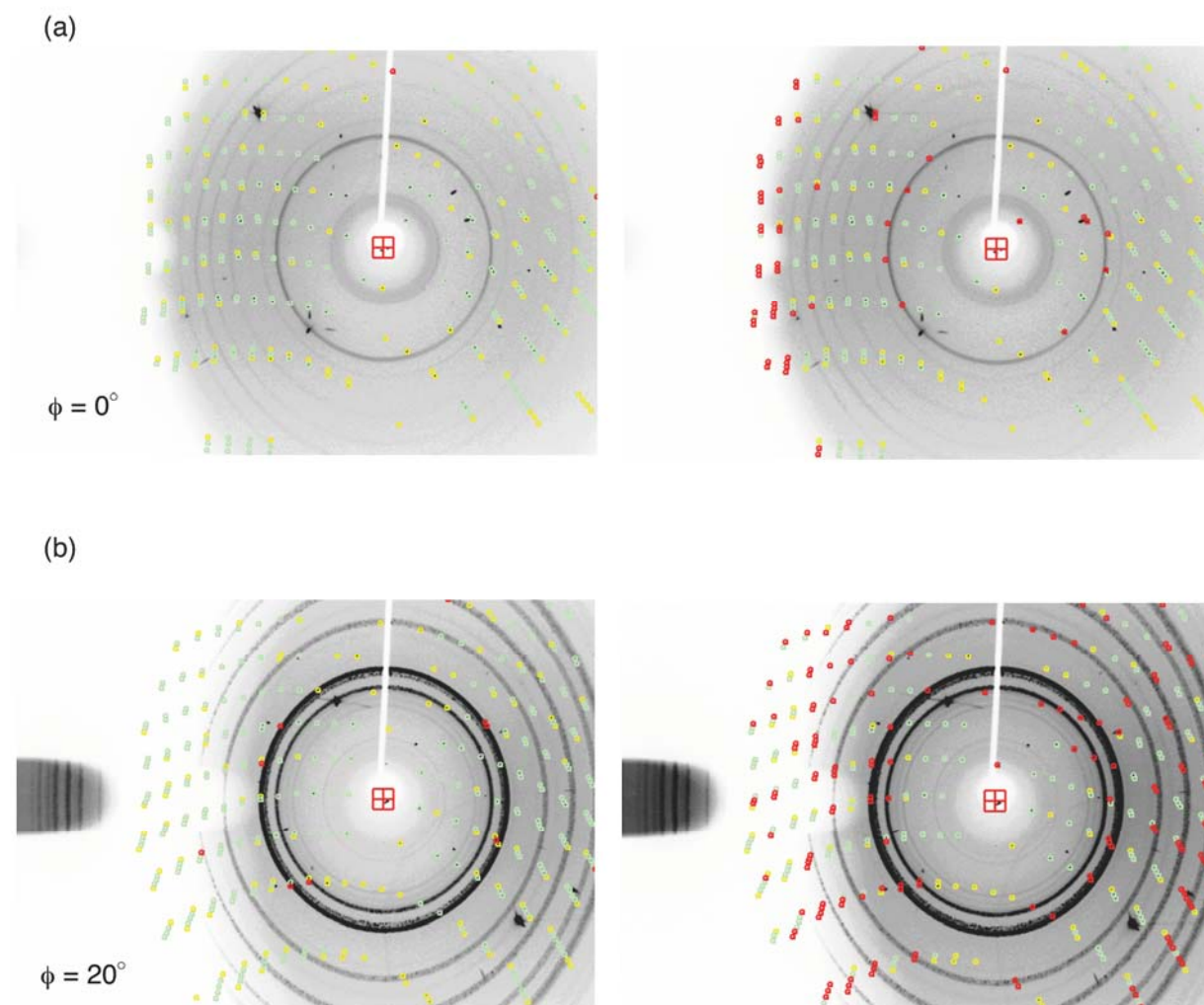


FIGURE 2-6. The diffraction photograph with indexing using various reject values measured at $\phi = 0^\circ$ (a) and 20° (b). reject slope and systematic were 300 and 0.4 (left), and 50 and 0.01 (right), respectively. Red circles mean rejected spots.

2-2-4. Absorption Correction

In the measurement using DAC, the incident and the diffracted X-ray were absorbed by Be backing disks, diamonds and gasket because the crystal was encapsulated in the DAC. In order to perform the structural analysis, the absorption correction to the diffraction intensity calculated by *Denzo* needs to take into account the absorption by the DAC.

Attenuation Factor

The schematic viewing of relationship between X-ray and DAC in the diffraction measurement was shown in Fig. 2-7. The degrees of the absorption of X-ray by DAC depend on the path length of X-ray through the Be backing disks, diamonds and gasket of the DAC. Since the diffraction measurement was performed rotating the DAC, the path length depends on the angle to DAC of X-ray. The angle between the cell axis and X-ray was defined as ϕ , and then the angle when the X-ray enters along the cell axis is 0° . Moreover, since the relative intensity needs to X-ray crystal structural analysis, the equation for the degrees of the absorption was defined as later,

$$I(\phi) = I(0) \exp\{-2\mu t(\phi)\} = I(0) \{A(\phi)\}^2$$

Here the $I(\phi)$ and $I(0)$ are the intensity of the X-ray at ϕ and 0° , μ is the absorption coefficient, and $2t(\phi)$ is the path length, respectively. It is necessary to determine the attenuation factor $A(\phi)$ for performing the absorption correction.

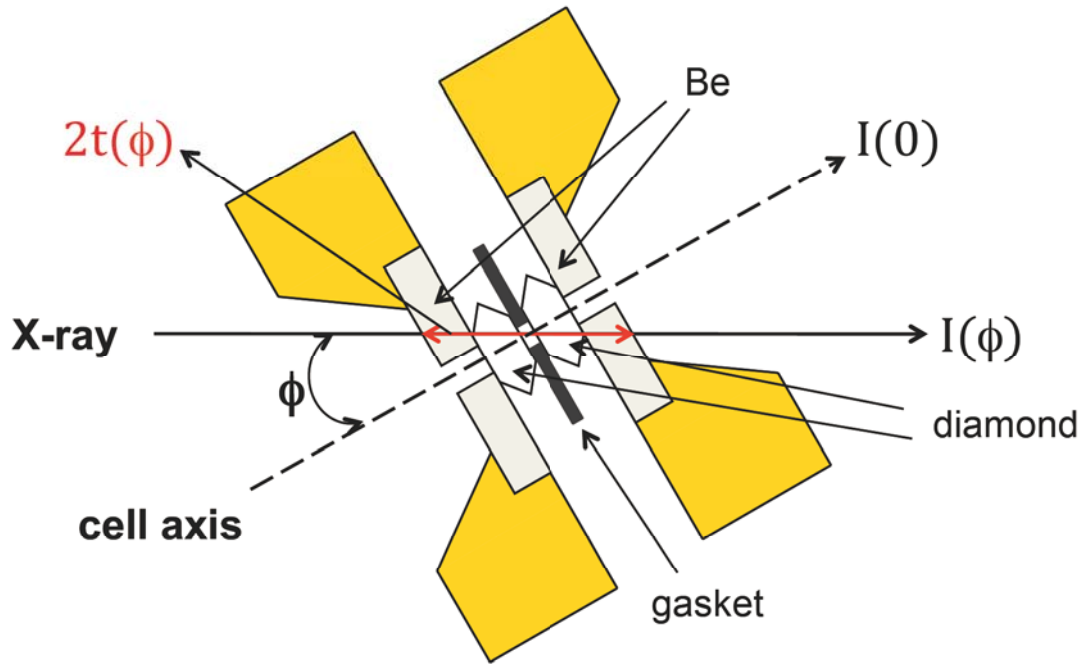


FIGURE 2-7. The schematic viewing of relationship between X-ray and DAC in the diffraction measurement.

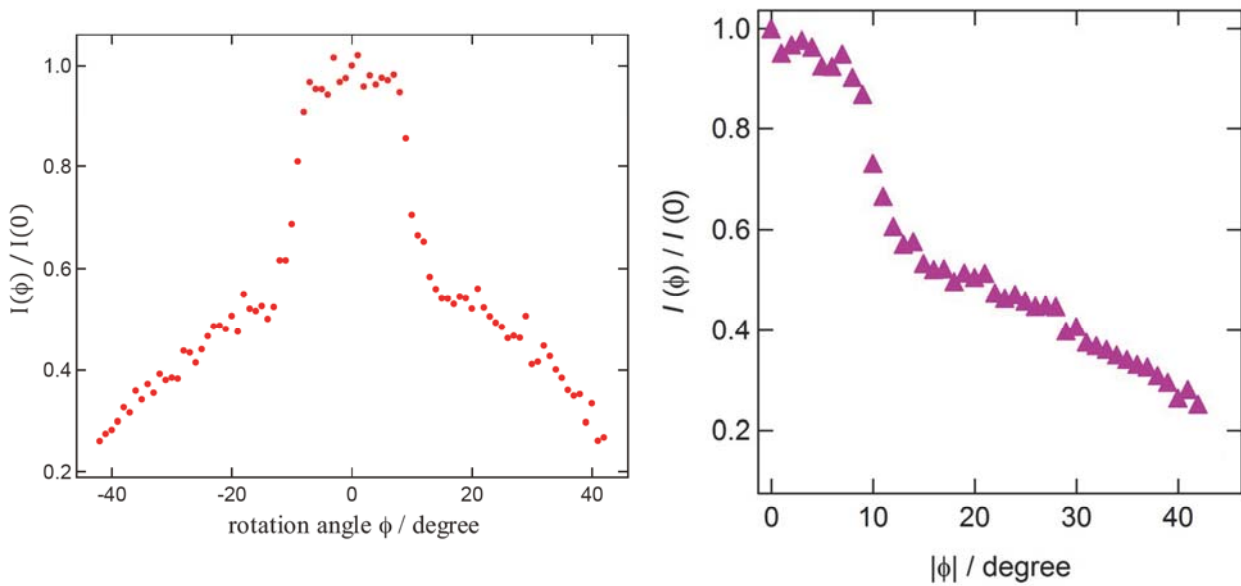


FIGURE 2-8. Angler (**left**) and the absolute value of the angle (**right**) dependence of the direct beam intensity.

Intensity of Direct Beam

In order to determine the attenuation factor $A(\phi)$, the angler dependence of direct X-ray beam intensity was investigated. This measurement was carried out on the condition of which the DAC was set to goniometer head after centering and the beam stopper was removed (Fig. 2-4). X-ray tube voltage and current was 20 kV and 10 mA, and the photograph was taken without oscillating, that is still mode, every 1° for each expose of 10 sec. The angles that the direct beam was not observed near the both edges of the measurement angle range were determined, and then the center of these angles was defined as $\phi = 0^\circ$. The angler dependence of the direct beam intensity was shown in Fig. 2-8. The vertical axis is the intensity $I(\phi)$ normalized by $I(0)$, that is square of the attenuation factor $\{A(\phi)\}^2$. The symmetrical graph at the positive and negative of the angle ϕ that is the horizontal axis was obtained. The direct beam intensity decreased rapidly near 10° where the X-ray began to be strongly absorbed by Be backing disks. And after that, it decreased gradually to near 40° , at that the intensity of X-ray was decreased to about 20 % by DAC. The plot that the attenuation factor was averaged with the absolute value of the angle ϕ was also shown in Fig. 2-8. Actual absorption correction was carried out using these results.

Diffracted X-ray

Taking into account the diffracted X-ray, the path lengths which influences the absorption depends on incident angle ϕ_i and diffracted angle ϕ_d , respectively. Therefore, the formula of absorption shown above is changed as follow.

$$I(\phi) = I(0) \exp\{-\mu t(\phi_i)\} \exp\{-\mu t(\phi_d)\}$$

ϕ_i is decided by measurement since the X-ray diffraction measurement is performed rotating ϕ_i . On the other hand, it is necessary to calculate the ϕ_d using the position coordinates of each diffraction spot on diffraction images.

Coordinates of Each Diffraction Spot

DIP320V imaging Plate (IP) detector using the X-ray diffraction measurement is cylinder-type (Fig. 2-4), but the diffraction image is obtained as a two-dimensional photograph. The schematic drawing of the coordinate system on the X-ray diffraction measurement is shown in Fig. 2-10. O' is the center of the bottom of the cylinder of the detector and it is assumed that the sample crystal is here. O is a position of the X-ray beam center in a diffraction photograph (Fig. 2-10), and $\overrightarrow{O'O}$ and $\overrightarrow{O'P}$ is incident and diffracted X-ray, respectively. The dashed blue line (Fig. 2-10) CO' is cell axis, and then $\angle CO'O$ and $\angle CO'P$ is ϕ_i and ϕ_d , respectively. The position coordinates of the beam center, $(x_{\text{center}}, y_{\text{center}})$, and of the each diffraction spot, (x, y) , in a photograph are refined by indexing, and the estimated values are listed in .x files. The coordinate transformation to the value of $(x_{\text{spot}}, y_{\text{spot}})$, that O is origin, for the value of (x, y) is performed.

$$x_{\text{spot}} = x - x_{\text{center}}, y_{\text{spot}} = y - y_{\text{center}}$$

The three-dimensional coordinate system that O' is origin is considered. The inner product of the two vectors $\overrightarrow{CO'}$ and $\overrightarrow{O'P}$ is represented as follows.

$$\overrightarrow{CO'} \cdot \overrightarrow{O'P} = |\overrightarrow{CO'P}| |\overrightarrow{O'P}| \cos \phi_d$$

$$\overrightarrow{CO'} = (0, d \sin \phi_i, d \sin \phi_i), |\overrightarrow{CO'}| = d$$

The crystal to detector distance, d ($|OO'| = |CO'|$), is also refined by indexing and the estimated values of d are listed in .x file. $\overrightarrow{O'P}$ is projected on the bottom of the cylinder and incident X-ray, and the foot of the perpendicular is P and Q, and $\angle P'O'Q = \theta'$, respectively. The vector $\overrightarrow{O'P}$ and y_{spot} are represented as follows.

$$y_{\text{spot}} = 2\pi d \frac{\theta'}{360}$$

$$\overrightarrow{O'P} = (x_{\text{spot}}, d \sin \theta', d \cos \theta'), |\overrightarrow{O'P}| = \sqrt{d^2 + x_{\text{spot}}^2}$$

As a result, ϕ_d is calculated from the following.

$$\cos \phi_d = \frac{0 \times x_{\text{spot}} + d^2 \sin \phi_i \sin \theta' + d^2 \cos \phi_i \cos \theta'}{d \sqrt{d^2 + x_{\text{spot}}^2}} = \frac{d \cos(\phi_i - \theta')}{\sqrt{d^2 + x_{\text{spot}}^2}}$$

Programming

Since the relative intensity is needed for the structure analysis, the formula of absorption is represented as follow.

$$I_{\text{obs.}} = I_{\text{cor.}} \{A(\phi_i)\} \{A(\phi_d)\}$$

The angle ϕ_i and ϕ_d of each spot are determined and the corrected intensity $I_{\text{cor.}}$ for each spot is calculated by performing against observed intensity $I_{\text{obs.}}$ using attenuation factor $A(\phi)$ obtained by direct beam measurement. The program that the all calculations shown above are performed is created using Perl. The source code of the program for absorption correction is shown in Appendix.

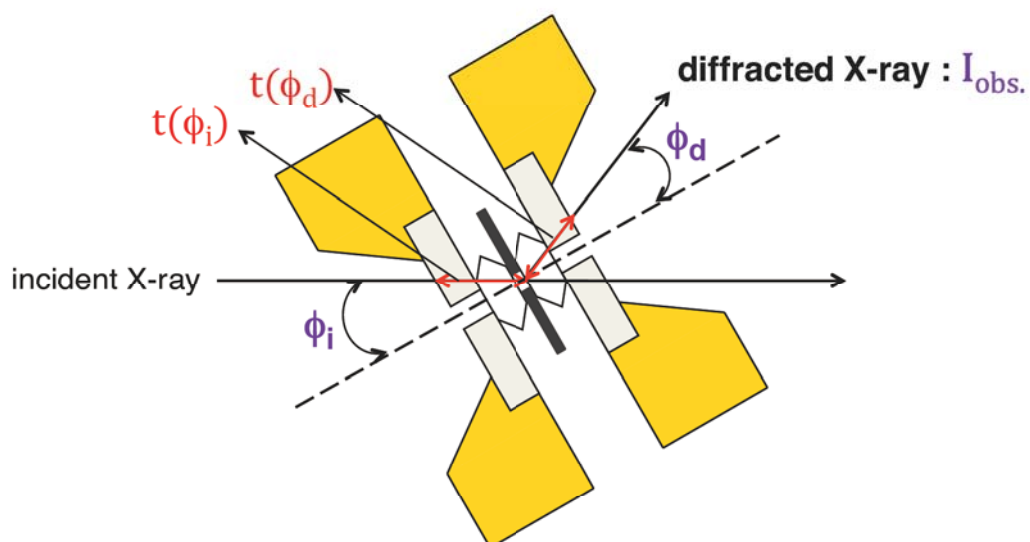


FIGURE 2-9. The schematic viewing of incident and diffracted X-ray, and DAC in the diffraction measurement.

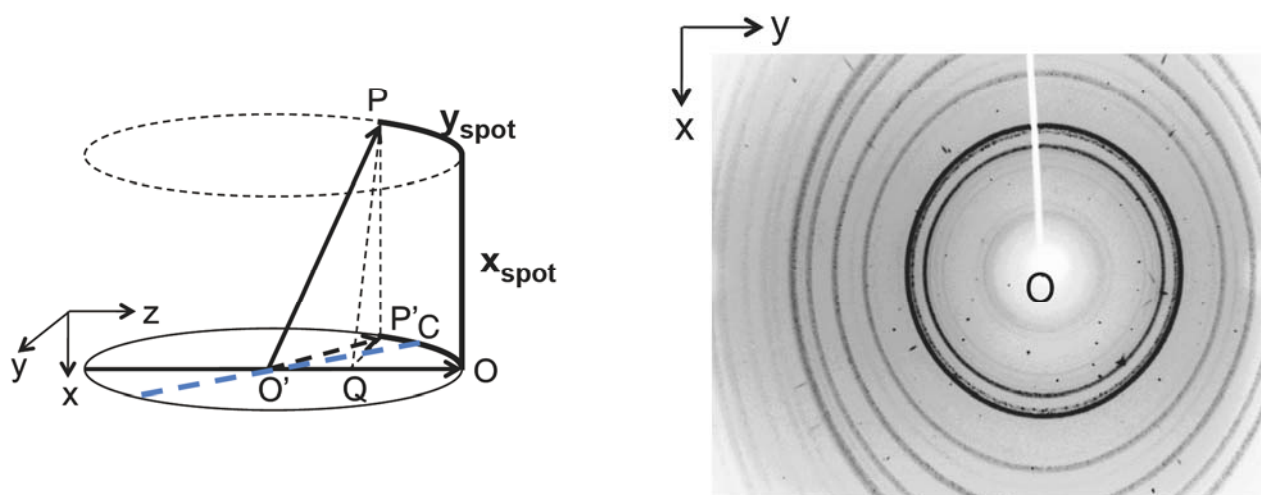


FIGURE 2-10. The schematic drawing of the coordinate system on the X-ray diffraction measurement (**left**), and in the diffraction photograph (**right**).

2-3. DISCUSSION

In order to evaluate the method of structure analysis under pressure described above, X-ray diffraction measurements were performed for the sample crystal that was enclosed with the DAC and wasn't pressurized. The results of the structure analysis are compared with the crystal structure obtained by normal measurement. Henceforth, The normal measurement is called "normal", and measurement using DAC is called "DAC". β -(BDA-TTP)₂FeCl₄ and (*R*)-GN were used for sample crystal. Detailed structure and physical properties of these materials are described in Chapter III [β -(BDA-TTP)₂FeCl₄] and IV [(*R*)-GN].

β -(BDA-TTP)₂FeCl₄

Table 3-II shows crystallographic data for β -(BDA-TTP)₂FeCl₄ in "normal" and "DAC". The cell parameters of "DAC" are good agreed with these of "normal". Since the range of the measured angle was restricted by DAC, observed reflections in "DAC" decreased 1630 that were about to 1/5 as compared with these in "normal". Because the number of the reflections was not enough to refine all non-Hydrogen atoms anisotropically in "DAC", S, Fe, and Cl atoms were refined with the anisotropic temperature factor for analysis in "DAC". For this reason, the refinement parameters decreased in "DAC". ORTEP drawing of the crystallographically independent part for β -(BDA-TTP)₂FeCl₄ in "DAC" is shown in Fig. 2-10. Bond lengths and angles in "normal" and "DAC" are summarized in Table 2-III and IV, respectively. Almost lengths and angles in "DAC" are good agree with these in "normal" within range of error, and *R*-factor is also about 6 % in "DAC". It indicates that the structure analysis for using DAC is succeeded.

TABLE 2-I. Crystallographic data for β -(BDA-TTP)₂FeCl₄ under normal condition and measured at DAC.

Condition	“normal”	“DAC”
Formula, F_w	C ₂₄ H ₂₄ S ₁₆ FeCl ₄ , 1023.04	
Crystal shape, color, size / mm ³	block, black, 0.25 × 0.20 × 0.10	
Crystal system, Space group	monoclinic, $P2_1/a$	
$a / \text{\AA}$	12.4530(7)	12.4710(18)
$b / \text{\AA}$	38.7650(16)	38.812(6)
$c / \text{\AA}$	7.7240(5)	7.7330(17)
$\beta / ^\circ$	91.143(3)	91.140(12)
$V / \text{\AA}^3$	3727.9(4)	3742.2(11)
Z	4	4
$D_{\text{calcd.}} / \text{g cm}^{-3}$	1.823	1.816
μ / mm^{-1}	1.610	1.604
Index range	$-16 \leq h \leq 16$	$-12 \leq h \leq 12$
	$0 \leq k \leq 47$	$0 \leq k \leq 36$
	$0 \leq l \leq 10$	$0 \leq l \leq 7$
Reflections	8794	1630
Parameters	406	286
GOF	0.968	1.138
R, wR	0.0526, 0.0896	0.0601, 0.1289
T / K	295	295

TABLE 2-II. Bond Lengths for β -(BDA-TTP)₂FeCl₄ in normal measurement and measured at DAC.

		distance / Å				distance / Å	
atom	atom	normal	DAC	atom	atom	normal	DAC
C1	C2	1.512(4)	1.496(18)	C14	S9	1.805(3)	1.813(16)
C1	C3	1.511(4)	1.52(2)	C15	S10	1.813(3)	1.825(16)
C2	S1	1.796(3)	1.798(16)	C16	C17	1.344(4)	1.33(2)
C3	S2	1.801(3)	1.821(17)	C16	S9	1.755(3)	1.754(14)
C4	C5	1.359(4)	1.33(2)	C16	S10	1.756(3)	1.776(16)
C4	S1	1.741(3)	1.771(15)	C17	S12	1.767(3)	1.767(15)
C4	S2	1.748(3)	1.724(15)	C17	S11	1.767(3)	1.784(15)
C5	S3	1.756(3)	1.775(15)	C18	C19	1.338(4)	1.36(2)
C5	S4	1.761(3)	1.774(14)	C18	S13	1.732(3)	1.743(17)
C6	C7	1.346(4)	1.33(2)	C18	S11	1.737(3)	1.720(16)
C6	S3	1.732(3)	1.721(16)	C19	S14	1.731(3)	1.730(17)
C6	S5	1.741(3)	1.740(16)	C19	S12	1.742(3)	1.727(17)
C7	S4	1.729(3)	1.747(17)	C20	C21	1.361(4)	1.35(2)
C7	S6	1.732(3)	1.742(17)	C20	S13	1.756(3)	1.757(15)
C8	S9	1.351(4)	1.32(2)	C20	S14	1.762(3)	1.765(16)
C8	S5	1.761(3)	1.777(14)	C21	S16	1.736(3)	1.723(16)
C8	S6	1.767(3)	1.774(16)	C21	S15	1.741(3)	1.766(16)
C9	S8	1.755(3)	1.745(14)	C22	C24	1.510(4)	1.54(2)
C9	S7	1.757(3)	1.788(15)	C22	S15	1.802(3)	1.816(18)
C10	C12	1.513(5)	1.54(2)	C23	C24	1.511(5)	1.486(18)
C10	S7	1.804(3)	1.799(17)	C23	S16	1.802(3)	1.820(17)
C11	C12	1.515(5)	1.51(2)	Fe1	Cl2	2.1743(12)	2.177(5)
C11	S8	1.810(3)	1.808(17)	Fe1	Cl4	2.1765(11)	2.182(6)
C13	C15	1.508(5)	1.51(2)	Fe1	Cl1	2.1833(11)	2.184(5)
C13	C14	1.514(5)	1.50(2)	Fe1	Cl3	2.1848(11)	2.189(5)

Table 2-III. Bond angles for β -(BDA-TTP)₂FeCl₄ in normal measurement and measured at DAC.

			angle / °						
atom	atom	atom	normal	DAC	atom	atom	atom	atom	atom
C3	C1	C2	114.3(3)	113.8(15)	S13	C18	S11	123.61(18)	123.9(8)
C1	C2	S1	114.7(2)	116.5(10)	C18	C19	S14	118.5(3)	117.8(12)
C1	C3	S2	114.7(2)	114.0(14)	C18	C19	S12	118.4(3)	118.1(12)
C5	C4	S1	116.3(2)	118.4(11)	S14	C19	S12	123.02(18)	123.9(9)
C5	C4	S2	117.0(2)	114.9(12)	C21	C20	S13	122.6(2)	123.3(11)
S1	C4	S2	125.81(19)	125.4(10)	C21	C20	S14	121.8(2)	120.8(11)
C4	C5	S3	122.3(2)	121.5(11)	S13	C20	S14	115.63(18)	115.8(10)
C4	C5	S4	121.7(2)	124.0(11)	C20	C21	S16	116.7(2)	118.3(12)
S3	C5	S4	115.97(18)	114.4(9)	C20	C21	S15	116.4(2)	115.4(11)
C7	C6	S3	118.3(2)	118.8(11)	S16	C21	S15	125.91(19)	125.3(10)
C7	C6	S5	118.2(2)	117.2(11)	C24	C22	S15	115.8(2)	113.7(14)
S3	C6	S5	123.33(18)	123.9(8)	C24	C23	S16	114.5(2)	114.5(10)
C6	C7	S4	118.1(2)	119.7(12)	C22	C24	C23	113.7(3)	113.3(15)
C6	C7	S6	118.3(2)	118.1(12)	C4	S1	C2	106.27(16)	105.4(8)
S4	C7	S6	123.43(18)	122.2(8)	C4	S2	C3	105.10(16)	105.7(7)
C9	C8	S5	122.3(2)	121.7(11)	C6	S3	C5	93.75(15)	94.6(7)
C9	C8	S6	121.7(2)	123.6(11)	C7	S4	C5	93.85(15)	94.1(8)
S5	C8	S6	115.97(17)	114.6(9)	C6	S5	C8	93.14(15)	94.4(8)
C8	C9	S8	118.8(2)	120.3(11)	C7	S6	C8	93.22(14)	93.4(7)
C8	C9	S7	117.9(2)	117.3(11)	C9	S7	C10	102.21(16)	102.6(8)
S8	C9	S7	122.18(19)	121.1(9)	C9	S8	C11	102.09(16)	103.0(7)
C12	C10	S7	114.6(3)	115.4(10)	C16	S9	C14	101.55(17)	101.2(7)

C12	C11	S8	114.7(2)	115.8(14)	C16	S10	C15	102.28(16)	102.5(8)
C10	C12	C11	113.6(3)	112.7(16)	C18	S11	C17	93.53(15)	93.9(7)
C15	C13	C14	112.8(3)	114.0(17)	C19	S12	C17	93.29(15)	94.2(8)
C13	C14	S9	114.2(3)	114.9(13)	C18	S13	C20	94.06(15)	94.2(7)
C13	C15	S10	114.6(3)	114.8(11)	C19	S14	C20	93.78(15)	94.3(7)
C17	C16	S9	118.6(2)	119.8(11)	C21	S15	C22	105.79(16)	106.1(7)
C17	C16	S10	118.2(2)	117.4(11)	C21	S16	C23	104.98(16)	105.3(9)
S9	C16	S10	122.34(19)	121.5(10)	Cl2	Fe1	Cl4	109.44(5)	109.6(3)
C16	C17	S12	122.4(2)	123.8(11)	Cl2	Fe1	Cl1	107.78(5)	107.9(2)
C16	C17	S11	122.1(2)	121.7(10)	Cl4	Fe1	Cl1	109.94(5)	109.7(2)
S12	C17	S11	115.49(18)	114.5(9)	Cl2	Fe1	Cl3	112.26(5)	111.9(2)
C19	C18	S13	118.0(3)	118.5(12)	Cl4	Fe1	Cl3	108.56(5)	108.5(3)
C19	C18	S11	118.3(3)	117.6(12)	Cl1	Fe1	Cl3	108.84(5)	109.2(3)

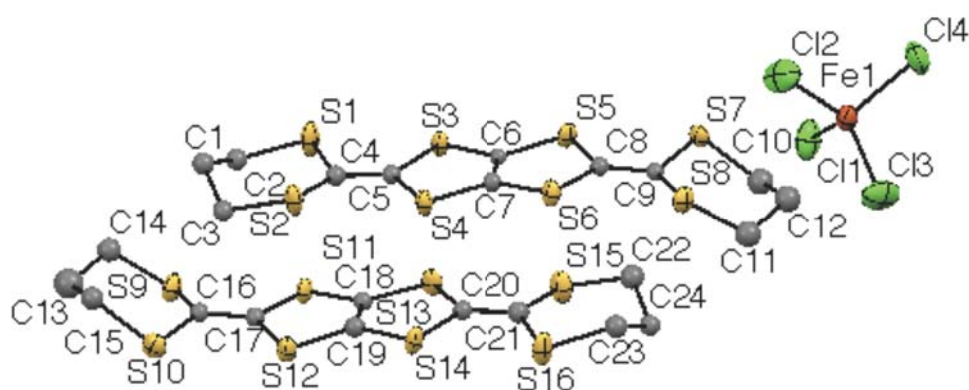


FIGURE 2-11. ORTEP drawing for β -(BDA-TTP) $_2$ FeCl $_4$ in “DAC”.

Table 2-V shows crystallographic data for (*R*)-GN in “normal” and “DAC”. The cell parameters in “DAC” are also good agree with these in “normal”. The Cr and Mn atoms were refined with anisotropic temperature factor since the observed reflections decreased to about 1/4 as compared with these in “normal”. ORTEP drawing of crystallographically independent part for (*R*)-GN in “DAC” is shown in Fig. 2-11. Bond length and angles in “normal” and “DAC” are summarized in Table 2-III and IV, respectively. The bond lengths and angles in “DAC” are also good agree with these in “normal”, and the *R*-factor is about 7% in “DAC”, indicating that the X-ray structure analysis under pressure using DAC are also succeeded for (*R*)-GN.

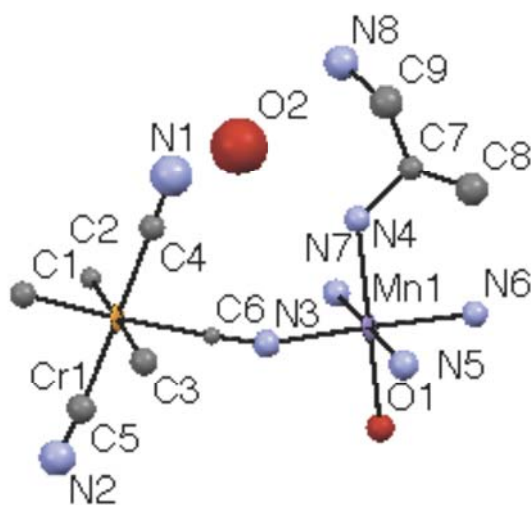


FIGURE 2-11. ORTEP drawing for (R)-GN in “DAC”.

TABLE 2-IV. Crystallographic data for (*R*)-GN in “normal” and “DAC”.

Condition	“normal”	“DAC”
Formula, F_w	$C_9H_{15}SCrMnN_8O_2$, 374.23	
Crystal shape, color, size / mm ³	block, yellowish-green, $0.20 \times 0.10 \times 0.05$	
Crystal system, Space group	orthorhombic, $P2_12_12_1$	
$a / \text{\AA}$	7.6370(4)	7.64700(7)
$b / \text{\AA}$	14.5270(11)	14.534(4)
$c / \text{\AA}$	14.9470(9)	14.958(3)
$V / \text{\AA}^3$	1658.26(18)	1662.5(6)
Z	4	4
$D_{\text{calcd.}} / \text{g cm}^{-3}$	1.499	1.495
μ / mm^{-1}	1.432	1.428
Index range	$0 \leq h \leq 9$	$0 \leq h \leq 8$
	$0 \leq k \leq 19$	$0 \leq k \leq 12$
	$0 \leq l \leq 19$	$0 \leq l \leq 13$
Reflections	2141	544
Parameters	191	96
GOF	1.116	1.135
R, wR	0.0465, 0.1252	0.0685, 0.1803
Flack	0.42(6)	0.27(16)
T / K	295	295

TABLE 2-V. Bond lengths for (*R*)-GN in “normal” and “DAC”.

atom	atom	distance / Å	
		“normal”	“DAC”
C1	N4	1.131(9)	1.13(2)
C1	Cr1	2.073(7)	2.076(19)
C2	N5	1.141(8)	1.18(2)
C2	Cr1	2.071(7)	2.031(16)
C3	N6	1.158(9)	1.12(2)
C3	Cr1	2.066(7)	2.10(2)
C4	N1	1.153(6)	1.17(3)
C4	Cr1	2.069(5)	2.024(18)
C5	N2	1.150(8)	1.17(2)
C5	Cr1	2.053(5)	2.089(18)
C6	N3	1.155(8)	1.18(2)
C6	Cr1	2.068(6)	2.036(17)
C7	N7	1.480(7)	1.48(2)
C7	C9	1.508(7)	1.49(3)
C7	C8	1.535(8)	1.53(3)
C9	N8	1.491(8)	1.51(3)
Mn1	N6	2.194(6)	2.187(17)
Mn1	N4	2.199(6)	2.206(16)
Mn1	N5	2.204(5)	2.213(16)
Mn1	N3	2.222(6)	2.253(16)
Mn1	O1	2.239(3)	2.241(13)
Mn1	N7	2.330(4)	2.341(16)
N4	C1	1.131(9)	1.12(2)
N5	C2	1.141(8)	1.13(2)
N6	C3	1.158(9)	1.19(2)

TABLE 2-VI. Bond angles for (*R*)-GN in “normal” and “DAC”.

angle / °					angle / °				
atom	atom	atom	“normal”	“DAC”	atom	atom	atom	“normal”	“DAC”
N4	C1	Cr1	176.9(6)	174(2)	C4	Cr1	C1	92.4(2)	90.5(8)
N5	C2	Cr1	177.8(6)	177.7(18)	C2	Cr1	C1	90.5(3)	92.4(9)
N6	C3	Cr1	176.7(7)	173(2)	N6	Mn1	N4	92.14(19)	92.2(6)
N1	C4	Cr1	176.1(5)	176(2)	N6	Mn1	N5	88.8(2)	89.2(5)
N2	C5	Cr1	179.6(6)	179(2)	N4	Mn1	N5	177.7(2)	177.6(7)
N3	C6	Cr1	176.4(5)	177.4(19)	N6	Mn1	N3	178.18(19)	177.8(7)
N7	C7	C9	113.8(5)	110.7(16)	N4	Mn1	N3	87.48(19)	85.9(6)
N7	C7	C8	109.9(5)	109.9(15)	N5	Mn1	N3	91.51(17)	90.5(5)
C9	C7	C8	108.2(5)	109.0(15)	N6	Mn1	O1	86.38(18)	87.9(5)
N8	C9	C7	114.1(6)	116.0(16)	N4	Mn1	O1	94.20(18)	94.4(6)
C5	Cr1	C3	88.5(3)	86.8(8)	N5	Mn1	O1	83.72(17)	83.7(5)
C5	Cr1	C6	90.7(3)	91.4(8)	N3	Mn1	O1	91.87(16)	91.9(6)
C3	Cr1	C6	90.7(3)	90.4(7)	N6	Mn1	N7	92.87(19)	93.2(6)
C5	Cr1	C4	178.0(3)	176.7(9)	N4	Mn1	N7	86.12(19)	85.8(6)
C3	Cr1	C4	93.4(3)	89.4(6)	N5	Mn1	N7	95.98(18)	96.0(6)
C6	Cr1	C4	89.0(2)	90.0(8)	N3	Mn1	N7	88.88(18)	89.0(6)
C5	Cr1	C2	90.2(3)	86.3(8)	O1	Mn1	N7	179.20(16)	179.1(4)
C3	Cr1	C2	178.8(3)	177.6(10)	C6	N3	Mn1	151.7(5)	152.9(17)
C6	Cr1	C2	89.2(2)	92.5(8)	C1	N4	Mn1	162.9(6)	161.7(16)
C4	Cr1	C2	87.8(2)	90.7(9)	C2	N5	Mn1	164.8(6)	163.2(18)
C5	Cr1	C1	87.9(3)	90.0(9)	C3	N6	Mn1	177.9(6)	179.3(19)
C3	Cr1	C1	89.6(2)	89.8(6)	C7	N7	Mn1	123.4(3)	122.4(11)
C6	Cr1	C1	178.6(3)	178.7(9)					

2-4. CONCLUSION

The author succeeds in developing the single crystal X-ray structure analysis under pressure using diamond anvil cell (DAC). The diffraction spots observed by overlapping with the diffraction from DAC, such as the halo pattern from Be backing-disks and gasket, and strong spots from diamond anvils, were deleted, and the program of the absorption correction for DAC was developed. When the the sample crystals were encapsulated in DAC without pressurized, the single crystal X-ray structure analysis for molecule-based materials β -(BDA-TTP)₂FeCl₄ and (*R*)-GN were carried out for application of this method. The structures obtained by measurements using DAC were good agreed with the results measured by normal condition. The method established in this work is very useful to the structural analysis for other various molecule-based materials under pressure, and wide application for this method are expected.

2-5. REFERENCES

- [1] a) R. J. Angel, R. T. Downs, and L. W. Finger, *Rev. Mineral. Geochem.* 41 (2000) 559.
b) R. J. Hemley, and P. Dera, *Rev. Mineral. Geochem.* 41 (2000) 335.
- [2] L. Merrill and W. A. Bassett: *Rev. Sci. Instrum.* 45 (1974) 290.
- [3] T. Isono: Master's thesis (2008) Tokyo Metropolitan Univesity.
- [4] T. Nagae: Graduation work (2005) Tokyo Metropolitan Univesity.
- [5] K. Takahashi: Master's thesis (2012) Tokyo Metropolitan Univesity.
- [6] G. J. Piermarini, S. Block, J. D. Barnett, and R. A. Forman, *J. Appl. Phys.* 46 (1975) 2274.
- [7] Z. Otwinowski and W. Minor: *Methods Enzymology, Macromolecular Crystallography, part A* (Eds.: C. W. Carter Jr. and R. M. Sweet) Academic Press, New York 276 (1997) 307.
- [8] G. M. Sheldrick, SHELX-97, University of Göttingen, Germany (1997).

2-6. APPENDIX

The source code of the program for absorption correction shows below.

```
use strict;
use warnings;

use Math::Trig;

# ----list of variables----
# -----input-----
my $phi_center = 46;
my $phi_limit = 41;

# ---direct beam---
my $db_phi_gonio;
my $db_phi;
my $db_int;
my %db;
my %db_ratio_sqrt;
my %db_avg;
my %db_avg_ratio_sqrt;

# ---from x file---
my $phi_gonio;
my $phi_i;
my $phi_i_round;
my $x_beam;
my $y_beam;
my $distance;

my $h;
my $k;
my $l;
my $flag;
```

```

my $int_prof;
my $int_sum;
my $chi_sq;
my $sigma;
my $cos;
my $x;
my $y;
my $factor;
my $strength;

my $x_spot;
my $y_spot;
my $theta_dash;
my $phi_d;
my $phi_d_round;
my $int_prof_cor;
my $int_sum_cor;

open (FILE, 'direct_beam.csv') or die "$!";
while (my $line = <FILE>) {
    my @line = split ('', $line);
    $db_phi_gonio = $line[1];
    $db_int = $line[2];
    $db_phi = $phi_center - $db_phi_gonio;
    $db{$db_phi} = $db_int;
}

foreach my $key1 (keys (%db)) {
    $db_ratio_sqrt{$key1} = ($db{$key1} / $db{0})**(1/2);
    foreach my $key2 (keys (%db)) {
        if ($key1 >= 0 and $key2 <= 0 and $key1 = abs ($key2)) {
            $db_avg{$key1} = ($db{$key1} + $db{$key2}) / 2;
        }
    }
    $db_avg{0} = $db{0};
}

```

```

foreach my $key (keys (%db_avg)) {
    $db_avg_ratio_sqrt{$key} = ($db_avg{$key} / $db_avg{0})**(1/2);
}

close (FILE);

my $dirname = '.';
opendir (DIR, $dirname) or die "$dirname: $!";
while (my $dir = readdir(DIR)) {
    next unless (-f $dir);
    next unless ($dir =~ /^os.¥d+¥.x$/);
    open (FILE, $dir) or die "$dir: $!";
    while (my $line = <FILE>) {
        if ($line =~ /x beam.+/) {
            my @xy_beam = split (' ', $line);
            $x_beam = $xy_beam[2];
            $y_beam = $xy_beam[5];
        } elsif ($line =~ /distance.+/) {
            my @distance = split (' ', $line);
            $distance = $distance[1];
        } elsif ($line =~ /^ +¥d+¥.¥d{5} /) {
            my @phi_start2end = split (' ', $line);
            $phi_gonio = ($phi_start2end[0] + $phi_start2end[1]) / 2;
            $phi_i = ($phi_gonio - $phi_center) * (-1);
            $phi_i_round = int ($phi_i + 0.5);
        } else {
            next;
        }
    }
}

my $dir_origin = $dir;
$dir =~ s/os/cor_os/;
open (FILE, $dir_origin) or die "$dir: $!";
open (NEWFILE, "> $dir") or die "$!";
while (my $line = <FILE>) {
    if ($line =~ /^ +-?¥d+ +-?¥d+ +-?¥d+ +/) {
        my @line = split (' ', $line);
        if (@line < 13) {

```

```

foreach my $data (@line) {
    if (length ($data) == 10) {
        $data =  $\sqrt{(.{4})/(.{6})}$ ;
        $chi_sq = $1;
        $sigma = $2;
        my @line = splice (@line, 6, 1, ($chi_sq, $sigma));
    } elsif (length ($data) == 11) {
        $data =  $\sqrt{(.{5})/(.{6})}$ ;
        $chi_sq = $1;
        $sigma = $2;
        my @line = splice (@line, 6, 1, ($chi_sq, $sigma));
    } elsif (length ($data) == 17) {
        $data =  $\sqrt{(.{1})/(.{8})/(.{8})}$ ;
        $flag = $1;
        $int_prof = $2;
        $int_sum = $3;
        my @line = splice (@line, 3, 1, ($flag, $int_prof,
$int_sum));
    }
}

$h = $line[0];
$k = $line[1];
$l = $line[2];
$flag = $line[3];
$int_prof = $line[4];
$int_sum = $line[5];
$chi_sq = $line[6];
$sigma = $line[7];
$cos = $line[8];
$x = $line[9];
$y = $line[10];
$factor = $line[11];
$strength = $line[12];
} else {
    $h = $line[0];
    $k = $line[1];
    $l = $line[2];
    $flag = $line[3];

```



```

    $int_prof = $line[4];
    $int_sum = $line[5];
    $chi_sq = $line[6];
    $sigma = $line[7];
    $cos = $line[8];
    $x = $line[9];
    $y = $line[10];
    $factor = $line[11];
    $strength = $line[12];
}
my $count = ($sigma =~ tr/0-9%.%-/0-9%.%-/);
if ($count > 6) {
    $sigma = int ($sigma + 0.5);
}

$x_spot = $x / 10 - $x_beam;
$y_spot = $y / 10 - $y_beam;
$theta_dash = rad2deg ($y_spot / $distance);
$phi_d = rad2deg (
    acos (($distance * cos (deg2rad ($phi_i - $theta_dash))) /
(($distance**2 + $x_spot**2)**(1/2)))
);

if ($phi_d > $phi_limit) {
    my $line = join ('', @line);
    $line = s/$line//;
} else {
    $phi_d_round = int ($phi_d + 0.5);
    $int_prof_cor = sprintf "%.1f", (
        $int_prof / ($db_ratio_sqrt{$phi_i_round} *
$db_avg_ratio_sqrt{$phi_d_round})
    );
    my $count1 = ($int_prof_cor =~ tr/0-9%.%-/0-9%.%-/);
    if ($count1 > 8) {
        $int_prof_cor = int ($int_prof_cor + 0.5);
    }
    $int_sum_cor = sprintf "%.1f", (

```

```

                                $int_sum      /      ($db_ratio_sqrt{$phi_i_round}      *
$db_avg_ratio_sqrt{$phi_d_round})
                                );
                                my $count2 = ($int_sum_cor = tr/0-9¥.¥-/0-9¥.¥-/);
                                if ($count2 > 8) {
                                    $int_sum_cor = int ($int_sum_cor + 0.5);
                                }

                                @line = (

                                    $h, $k, $l, $flag, $int_prof_cor, $int_sum_cor,
                                    $chi_sq, $sigma, $cos, $x, $y, $factor, $strength
                                );
                                printf NEWFILE ("%4s%4s%4s%2s%8s%8s%7s%6s%6s%7s%7s%6s%8s¥n",
@line);

                                }
                                } else {
                                    print NEWFILE $line;
                                }
                                }
                                close (NEWFILE);
                                close (FILE);
                                }
                                closedir(DIR);

```

TABLE S2-I. Atomic coordinates in β -(BDA-TTP)₂FeCl₄ under ambient pressure.

	x	y	z	$U_{\text{eq}} / \text{\AA}^2$
C1	0.1620(3)	-0.13928(8)	1.0315(5)	0.0335(9)
H1A	0.1597	-0.1422	0.9068	0.04
H1B	0.1477	-0.1616	1.0833	0.04
C2	0.2738(3)	-0.12792(8)	1.0861(5)	0.0353(9)
H2A	0.3235	-0.1466	1.0631	0.042
H2B	0.2751	-0.1239	1.21	0.042
C3	0.0741(3)	-0.11454(8)	1.0812(5)	0.0348(9)
H3A	0.0801	-0.1102	1.2047	0.042
H3B	0.0052	-0.1255	1.0589	0.042
C4	0.2110(2)	-0.06173(8)	0.9671(4)	0.0279(8)
C5	0.2329(2)	-0.02855(8)	0.9230(4)	0.0276(8)
C6	0.3237(2)	0.02734(8)	0.8333(4)	0.0251(8)
C7	0.2178(2)	0.03437(8)	0.8294(4)	0.0239(8)
C8	0.3091(2)	0.09019(8)	0.7416(4)	0.0238(8)
C9	0.3300(2)	0.12382(8)	0.7109(4)	0.0259(8)
C10	0.4713(3)	0.17825(8)	0.7633(5)	0.0413(10)
H10A	0.4697	0.1762	0.8884	0.05
H10B	0.5397	0.1884	0.7339	0.05
C11	0.2725(3)	0.19196(8)	0.7662(5)	0.0387(9)
H11A	0.222	0.2103	0.7382	0.046
H11B	0.2754	0.1896	0.8913	0.046
C12	0.3825(3)	0.20252(9)	0.7051(5)	0.0427(10)
H12A	0.381	0.2036	0.5796	0.051
H12B	0.3987	0.2255	0.7484	0.051
C13	0.1322(3)	-0.20258(9)	1.5531(6)	0.0472(10)
H13A	0.1194	-0.2259	1.5121	0.057

H13B	0.1317	-0.203	1.6787	0.057
C14	0.2416(3)	-0.19082(8)	1.4950(5)	0.0417(10)
H14A	0.2395	-0.1881	1.3702	0.05
H14B	0.2937	-0.2087	1.5227	0.05
C15	0.0424(3)	-0.17960(8)	1.4878(5)	0.0428(10)
H15A	-0.0256	-0.1904	1.5146	0.051
H15B	0.0464	-0.178	1.3627	0.051
C16	0.1775(2)	-0.12355(8)	1.5461(4)	0.0274(8)
C17	0.1970(2)	-0.09011(8)	1.5128(4)	0.0264(8)
C18	0.2856(2)	-0.03363(8)	1.4237(4)	0.0267(8)
C19	0.1800(2)	-0.02723(8)	1.4189(4)	0.0275(8)
C20	0.2680(2)	0.02924(8)	1.3290(4)	0.0276(8)
C21	0.2869(2)	0.06273(8)	1.2866(4)	0.0280(8)
C22	0.4215(3)	0.11692(9)	1.1775(5)	0.0366(9)
H22A	0.489	0.1283	1.2062	0.044
H22B	0.4192	0.1134	1.0531	0.044
C23	0.2213(3)	0.12794(8)	1.1669(5)	0.0352(9)
H23A	0.2227	0.1228	1.0441	0.042
H23B	0.1694	0.1463	1.183	0.042
C24	0.3309(3)	0.14088(9)	1.2237(5)	0.0346(9)
H24A	0.3432	0.1632	1.1706	0.042
H24B	0.3317	0.1442	1.3482	0.042
S1	0.32037(7)	-0.08968(2)	0.97988(15)	0.0457(3)
S2	0.07587(7)	-0.07380(2)	0.96922(14)	0.0413(3)
S3	0.36449(6)	-0.01385(2)	0.89166(12)	0.0320(2)
S4	0.12999(6)	0.00186(2)	0.88530(13)	0.0323(2)
S5	0.41186(6)	0.05925(2)	0.76586(12)	0.0303(2)
S6	0.17639(7)	0.07452(2)	0.75578(12)	0.0307(2)

S7	0.46327(7)	0.13564(2)	0.66995(12)	0.0330(2)
S8	0.22189(7)	0.15209(2)	0.67396(13)	0.0332(2)
S9	0.28675(7)	-0.15087(2)	1.59194(13)	0.0347(2)
S10	0.04397(7)	-0.13634(2)	1.57689(13)	0.0362(2)
S11	0.32883(7)	-0.07378(2)	1.49654(12)	0.0318(2)
S12	0.09306(6)	-0.05937(2)	1.48820(12)	0.0325(2)
S13	0.37190(6)	-0.00055(2)	1.36839(13)	0.0322(2)
S14	0.13673(6)	0.01348(2)	1.35718(13)	0.0332(2)
S15	0.42105(7)	0.07534(2)	1.28174(15)	0.0437(3)
S16	0.17661(7)	0.09013(2)	1.28053(14)	0.0409(3)
Fe1	0.11024(4)	0.248696(12)	0.11977(7)	0.03383(15)
Cl1	0.20128(9)	0.22139(3)	0.32167(15)	0.0599(3)
Cl2	0.01936(10)	0.21060(3)	-0.02887(18)	0.0831(4)
Cl3	0.00644(9)	0.28670(3)	0.24145(16)	0.0678(3)
Cl4	0.21958(9)	0.27564(3)	-0.05008(15)	0.0612(3)

TABLE S2-II. Atomic coordinates in β -(BDA-TTP)₂FeCl₄ under ambient pressure measured at DAC.

	x	y	z	$U_{eq} / \text{\AA}^2$
C1	0.1616(11)	-0.1396(4)	1.031(2)	0.029(4)
H1A	0.1482	-0.1618	1.0833	0.035
H1B	0.1583	-0.1425	0.9065	0.035
C2	0.2721(11)	-0.1280(4)	1.083(2)	0.027(4)
H2A	0.3216	-0.1466	1.059	0.033
H2B	0.2738	-0.1242	1.2068	0.033
C3	0.0740(11)	-0.1148(4)	1.083(2)	0.026(4)
H3A	0.081	-0.1105	1.2064	0.031
H3B	0.005	-0.1257	1.062	0.031
C4	0.2092(11)	-0.0614(4)	0.969(2)	0.025(4)
C5	0.2322(11)	-0.0292(4)	0.924(2)	0.022(4)
C6	0.3239(11)	0.0270(4)	0.832(2)	0.017(4)
C7	0.2196(11)	0.0342(4)	0.826(2)	0.023(4)
C8	0.3088(11)	0.0907(4)	0.738(2)	0.021(4)
C9	0.3280(11)	0.1236(4)	0.712(2)	0.019(4)
C10	0.4716(13)	0.1783(4)	0.762(3)	0.041(5)
H10A	0.4708	0.1762	0.8867	0.049
H10B	0.5399	0.1883	0.7314	0.049
C11	0.2723(12)	0.1922(5)	0.764(3)	0.041(5)
H11A	0.2212	0.2103	0.7363	0.049
H11B	0.2751	0.1899	0.8893	0.049
C12	0.3817(12)	0.2034(5)	0.705(3)	0.040(5)
H12A	0.3975	0.2261	0.7507	0.048
H12B	0.3803	0.205	0.5793	0.048
C13	0.1326(13)	-0.2029(5)	1.550(3)	0.052(5)

H13A	0.132	-0.204	1.6749	0.062
H13B	0.1206	-0.226	1.5059	0.062
C14	0.2413(11)	-0.1909(4)	1.495(2)	0.034(4)
H14A	0.2398	-0.188	1.37	0.041
H14B	0.2932	-0.2088	1.5223	0.041
C15	0.0416(12)	-0.1801(4)	1.488(2)	0.030(4)
H15A	-0.0256	-0.1909	1.5179	0.036
H15B	0.0434	-0.1786	1.3627	0.036
C16	0.1785(11)	-0.1235(4)	1.543(2)	0.021(4)
C17	0.1963(11)	-0.0903(4)	1.513(2)	0.022(4)
C18	0.2860(11)	-0.0337(4)	1.426(2)	0.022(4)
C19	0.1786(11)	-0.0273(4)	1.418(2)	0.025(4)
C20	0.2678(11)	0.0292(4)	1.328(2)	0.022(4)
C21	0.2848(12)	0.0626(4)	1.287(2)	0.028(4)
C22	0.4223(12)	0.1168(4)	1.174(3)	0.035(5)
H22A	0.49	0.1281	1.2002	0.042
H22B	0.4181	0.113	1.0501	0.042
C23	0.2226(11)	0.1283(4)	1.167(2)	0.032(4)
H23A	0.2248	0.1233	1.0447	0.039
H23B	0.1709	0.1466	1.1833	0.039
C24	0.3300(10)	0.1408(4)	1.226(2)	0.026(4)
H24A	0.3308	0.1433	1.3506	0.031
H24B	0.3421	0.1635	1.1766	0.031
S1	0.3205(3)	-0.08966(11)	0.9799(8)	0.0426(16)
S2	0.0765(3)	-0.07380(11)	0.9691(7)	0.0369(15)
S3	0.3643(3)	-0.01370(10)	0.8927(6)	0.0261(13)
S4	0.1301(3)	0.00185(10)	0.8855(7)	0.0271(13)
S5	0.4113(3)	0.05926(10)	0.7669(6)	0.0278(14)

S6	0.1764(3)	0.07461(11)	0.7562(6)	0.0291(14)
S7	0.4633(3)	0.13580(11)	0.6699(6)	0.0279(14)
S8	0.2220(3)	0.15220(11)	0.6739(6)	0.0301(14)
S9	0.2867(3)	-0.15094(11)	1.5930(7)	0.0344(15)
S10	0.0439(3)	-0.13646(12)	1.5763(7)	0.0352(15)
S11	0.3289(3)	-0.07352(10)	1.4958(6)	0.0267(13)
S12	0.0935(3)	-0.05925(11)	1.4887(7)	0.0294(14)
S13	0.3719(3)	-0.00042(11)	1.3675(7)	0.0297(14)
S14	0.1366(3)	0.01349(10)	1.3578(7)	0.0306(14)
S15	0.4207(3)	0.07535(12)	1.2828(7)	0.0408(16)
S16	0.1764(3)	0.09008(11)	1.2800(7)	0.0405(16)
Fe1	0.11025(17)	0.24867(6)	0.1199(4)	0.0332(9)
Cl1	0.2015(4)	0.22132(12)	0.3210(8)	0.0604(19)
Cl2	0.0187(4)	0.21072(16)	-0.0285(9)	0.080(2)
Cl3	0.0063(4)	0.28680(15)	0.2408(8)	0.065(2)
Cl4	0.2201(4)	0.27554(14)	-0.0500(8)	0.0621(18)

TABLE S2-III. Atomic coordinates in (*R*)-GN under ambient pressure.

	<i>x</i>	<i>y</i>	<i>z</i>	$U_{eq} / \text{\AA}^2$
C1	1.1835(9)	0.1507(5)	0.7142(4)	0.0242(14)
C2	1.1958(9)	0.3351(4)	0.7956(4)	0.0230(14)
C3	0.8027(9)	0.1516(5)	0.7290(5)	0.0267(14)
C4	0.9848(10)	0.3099(3)	0.6386(3)	0.0281(12)
C5	1.0191(11)	0.1814(4)	0.8838(3)	0.0342(14)
C6	0.8165(8)	0.3355(4)	0.8107(4)	0.0224(13)
C7	0.4646(8)	0.4169(4)	0.5951(3)	0.0337(14)
H7A	0.3397	0.4293	0.6041	0.04
C8	0.4999(12)	0.3160(4)	0.6197(4)	0.0444(14)
H8A	0.6199	0.3013	0.6071	0.067
H8B	0.4247	0.2767	0.5851	0.067
H8C	0.4771	0.3068	0.6822	0.067
C9	0.5060(11)	0.4297(5)	0.4973(3)	0.0471(15)
H9A	0.6321	0.4301	0.4898	0.057
H9B	0.4604	0.3774	0.4643	0.057
Cr1	0.99906(17)	0.24373(4)	0.76090(4)	0.0163(2)
Mn1	0.50842(10)	0.49330(4)	0.80747(4)	0.0178(2)
N1	0.9768(10)	0.3516(4)	0.5730(3)	0.0496(15)
N2	1.0306(13)	0.1460(4)	0.9523(4)	0.078(3)
N3	0.7151(8)	0.3893(4)	0.8344(3)	0.0330(14)
N4	0.7166(7)	0.5979(4)	0.8078(4)	0.0307(12)
N5	0.3021(7)	0.3874(4)	0.8129(4)	0.0283(12)
N6	0.3046(8)	0.5973(4)	0.7854(4)	0.0347(13)
N7	0.5654(6)	0.4783(3)	0.6550(3)	0.0312(11)
N8	0.4328(7)	0.5157(4)	0.4578(4)	0.0535(16)
O1	0.4500(5)	0.5086(2)	0.9535(2)	0.0310(9)
O2	1.0091(16)	0.8305(4)	0.4363(5)	0.139(4)

TABLE S2-IV. Atomic coordinates in (*R*)-GN under ambient pressure measured at DAC.

atom	<i>x</i>	<i>y</i>	<i>z</i>	$U_{eq} / \text{\AA}^2$
C1	1.184(2)	0.6657(14)	0.3137(15)	0.029(5)
C2	0.8086(18)	0.6656(13)	0.2922(14)	0.019(5)
C3	1.202(2)	0.8483(15)	0.2253(17)	0.032(5)
C4	0.979(2)	0.8185(14)	0.3812(12)	0.029(5)
C5	1.013(2)	0.6893(15)	0.1373(12)	0.036(5)
C6	0.8199(17)	0.8478(13)	0.2158(14)	0.013(4)
C7	0.4620(17)	1.0835(14)	0.4041(12)	0.027(4)
H7A	0.3375	1.0699	0.3962	0.032
C8	0.496(2)	1.1841(15)	0.3790(13)	0.046(5)
H8A	0.4255	1.2235	0.416	0.069
H8B	0.4656	1.1937	0.3174	0.069
H8C	0.6171	1.1983	0.3878	0.069
C9	0.510(2)	1.0694(16)	0.5000(13)	0.048(5)
H9A	0.4721	1.1229	0.5336	0.058
H9B	0.6364	1.0664	0.5043	0.058
Cr1	1.0012(4)	0.75614(18)	0.26073(19)	0.0186(11)
Mn1	0.5086(2)	1.00649(17)	0.19238(17)	0.0207(10)
N1	0.967(3)	0.8532(17)	0.4515(16)	0.077(6)
N2	1.023(2)	0.6471(14)	0.0709(13)	0.057(5)
N3	0.7161(17)	0.9029(14)	0.1929(12)	0.034(4)
N4	0.3041(16)	0.9017(13)	0.2139(12)	0.032(4)
N5	0.7157(17)	1.1130(13)	0.1648(12)	0.037(5)
N6	0.3030(17)	1.1134(13)	0.1864(12)	0.029(4)
N7	0.5658(14)	1.0219(12)	0.3454(11)	0.030(4)
N8	0.4346(17)	0.9844(15)	0.5443(13)	0.052(5)
O1	0.4499(11)	0.9905(10)	0.0464(9)	0.034(3)
O2	0.511(3)	0.8324(19)	0.4386(19)	0.139(8)

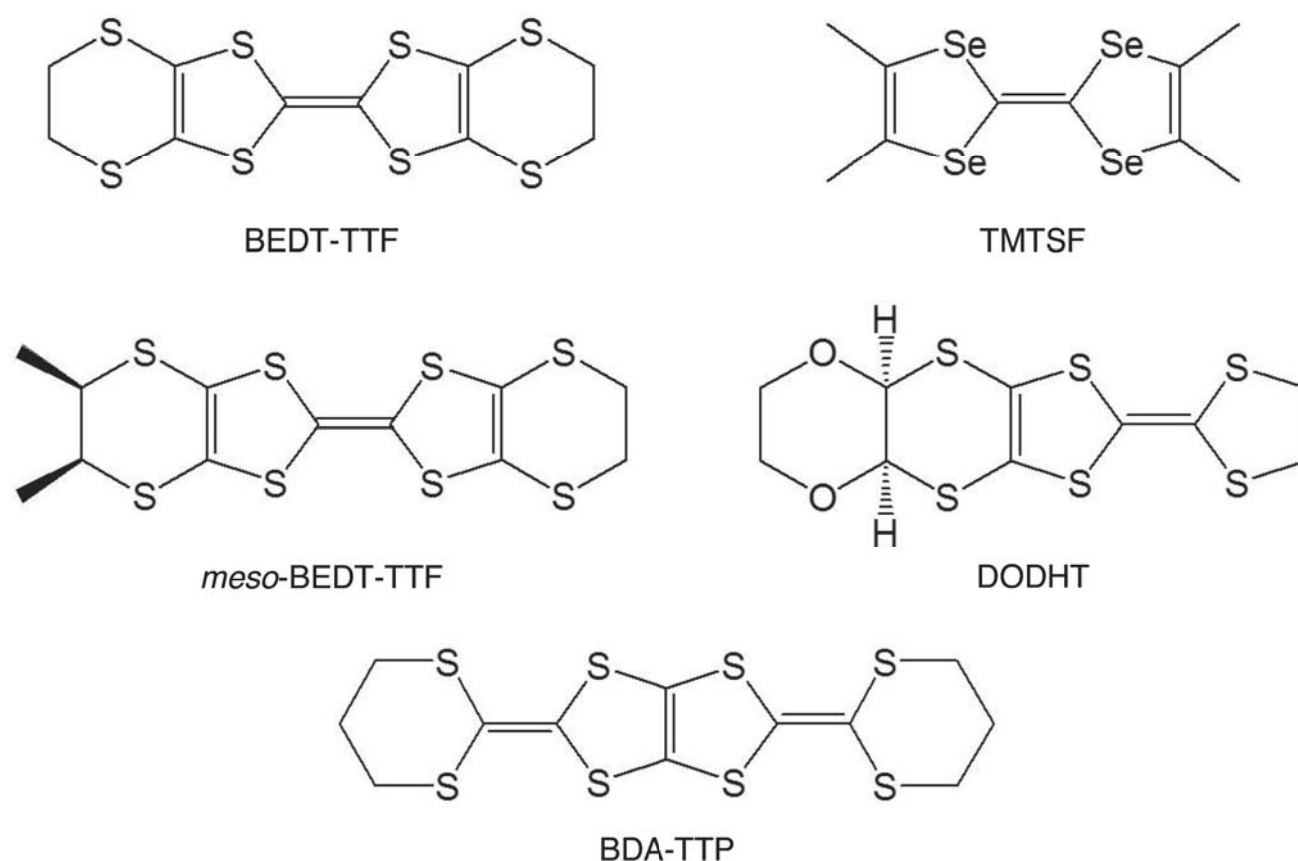
Chapter III. Crystal Structural Study of Pressure-Induced Molecule-based Superconductor β -(BDA-TTP) $_2$ FeCl $_4$ at Low Temperature and under High Pressure

3-1. INTRODUCTION

Molecule-based Superconductor

From the viewpoints of the development of new organic superconductors and the clarification of the mechanism of superconductivity, there has been growing interest in layered organic superconductors with the quarter-filled band structure such as θ -(BEDT-TTF) $_2$ I $_3$ [BEDT-TTF = bis(ethylenedithio)tetrathiafulvalene] [1], α -(BEDT-TTF) $_2$ I $_3$ [2], β'' -(DODHT) $_2$ PF $_6$ [DODHT = (1,4-dioxane-2,3-diylidithio)dihydrotetrathiafulvalene] [3], and β -(*meso*-DMBEDT-TTF) $_2$ X (X = PF $_6$, AsF $_6$) [DMBEDT-TTF = (1,2-dimethylethylenedithio)ethylenedithiotetrathiafulvalene] [4], in which the superconducting phase is adjacent to the charge-ordered insulating phase [5]. The donor molecule BDA-TTP [2,5-bis(1,3-dithian-2-ylidene)-1,3,4,6-tetrathiapentalene], akin to TMTSF (tetramethyltetraselenafulvalene) and BEDT-TTF, has the ability to produce many organic superconductors [6, 7]. The uniaxial strain experiment using the pressure-induced BDA-TTP superconductor β -(BDA-TTP) $_2$ I $_3$ revealed that the quarter-filled band system rather than the half-filled one is favorable for achieving superconductivity [8, 9], and theoretical study of β -(BDA-TTP) $_2$ I $_3$ suggested that a short-range charge ordering (CO) is likely to contribute to an enhancement of spin-fluctuation-mediated superconductivity [10].

Besides β -(BDA-TTP) $_2$ I $_3$, superconductivity occurs in β -(BDA-TTP) $_2$ FeCl $_4$ above a critical pressure of 6.5 kbar (the room temperature value of pressure) [11]. Temperature dependence of resistance ratio and temperature-pressure phase diagram of β -(BDA-TTP) $_2$ FeCl $_4$ are shown in Fig. 3-1. The FeCl $_4$ salt at ambient pressure undergoes an MI transition at 113 K and an antiferromagnetic (AF) ordering below a Néel temperature of 8.5 K with decreasing temperature [12, 13]: the MI transition is suppressed by pressure [11]. However, the X-ray study at 95 K showed almost no remarkable change in the arrangement of two independent BDA-TTP molecules in β -(BDA-TTP) $_2$ FeCl $_4$ compared to those at room temperature [13].



SCHEME 3-1. Chemical structure of BDA-TTP and some donor molecules of the organic superconductor.

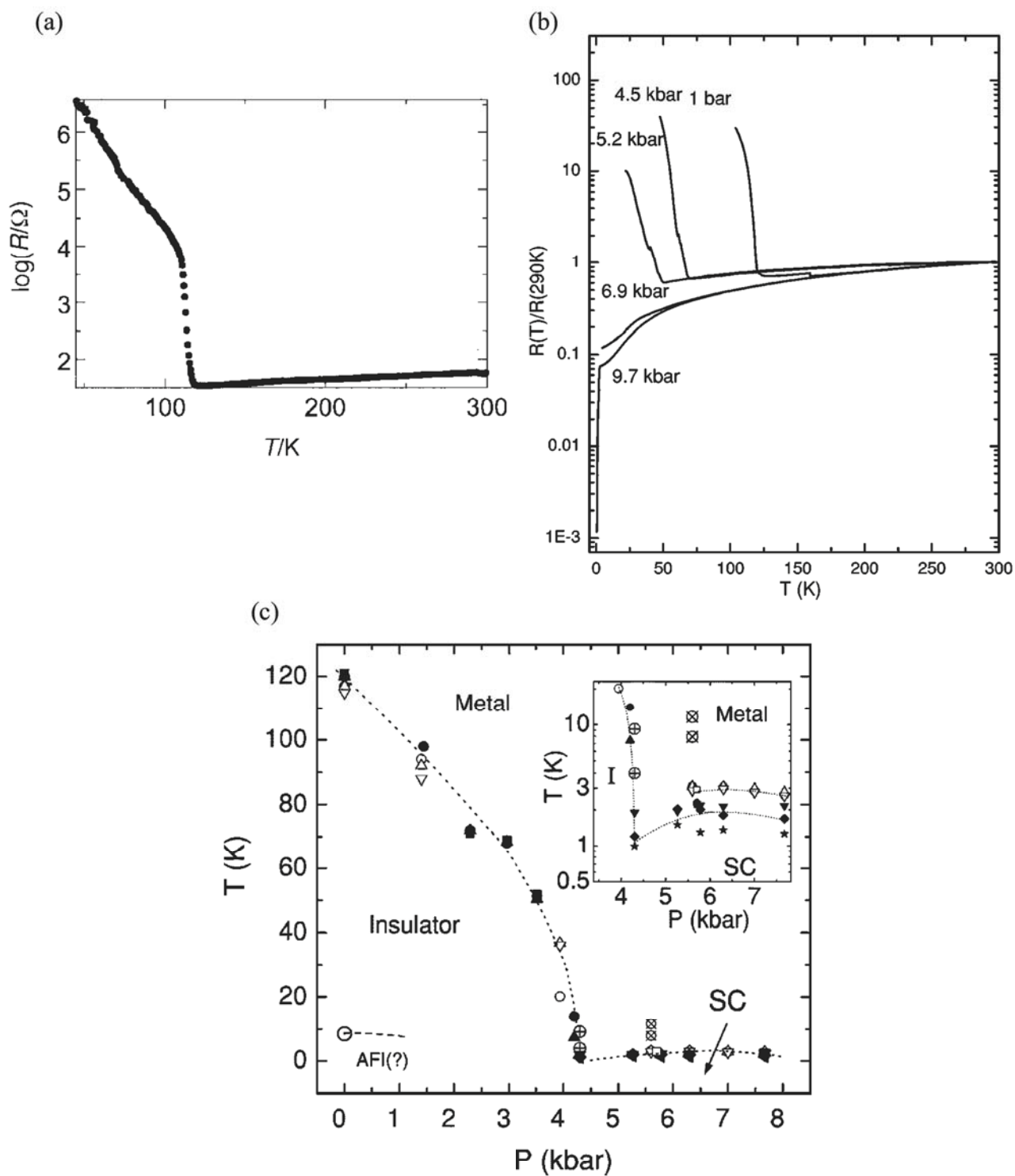


FIGURE 3-1. Temperature dependence of resistance ratio of β -(BDA-TTP)₂FeCl₄ under (a) ambient pressure [11] and (b) various pressures [13]. (c) Temperature-pressure phase diagram of β -(BDA-TTP)₂FeCl₄ [13].

This Work

Meanwhile, electron spin resonance (ESR) measurement and Raman spectroscopy of β -(BDA-TTP)₂FeCl₄ have been strongly indicative of CO at the MI transition [14]. Stimulated by the result, the author undertook X-ray studies of the FeCl₄ salt at different temperatures below $T_{\text{MI}} = 113$ K to obtain structural evidence for the CO. In addition, the author performed room-temperature X-ray studies by applying hydrostatic pressures up to 21 kbar to gain a better understanding of the suppression of MI transition and subsequent occurrence of superconductivity. In this chapter, the variations in the crystal and electronic structures of β -(BDA-TTP)₂FeCl₄ induced by lowering temperature and by increasing pressure is reported.

3-2. EXPERIMENTAL DETAILS

X-ray Diffraction Measurement

The crystal size used for X-ray diffraction measurements at 10, 54, 82, 92, 103, and 113 K was $0.45 \times 0.30 \times 0.10 \text{ mm}^2$, whereas that at room temperature (295 K) under ambient pressure and hydrostatic pressures of 3, 8, 11, 16, and 21 kbar was $0.25 \times 0.20 \times 0.10 \text{ mm}^3$. A curved imaging plate (MACScience DIP320V) equipped with a 6 kW rotating-anode X-ray generator with a graphite monochromated MoK α radiation ($\lambda = 0.71073 \text{ \AA}$) and with a closed-cycle helium refrigerator (DAIKIN U110DW) was used for data collection. Oscillation photographs were taken with the angle of 3° for each exposure of 1 hour. The image data processing of IP digital data, cell refinements and data reduction were performed using the *Denzo* and *Scalepack* programs [15].

High-Pressure Procedure

The measurements under pressures up to 21 kbar were performed using a diamond anvil cell (DAC) with a 1.0 mm culet and a sample chamber of 0.5 mm diameter. The X-ray beam can enter and exit in a cone of 45° half-angle through the beryllium backing-disc. Daphne 7373 (Idemitsu Co. Ltd.) was employed as a pressure medium, and the value of pressure at room temperature was determined by the ruby fluorescence method [16]. The intensity data were corrected for the absorption of the incident and the diffraction beam through the DAC before the merging process. Detailed procedures and analysis under pressure are described in Chapter II.

Structure Analysis

Structures were solved by direct methods and refined by least-squares method on F^2 using the SHELXS-97 program [17]. Hydrogen atoms are located in their calculated positions. Although all non-Hydrogen atoms were refined anisotropically at room temperature, only Fe atoms were refined with the anisotropic temperature factor for structure analysis at low temperature, and the anisotropic temperature factors were applied for S, Fe, and Cl atoms for structure analyses at all pressures up to 21 kbar.

Band Calculation

The band structure calculations were performed using the programs reported previously [18]. The overlap integrals S_{ij} between HOMOs of adjacent donor molecules were calculated by the extended Hückel method. The band dispersions were obtained by the tight-binding method using the transfer integrals t_{ij} derived from the following equation: $t_{ij} = E (-10 \text{ eV}) \times S_{ij}$, where E is the energy level of the HOMO of donor molecule.

3-3. RESULTS & DISCUSSION

3-3-1. Low-Temperature Crystal and Electric Structures

Satellite Reflections

In a low temperature range from 103 to 10 K, some satellite reflections for $l/2$ in the diffraction photographs of β -(BDA-TTP) $_2$ FeCl $_4$ were observed (Fig. 3-2(a)-(e)); however, any other satellite reflections could not be detected. Such satellite reflections could not be observed in the preceding X-ray diffraction pattern [13], probably because the sample was not sufficiently cooled to below $T_{\text{MI}} = 113$ K. Fig. 3-2(f) shows the change in the intensity ratio of the satellite reflection (2 18 5.5) to Bragg reflection (2 18 5) as a function of temperature. The intensity ratio rapidly increases as the temperature is lowered to 80 K, and its increase becomes gradual below 80 K. This temperature dependence implies that the MI transition is due to a structural phase transition associated with a displacing change in the position of the BDA-TTP donor molecules and/or FeCl $_4^-$ anions.

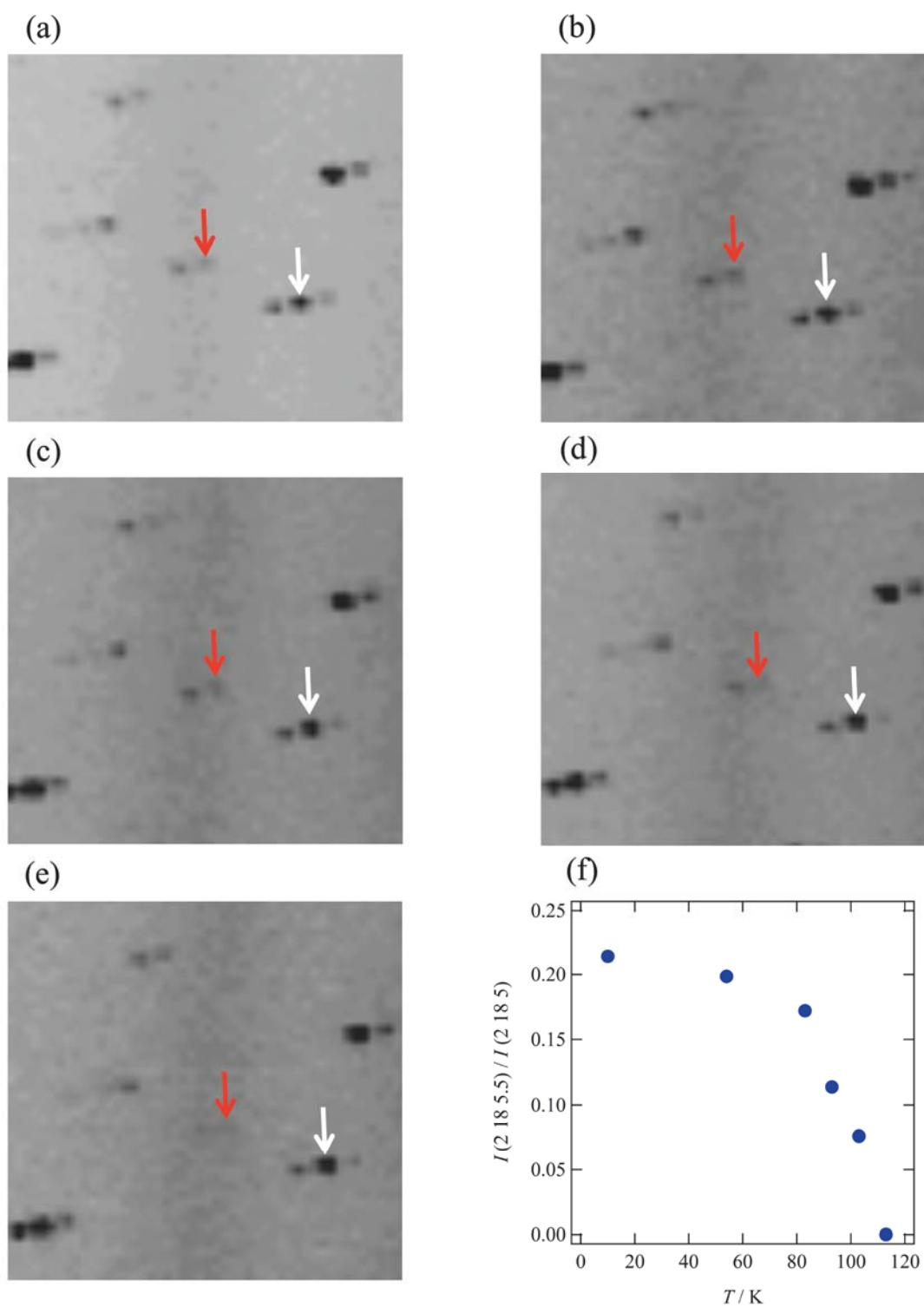


FIGURE 3-2. X-ray diffraction patterns at (a) 10, (b) 54, (c) 82, (d) 92, and (e) 103 K. White and Red arrows indicate Bragg reflection (2 18 5) and satellite reflection (2 18 5.5), respectively. (f) Temperature dependence of the intensity ratio of one satellite reflection (2 18 5.5) to Bragg reflection (2 18 5).

Crystal Structure of β -(BDA-TTP) $_2$ FeCl $_4$ at 295 (RT) & 10 (LT) K

X-ray structure analyses of β -(BDA-TTP) $_2$ FeCl $_4$ at both 295 (RT) and 10 (LT) K were carried out. Table 3-I summarizes the crystallographic data at RT and LT. The unit lattice at LT was determined to be $a_p \times b_p \times 2c_p$, where a_p , b_p , and c_p denote the lattice parameters at RT. It is therefore clear that the insulating state below $T_{\text{MI}} = 113$ K occurs as the result of structural phase transition accompanied by a change in one of the lattice parameters.

Fig. 3-3(a) and (b) show the crystal structures at RT and LT, respectively. The RT structure is identical with that previously reported within experimental error [12, 13], and the unit cell contains two crystallographically independent BDA-TTP molecules (molecules A and B) and one FeCl $_4^-$ anion. On the other hand, in the LT structure, there are four independent BDA-TTP molecules (molecules A, A', B, and B') and two FeCl $_4^-$ anions in the unit cell with a 2-fold periodicity along the c -axis.

TABLE 3-I. Crystallographic data for β -(BDA-TTP)₂FeCl₄ at 295 (RT) and 10 (LT) K.

T / K	295 (RT)	10 (LT)
Formula, F_w	$\text{C}_{24}\text{H}_{24}\text{S}_{16}\text{FeCl}_4$, 1023.04	
Crystal size / mm^3	$0.25 \times 0.20 \times 0.10$	$0.45 \times 0.30 \times 0.10$
Crystal shape, color	block, black	
Crystal system, Space Group	monoclinic, $P2_1/a$	
$a / \text{\AA}$	12.4530(7)	12.3750(7)
$b / \text{\AA}$	38.7650(16)	38.599(2)
$c / \text{\AA}$	7.7240(5)	15.1200(15)
$\beta / ^\circ$	91.143(3)	90.968(5)
$V / \text{\AA}^3$	3727.9(4)	7221.2(9)
Z	4	8
$D_{\text{calcd.}} / \text{g cm}^{-3}$	1.823	1.882
μ / mm^{-1}	1.610	1.662
Index range	$-16 \leq h \leq 16$	$-11 \leq h \leq 13$
	$0 \leq k \leq 47$	$0 \leq k \leq 51$
	$0 \leq l \leq 10$	$0 \leq h \leq 18$
Reflections / Parameters	8794 / 406	10677 / 371
R, wR	0.0526, 0.0896	0.1114 / 0.2896
GOF	0.968	1.101

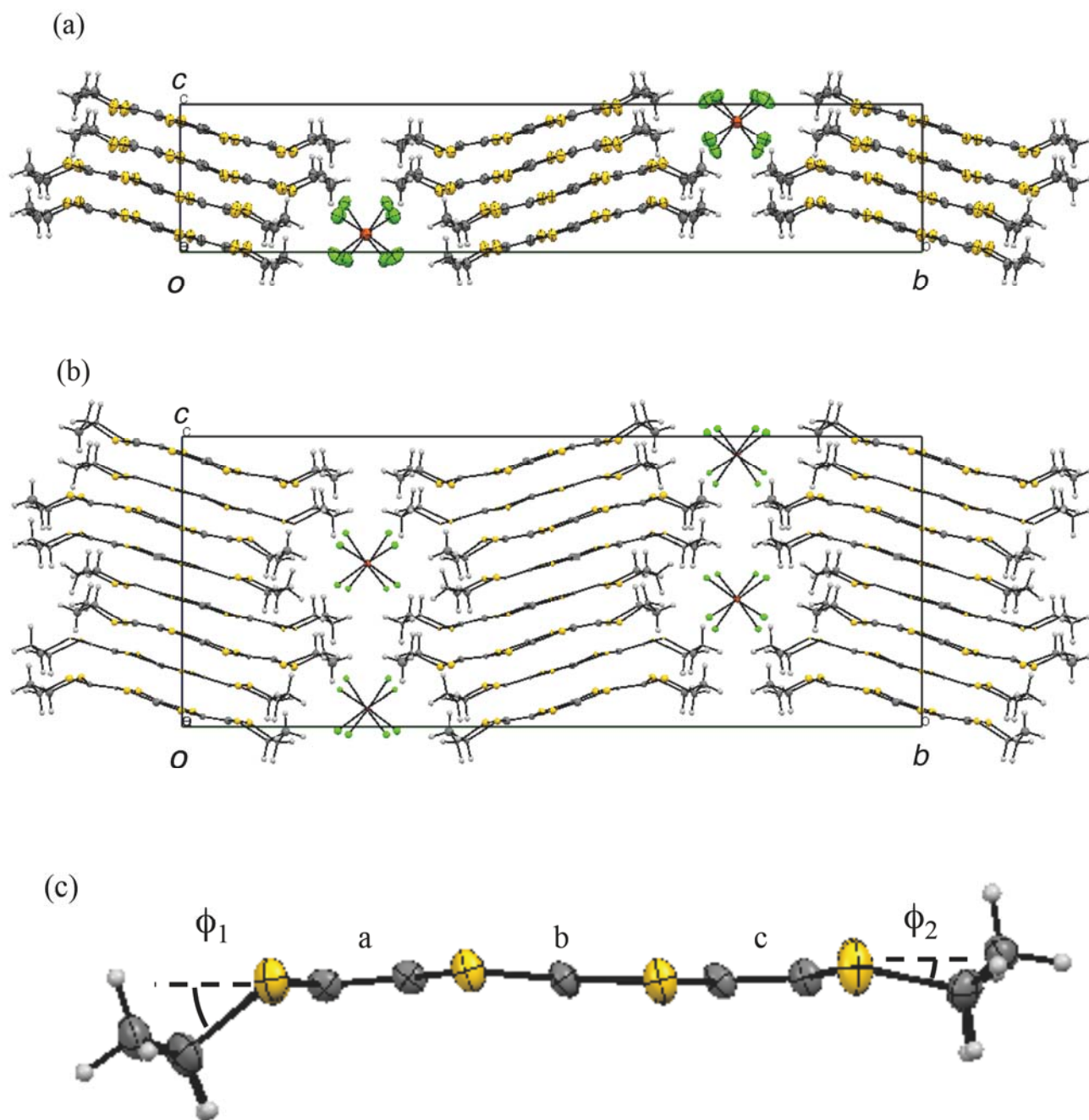


FIGURE 3-3. Crystal structures of β -(BDA-TTP) $_2$ FeCl $_4$ viewed along the a axis at **(a)** 295 (RT) and **(b)** 10 (LT) K, respectively. **(c)** Molecular structure of BDA-TTP in β -(BDA-TTP) $_2$ FeCl $_4$. The lengths of three C=C bonds a , b , and c and the values of the dihedral angles of ϕ_1 and ϕ_2 at RT and LT are summarized in TABLE 3-II and III, respectively.

Charge Separation in LT Structure

In the low-temperature X-ray analysis, the error range of the three C=C bond lengths [a , b , and c in Fig. 3-3(c)] in molecules A, A', B, and B' is larger than that of the corresponding bond lengths in molecules A and B in the RT structure (Table 3-II), so that it is difficult to estimate charges on molecules A, A', B, and B' from the empirical correlation between bond length and charge in BDA-TTP salts [19]. These charges were thus estimated by the folding dihedral angles around the intramolecular sulfur-to-sulfur axes of two outer dithiane rings in BDA-TTP, hereafter defined as ϕ , because, unlike the two outer dithiane rings with an equivalent ϕ (53.6°) in the neutral molecular structure of BDA-TTP [20], one outer dithiane ring of BDA-TTP in the charged state has planarity with a small ϕ in comparison with ϕ in the other outer dithiane ring as seen in molecules A ($\phi_1 = 38.7^\circ$ and $\phi_2 = 13.3^\circ$ in Table 3-III) and B ($\phi_1 = 38.8^\circ$, $\phi_2 = 13.1^\circ$) in the RT structure. In the LT structure, the values of one of two ϕ 's in molecules A ($\phi_2 = 18.6^\circ$) and B ($\phi_2 = 17.8^\circ$) are larger than those in molecules A' ($\phi_2 = 11.1^\circ$) and B' ($\phi_2 = 9.87^\circ$), thereby indicating that the charge separation occurs between a pair of molecules A and B and a pair of molecules A' and B'. However, judging from weak satellite peaks even at LT, the degree of the charge separation seems to be small.

TABLE 3-II. Three C=C bond lengths [a , b , and c in Fig. 3-3(c)] in two independent BDA-TTP molecules (A and B) at 295 (RT) K and in four independent BDA-TTP molecules (A, A', B, and B') at 10 (LT) K.

T / K	295 (RT)	10 (LT)
$a(\text{A}), b(\text{A}), c(\text{A}) / \text{\AA}$	1.351(4), 1.346(4), 1.360(4)	1.42(2), 1.35(3), 1.36(2)
$a(\text{A}'), b(\text{A}'), c(\text{A}') / \text{\AA}$	—	1.32(2), 1.35(2), 1.41(2)
$a(\text{B}), b(\text{B}), c(\text{B}) / \text{\AA}$	1.345(4), 1.338(4), 1.361(4)	1.36(2), 1.27(3), 1.37(2)
$a(\text{B}'), b(\text{B}'), c(\text{B}') / \text{\AA}$	—	1.37(2), 1.40(2), 1.40(2)

TABLE 3-III. Two dihedral angles [ϕ_1 and ϕ_2 in Fig. 3-3(c)] in two independent BDA-TTP molecules (A and B) at 295 (RT) K and in four independent BDA-TTP molecules (A, A', B, and B') at 10 (LT) K.

T / K	295 (RT)	10 (LT)
$\phi_1(\text{A}), \phi_2(\text{A}) / ^\circ$	38.7, 13.3	40.1, 18.6
$\phi_1(\text{A}'), \phi_2(\text{A}') / ^\circ$	—	39.0, 11.1
$\phi_1(\text{B}), \phi_2(\text{B}) / ^\circ$	38.8, 13.1	36.9, 17.8
$\phi_1(\text{B}'), \phi_2(\text{B}') / ^\circ$	—	41.7, 9.87

Checkerboard-type Donor Arrangement in LT Structure

The donor layer of LT structure is shown in Fig. 3-4(a). The charge distribution of four independent BDA-TTP molecules based on the above result leads to a checkerboard-type arrangement consisting of two charge-poor donors (molecule A and B) and two charge-rich ones (molecule A' and B'). Interplanar distances between BDA-TTP molecules are summarized in Table 3-IV. Interestingly, the two charge-poor donors and the two charge-rich ones form distinct dimers: a dimer being 3.47 Å apart (dimer A) and a dimer being 3.44 Å apart (dimer B), which alternate at separations of 3.85 and 3.83 Å. Comparison with the dimerization of two independent BDA-TTP molecules, observed at RT, with an intradimer spacing of 3.56 Å and an interdimer spacing of 3.89 Å (Table 3-IV) suggests strong interactions within both dimers A and B. The overlap integrals between BDA-TTP molecules are summarized in Table 3-V. Actually, compared to the absolute value ($c1 = 15.6 \times 10^{-3}$ in Table 3-V) of the overlap integral within a dimer in the RT structure, the corresponding value ($c1 = 17.7 \times 10^{-3}$ in Table 3-V) within dimer A is larger than that, and the corresponding value ($c1' = 16.0 \times 10^{-3}$) within dimer B is not less than that. The formation of a strong dimer in the donor stacking is expected to lead to a band gap responsible for the insulating state.

TABLE 3-IV. Interplanar distances between BDA-TTP molecules [d_1 , d_2 , d_3 , and d_4 in Fig. 3-4] and the shortest Fe···Fe distance between adjacent FeCl_4^- anions along the a -axis.

T / K	295 (RT)	10 (LT)
$d_1 / \text{Å}$	3.56	3.47
$d_2 / \text{Å}$	3.89	3.85
$d_3 / \text{Å}$	—	3.44
$d_4 / \text{Å}$	—	3.83
Fe···Fe / Å	6.23	6.19

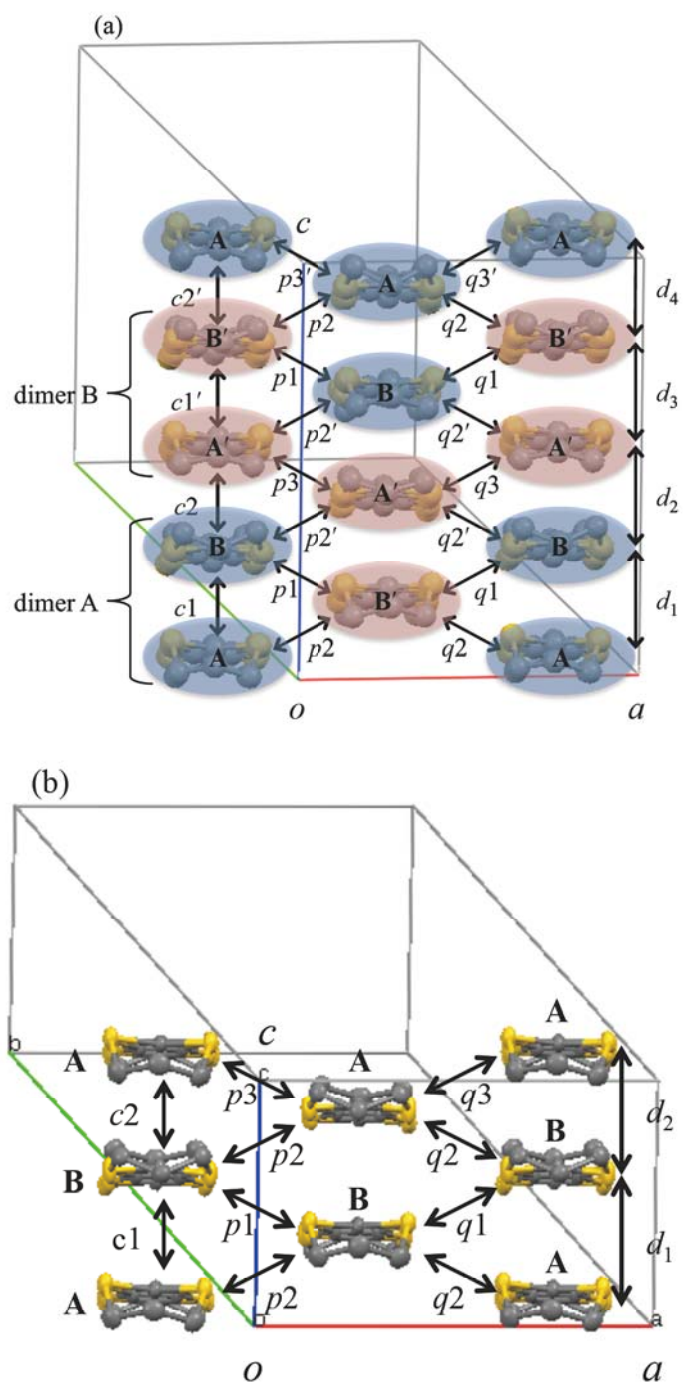


FIGURE 3-4. Donor arrangements of β -(BDA-TTP) $_2$ FeCl $_4$ at **(a)** 10 (LT) and **(b)** 295 (RT) K. Hydrogen atoms are omitted for clarify. In LT, donors marked in light blue and in light red indicate charge-poor and molecules A and B and charge-rich molecules A' and B', respectively.

TABLE 3-V. Intermolecular overlap integrals between BDA-TTP molecules at 295 (RT) and 10 (LT) K [for the notation, see Fig. 3-4].

T / K	295 (RT)	10 (LT)
$c1$	-15.6	-17.7
$c1'$	—	-16.0
$c2$	-13.6	-14.8
$c2'$	—	-13.8
$p1$	2.22	1.19
$p2$	7.33	7.87
$p2'$	—	6.71
$p3$	3.18	4.36
$p3'$	—	1.87
$q1$	7.04	7.42
$q2$	5.63	5.94
$q2'$	—	5.17
$q3$	5.48	5.73
$q3'$	—	5.57

Band Calculations

In order to obtain the band dispersion at LT, the tight-binding band calculation was carried out based on the assumption that all BDA-TTP donor molecules in the LT structure have an equivalent charge. Fig. 3-5(c) shows the band dispersion at LT. There exists a band gap of 5.3 meV in the vicinity of the Fermi level, which is in contrast to the fact that the RT structure has the open and closed Fermi surfaces [11, 21]. While the band gap is not large, the author would be able to find a larger band gap in a band dispersion taking account of accurate charges on the four independent BDA-TTP molecules. It is thus conceivable that the charge separation causes the MI transition observed at 113 K.

π -d Interaction

On the other hand, β -(BDA-TTP)₂FeCl₄ exhibits an AF transition at $T_N = 8.5$ K [12, 13]. Table 3-IV also shows the shortest Fe \cdots Fe distances. Although the shortest Fe \cdots Fe distance (6.19 Å) between adjacent FeCl₄[−] anions along the *a*-axis at LT is shorter than that (6.23 Å) at RT, any short H \cdots Cl contacts were unable to be observed between the BDA-TTP donor molecule and the FeCl₄[−] anion. Therefore, it is likely that there is no π -d interaction capable of inducing an AF d-electron exchange via π -electrons [14] at LT.

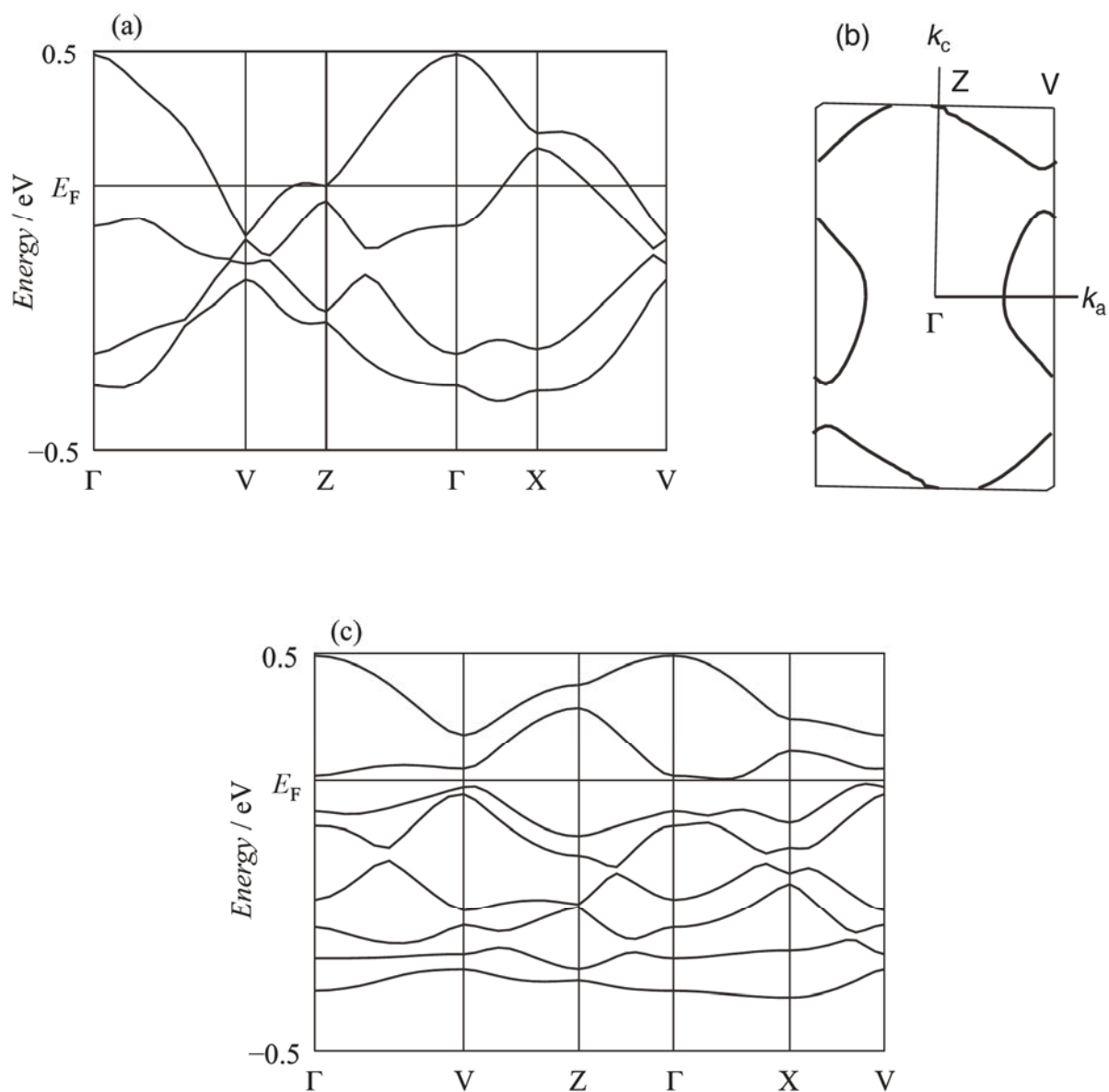


FIGURE 3-5. (a) Band dispersion and (b) Fermi surface at 295 (RT) K, and (c) band dispersion at 10 (LT) K for β -(BDA-TTP) $_2$ FeCl $_4$.

3-3-2. Crystal and Electric Structures under Pressure

Crystal Structures under Pressure

With the application of pressures to β -(BDA-TTP)₂FeCl₄, the suppression of MI transition is followed by the occurrence of superconductivity [12, 13]. In order to probe into the structural origin, room-temperature X-ray studies under pressures were performed up to 21 kbar (Table 3-VI). Figure 3-6 shows the pressure dependence of the unit cell parameters. The change in the *b*-axis, along which the donor and anion layers are alternately arranged, is smallest, whereas that in the *c*-axis, which is the donor stacking direction, is largest. Table 3-VII summarizes the respective two dihedral angles ϕ_1 and ϕ_2 [Fig. 3-3(c)] in two independent BDA-TTP molecules (molecules A and B) and the interplanar distances of intradimer [d_1 in Fig. 3-4(b)] and interdimer (d_2) at each pressure. With increasing pressure, the values of the larger dihedral angles (ϕ_1 's) in molecules A and B tend to gradually increase, meaning a slight increase in steric bulkiness. On the other hand, the variation of the smaller dihedral angles (ϕ_2 's) is less than that of ϕ_1 's; however, a comparison of the values of ϕ_2 's at each pressure with those at RT under ambient pressure indicates only a little increase in planarity. In addition, the BDA-TTP donor molecules mutually shift along the direction of the short molecular axis with slightly increasing the steric bulkiness of one dithiane ring, and the values of d_1 and d_2 decrease as the *c*-axis is shortened.

Table 3-VI. Crystallographic data for β -(BDA-TTP)₂FeCl₄ at different pressures.

Pressure / kbar	1×10^{-3}	3	8
Formula, F_w	C ₂₄ H ₂₄ S ₁₆ FeCl ₄ , 1023.04		
Crystal shape, color, size	block, black, $0.25 \times 0.20 \times 0.10$ mm ³		
Crystal system	monoclinic		
Space Group, Z	$P2_1/a$, $Z = 4$		
$a / \text{\AA}$	12.4530(7)	12.332(6)	12.2050(16)
$b / \text{\AA}$	38.7650(16)	38.62(4)	38.402(19)
$c / \text{\AA}$	7.7240(5)	7.614(4)	7.5050(14)
$\beta / ^\circ$	91.143(3)	91.054(9)	90.981(6)
$V / \text{\AA}^3$	3727.9(4)	3626(5)	3517.1(19)
$D_{\text{calcd.}} / \text{g cm}^{-3}$	1.823	1.874	1.932
μ / mm^{-1}	1.610	1.655	1.707
Index range	$-16 \leq h \leq 16$	$-10 \leq h \leq 9$	$-11 \leq h \leq 10$
	$0 \leq k \leq 47$	$0 \leq k \leq 23$	$0 \leq k \leq 26$
	$0 \leq l \leq 10$	$0 \leq l \leq 7$	$0 \leq l \leq 7$
Reflections / Parameters	8794 / 406	1013 / 286	1319 / 286
GOF	0.968	1.136	1.113
R, wR	0.0526 / 0.0896	0.0542 / 0.1420	0.0501 / 0.1193

Table 3-VI. (*continued*)

Pressure / kbar	11	16	21
Formula, F_w	$C_{24}H_{24}S_{16}FeCl_4$, 1023.04		
Crystal shape, color, size	block, black, $0.25 \times 0.20 \times 0.10$ mm ³		
Crystal system	monoclinic		
Space Group, Z	$P2_1/a$, $Z = 4$		
$a / \text{\AA}$	12.130(2)	12.0580(18)	11.970(3)
$b / \text{\AA}$	38.23(2)	38.10(2)	37.84(3)
$c / \text{\AA}$	7.4380(16)	7.3750(15)	7.291(2)
$\beta / ^\circ$	90.940(8)	90.881(7)	90.777(9)
$V / \text{\AA}^3$	3449(2)	3388(2)	3302(3)
$D_{\text{calcd.}} / \text{g cm}^{-3}$	1.970	2.006	2.058
μ / mm^{-1}	1.740	1.772	1.818
Index range	$-11 \leq h \leq 10$	$-11 \leq h \leq 10$	$-11 \leq h \leq 10$
	$0 \leq k \leq 25$	$0 \leq k \leq 25$	$0 \leq k \leq 24$
	$0 \leq l \leq 7$	$0 \leq l \leq 7$	$0 \leq l \leq 7$
Reflections / Parameters	1246 / 286	1171 / 286	957 / 286
GOF	1.171	1.160	1.091
R, wR	0.0475 / 0.01199	0.0528 / 0.1369	0.0491 / 0.1265

TABLE 3-VII. Two dihedral angles [ϕ_1 and ϕ_2 in Fig. 3-3(c)] in two independent BDA-TTP molecules (A and B) and interplanar distances [d_1 and d_2 in Fig. 3-4(b)] at different pressures.

P / kbar	1×10^{-3}	3	8	11	16	21
$\phi_1(\text{A}) / ^\circ$	38.7	39.2	41.1	41.0	41.5	41.6
$\phi_2(\text{A}) / ^\circ$	13.3	12.4	12.7	12.5	12.2	11.6
$\phi_1(\text{B}) / ^\circ$	38.8	39.0	40.6	41.4	42.6	44.0
$\phi_2(\text{B}) / ^\circ$	13.1	12.4	11.9	12.3	11.7	11.3
$d_1 / \text{\AA}$	3.56	3.51	3.49	3.42	3.39	3.35
$d_2 / \text{\AA}$	3.89	3.82	3.76	3.72	3.68	3.63

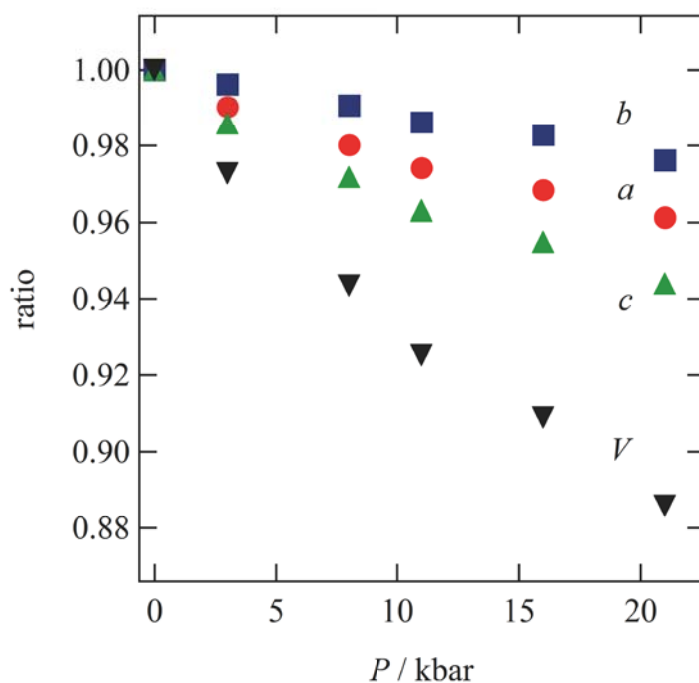


FIGURE 3-6. Pressure dependence of the unit cell parameters for β -(BDA-TTP) $_2$ FeCl $_4$.

Uniform Face-to-Face Interaction

Although the difference between d_1 and d_2 is found at all pressures up to 21 kbar, it should be noted that the ratio of the overlap integral of intradimer ($c1$ in Table 3-VIII) to the overlap integral of interdimer ($c2$) at each pressure is close to 1.0 as shown in Fig. 3-7. The result indicates an almost uniform face-to-face interaction in the donor stacking. On the other hand, probably due to the shift of donor molecules, one overlap integral ($p1$) between donor stacks decreases with increasing pressure, so that it is not necessarily the case that the side-by-side interaction is uniformly enhanced by pressure. Consequently, the suppression of MI transition should be attributed mainly to the almost uniform face-to-face interaction.

Increase of Bandwidth W

The value of bandwidth W in the energy dispersion at each pressure below 21 kbar were then calculated [Fig. 3-8], because the W value is a key parameter to control the effective electron correlation given by U/W and V/W , where U and V are the on-site and intersite Coulomb repulsions, respectively, in molecular conductors [22]. As shown in Fig. 3-9, the W value rises to 0.90 eV at 3 kbar and remains almost constant above 8 kbar, at which pressure β -(BDA-TTP)₂FeCl₄ is in the superconducting state [11]. Therefore, the almost uniform face-to-face interaction appears to play an important role in the increase of W required for achieving superconductivity as well as the suppression of MI transition.

Table 3-VIII. Intermolecular overlap integrals ($\times 10^{-3}$) at different pressures [for the notation, see Fig. 3-4(b)].

P / kbar	0.001	3	8	11	16	21
$c1$	-15.6	-15.7	-17.7	-18.6	-19.0	-21.3
$c2$	-13.6	-16.4	-17.7	-18.7	-20.1	-21.4
$p1$	2.22	2.04	1.06	1.27	0.811	0.451
$p2$	7.33	7.72	9.33	9.51	10.4	11.5
$p3$	3.18	2.75	3.66	3.70	4.24	4.14
$q1$	7.04	7.75	8.43	9.19	9.32	10.1
$q2$	5.63	5.88	5.98	6.54	6.57	6.10
$q3$	5.48	6.39	7.27	7.30	7.46	8.82

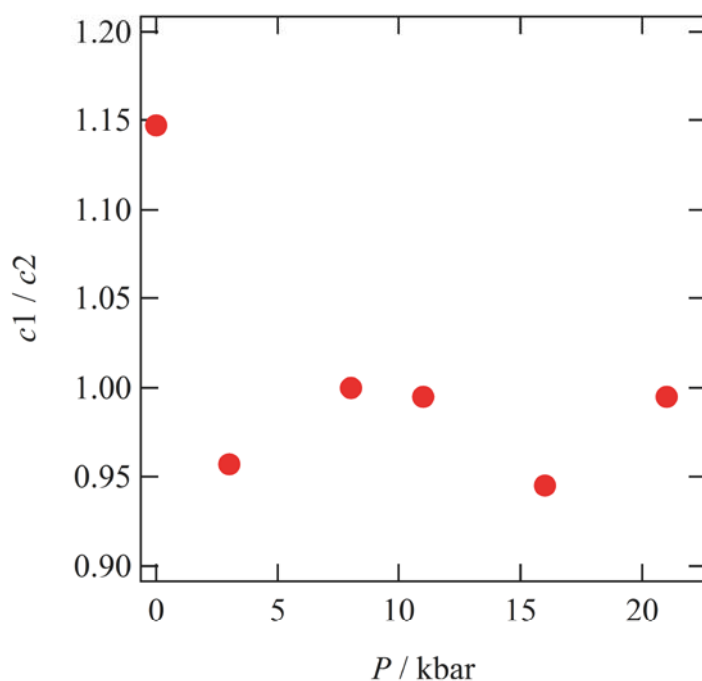


FIGURE 3-7. Pressure dependence of the ratio of overlap integral $c1/c2$ for β -(BDA-TTP) $_2$ FeCl $_4$ [for the notation, see Fig. 3-4(b)].

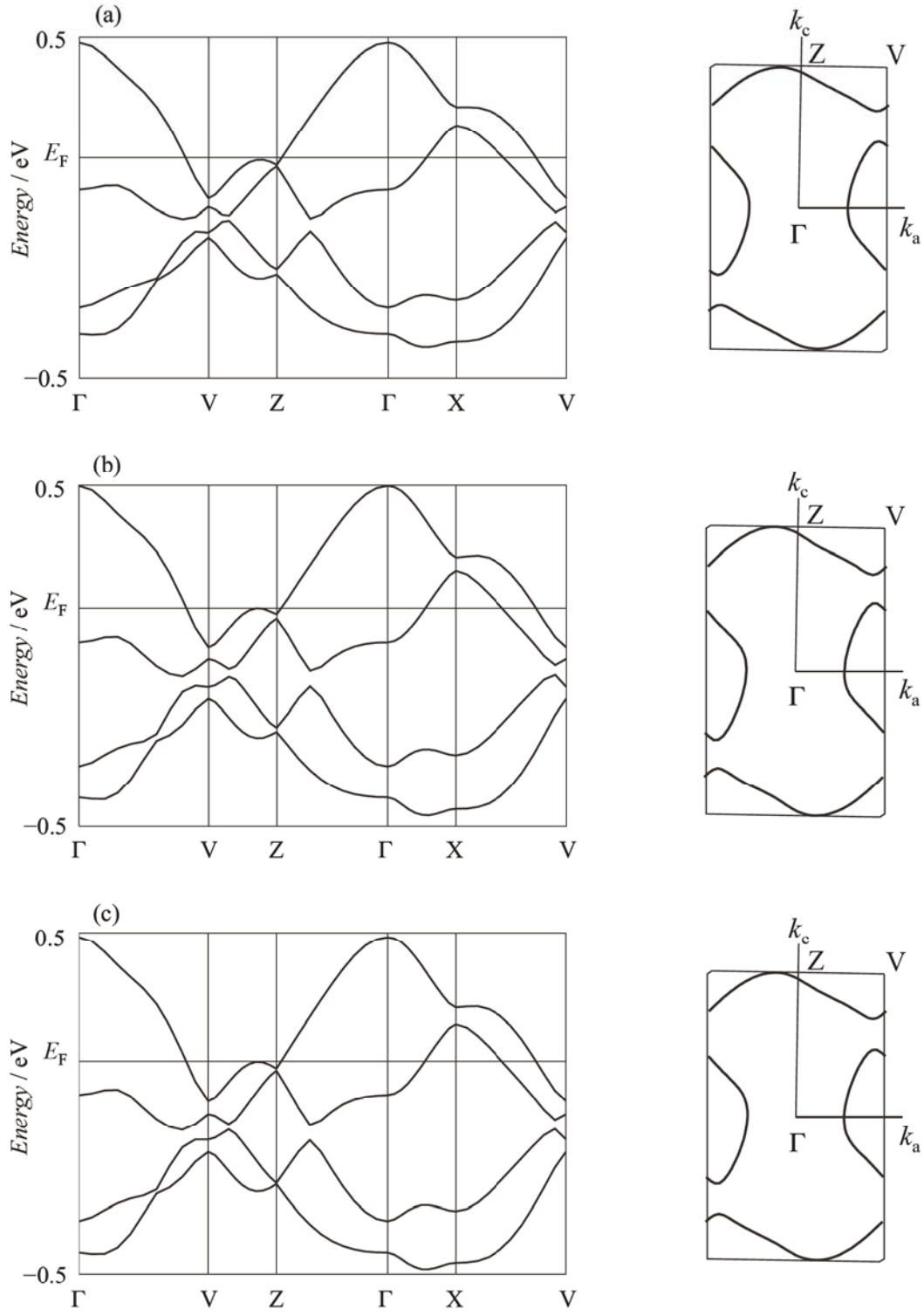


FIGURE 3-8. Band dispersions and Fermi surfaces for β -(BDA-TTP)₂FeCl₄ at (a) 3, (b) 8, (c) 11 kbar.

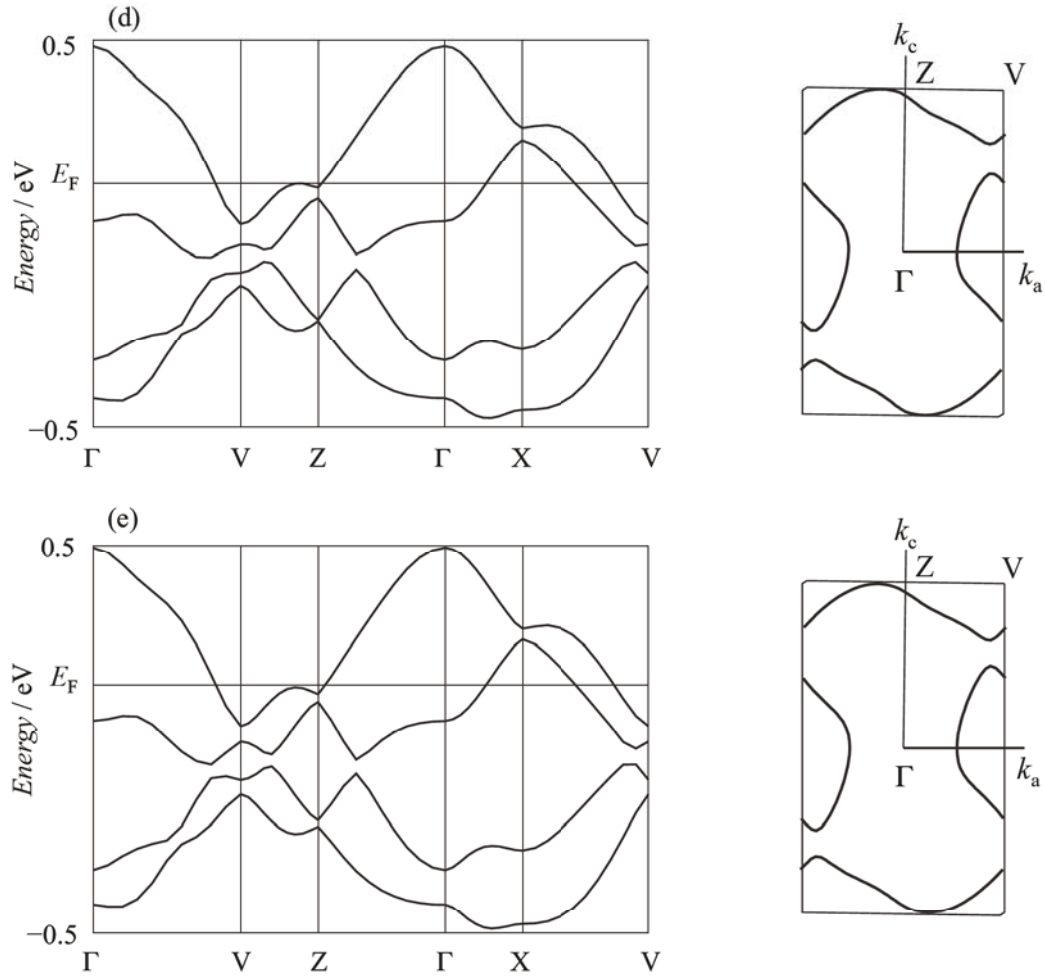


FIGURE 3-8 (*continued*). Band dispersions and Fermi surfaces for β -(BDA-TTP) $_2$ FeCl $_4$ at (d) 16, (e) 21 kbar.

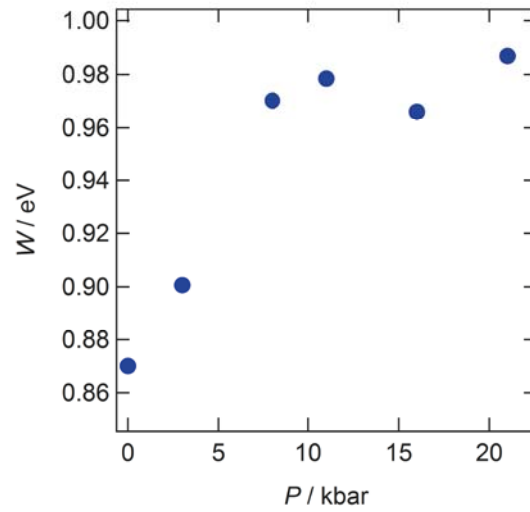


FIGURE 3-9. Pressure dependence of the bandwidth (W) for β -(BDA-TTP) $_2$ FeCl $_4$.

3-4. CONCLUSION

The author succeeded in providing structural evidence for the charge separation causing the MI transition in β -(BDA-TTP)₂FeCl₄ by X-ray studies below $T_{\text{MI}} = 113$ K, and in disclosing the structural origin of both the suppression of MI transition and the occurrence of superconductivity by X-ray studies under pressures up to 21 kbar. The changes in the crystal structure, described here, arise from the structural flexibility of two outer six-membered heterocycles (two dithiane rings) of BDA-TTP; that is, these heterocycles can adopt a variety of chair conformations [9]. In this study, the structural flexibility of chair conformation appears as variations of ϕ_1 and ϕ_2 induced by decrease in temperature and by increase in pressure. It is therefore demonstrated by this study that although the variations in one BDA-TTP molecule are subtle, such subtle variations affect the collective electronic structure of β -(BDA-TTP)₂FeCl₄ and enable the charge-ordered insulating state to transform into the superconducting state. Further structural study is to reveal what conformational variation takes place in the BDA-TTP donor molecule of β -(BDA-TTP)₂FeCl₄ by applying uniaxial strain, and the author hope that the resulting change in its electronic structure leads to a new physical phenomenon.

3-5. REFERENCES

- [1] H. Kobayashi, R. Kato, A. Kobayashi, Y. Nishio, K. Kajita, and W. Sasaki, *Chem. Lett.* 15 (1986) 789.
- [2] N. Tajima, A. Ebina-Tajima, M. Tamura, Y. Nishio, and K. Kajita, *J. Phys. Soc. Jpn.* 71 (2002) 1832.
- [3] H. Nishikawa, T. Morimoto, T. Kodama, I. Ikemoto, K. Kikuchi, J. Yamada, H. Yoshino, and K. Murata, *J. Am. Chem. Soc.* 124 (2002) 730.
- [4] T. Shikama, T. Shimokawa, S. Lee, T. Isono, A. Ueda, K. Takahashi, A. Nakao, R. Kumai, H. Nakao, K. Kobayashi, Y. Murakami, M. Kimata, H. Tajima, K. Matsubayashi, Y. Uwatoko, Y. Nishio, K. Kajita and H. Mori, *Crystals* 2 (2012) 1502.
- [5] A. Ardavan, S. Brown, S. Kagoshima, K. Kanoda, K. Kuroki, H. Mori, M. Ogata, S. Uji and J. Wosnitza, *J. Phys. Soc. Jpn.* 81 (2012) 011004.
- [6] J. Yamada, H. Akutsu, H. Nishikawa, and K. Kikuchi, *Chem. Rev.* 104 (2004) 5057.
- [7] J. Yamada, K. Fujimoto, H. Akutsu, S. Nakatsuji, A. Miyazaki, M. Aima, S. Kudo, T. Enoki, and K. Kikuchi, *Chem. Commun.* (2006) 1331.
- [8] K. Kikuchi, T. Isono, M. Kojima, H. Yoshimoto, T. Kodama, W. Fujita, K. Yokogawa, H. Yoshino, K. Murata, T. Kaihatsu, H. Akutsu, and J. Yamada, *J. Am. Chem. Soc.* 133 (2011) 19590.
- [9] J. Yamada and H. Akutsu, *Crystals* 2 (2012) 812.
- [10] Y. Nonoyama, Y. Maekawa, A. Kobayashi, Y. Suzumura, and J. Yamada, *J. Phys. Conference Series* 132 (2008) 012013.
- [11] E. S. Choi, D. Graf, J. S. Brooks, J. Yamada, H. Akutsu, K. Kikuchi, and M. Tokumoto, *Phys. Rev. B* 70 (2004) 024517.
- [12] J. Yamada, T. Toita, H. Akutsu, S. Nakatsuji, H. Nishikawa, I. Ikemoto, and K. Kikuchi, *Chem. Commun.* (2001) 2538.

- [13] K. Kikuchi, H. Nishikawa, I. Ikemoto, T. Toita, H. Akutsu, S. Nakatsuji, and J. Yamada, *J. Solid State Chem.* 168 (2002) 503.
- [14] T. Tokumoto, J. S. Brooks, Y. Oshima, E. S. Choi, L. C. Brunel, H. Akutsu, T. Kaihatsu, J. Yamada, and J. von Tol, *Phys. Rev. Lett.* 100 (2008) 147602.
- [15] Z. Otwinowski and W. Minor, *Methods Enzymology, Macromolecular Crystallography, part A* (Eds.: C. W. Carter Jr. and R. M. Sweet) Academic Press, New York 276 (1997) 307.
- [16] G. J. Piermarini, S. Block, J. D. Barnett, and R. A. Forman, *J. Appl. Phys.* 46 (1975) 2774.
- [17] G. M. Sheldrick, SHELX-97, University of Göttingen, Germany (1997).
- [18] T. Mori, A. Kobayashi, Y. Sasaki, H. Kobayashi, G. Saito, and H. Inokuchi, *Bull. Chem. Soc. Jpn.* 57 (1984) 627.
- [19] M. Uruichi, C. Nakano, M. Tanaka, K. Yakushi, T. Kaihatsu and J. Yamada, *Solid State Commun.* 147 (2008) 484.
- [20] J. Yamada, M. Watanabe, H. Akutsu, S. Nakatsuji, H. Nishikawa, I. Ikemoto, and K. Kikuchi, *J. Am. Chem. Soc.* 123 (2001) 4174.
- [21] J. Yamada, *J. Phys. IV France* 114 (2004) 439.
- [22] H. Seo, C. Hotta, and H. Fukuyama, *Chem. Rev.* 104 (2004) 5005.

3-6. APPENDIX

TABLE S3-I. Atomic coordinates in β -(BDA-TTP)₂FeCl₄ at 10 K (LT).

atom	<i>x</i>	<i>y</i>	<i>z</i>	$U_{\text{eq}} / \text{\AA}^2$
C1	0.1669(16)	-0.1396(5)	1.0175(15)	0.024(4)
H1A	0.1519	-0.1633	1.0348	0.029
H1B	0.1692	-0.1389	0.9534	0.029
C2	0.0739(14)	-0.1157(3)	1.0496(12)	0.009(3)
H2A	0.0845	-0.1102	1.1118	0.011
H2B	0.0049	-0.1274	1.0424	0.011
C3	0.2761(13)	-0.1290(3)	1.0553(11)	0.006(3)
H3A	0.3273	-0.1479	1.051	0.007
H3B	0.27	-0.1225	1.117	0.007
C4	0.2148(16)	-0.0621(4)	0.9797(14)	0.021(4)
C5	0.2327(15)	-0.0277(4)	0.9651(13)	0.012(3)
C6	0.2202(17)	0.0350(4)	0.9155(15)	0.021(4)
C7	0.3275(14)	0.0282(4)	0.9149(12)	0.008(3)
C8	0.3102(13)	0.0893(3)	0.8690(11)	0.006(3)
C9	0.3317(14)	0.1252(4)	0.8566(12)	0.011(3)
C10	0.2713(14)	0.1928(4)	0.8884(13)	0.013(3)
H10A	0.2196	0.2112	0.8772	0.016
H10B	0.2756	0.1893	0.9519	0.016
C11	0.4740(16)	0.1796(4)	0.8837(15)	0.020(4)
H11A	0.4733	0.1769	0.9474	0.024

H11B	0.5432	0.1896	0.8684	0.024
C12	0.3842(15)	0.2050(4)	0.8562(14)	0.018(4)
H12A	0.3823	0.2071	0.7923	0.021
H12B	0.4002	0.2276	0.8809	0.021
C13	0.1589(12)	-0.1411(3)	0.5227(11)	0.004(3)
H13	0.1521	-0.1492	0.4621	0.005
H14	0.1464	-0.1609	0.5609	0.005
C14	0.2765(15)	-0.1289(4)	0.5383(14)	0.017(4)
H15	0.3236	-0.1474	0.5189	0.02
H16	0.2876	-0.1266	0.6017	0.02
C15	0.0719(16)	-0.1154(4)	0.5378(14)	0.018(4)
H17	0.0694	-0.1113	0.6011	0.022
H18	0.004	-0.1263	0.5209	0.022
C16	0.2086(13)	-0.0635(3)	0.4885(11)	0.004(3)
C17	0.2327(13)	-0.0298(3)	0.4595(11)	0.006(3)
C18	0.3214(16)	0.0268(4)	0.4166(13)	0.016(4)
C19	0.2147(12)	0.0337(3)	0.4154(10)	0.000(3)
C20	0.3080(15)	0.0915(4)	0.3719(13)	0.014(4)
C21	0.3279(14)	0.1241(4)	0.3514(12)	0.010(3)
C22	0.4718(14)	0.1789(3)	0.3830(12)	0.007(3)
H19	0.4707	0.1765	0.4469	0.008
H20	0.5399	0.1895	0.3677	0.008
C23	0.2712(14)	0.1930(4)	0.3824(13)	0.013(4)
H21	0.2217	0.2115	0.3665	0.016
H22	0.2718	0.1909	0.4463	0.016

C24	0.3803(13)	0.2026(3)	0.3541(11)	0.006(3)
H23	0.396	0.2257	0.3761	0.007
H24	0.3796	0.2038	0.29	0.007
C25	0.3284(16)	0.1416(5)	0.6060(15)	0.023(4)
H25	0.3275	0.1438	0.6699	0.027
H26	0.3418	0.1644	0.5819	0.027
C26	0.2166(14)	0.1299(4)	0.5746(13)	0.012(3)
H27	0.2184	0.1234	0.5127	0.015
H28	0.1652	0.1487	0.5809	0.015
C27	0.4232(15)	0.1182(4)	0.5820(14)	0.016(4)
H29	0.4904	0.1303	0.5945	0.019
H30	0.4198	0.1133	0.5191	0.019
C28	0.2859(15)	0.0638(4)	0.6446(13)	0.016(4)
C29	0.2688(16)	0.0293(4)	0.6619(14)	0.018(4)
C30	0.1795(14)	-0.0268(4)	0.7123(13)	0.011(3)
C31	0.2801(15)	-0.0334(4)	0.7103(13)	0.013(3)
C32	0.1983(14)	-0.0895(3)	0.7602(12)	0.008(3)
C33	0.1775(15)	-0.1238(4)	0.7701(13)	0.014(3)
C34	0.0430(15)	-0.1807(4)	0.7492(14)	0.016(4)
H31	-0.0248	-0.1914	0.7654	0.019
H32	0.0448	-0.1801	0.6851	0.019
C35	0.2430(13)	-0.1910(3)	0.7473(12)	0.007(3)
H33	0.2395	-0.1883	0.6836	0.009
H34	0.2954	-0.209	0.7609	0.009
C36	0.1300(18)	-0.2026(5)	0.7805(17)	0.029(5)

H35	0.1164	-0.2262	0.7609	0.034
H36	0.131	-0.2026	0.8447	0.034
C37	0.1345(12)	-0.2036(3)	0.2781(11)	0.002(3)
H37	0.134	-0.2044	0.3422	0.003
H38	0.1229	-0.227	0.2566	0.003
C38	0.2419(15)	-0.1915(4)	0.2493(14)	0.017(4)
H39	0.2392	-0.1878	0.1859	0.02
H40	0.2945	-0.2097	0.2613	0.02
C39	0.0386(14)	-0.1800(4)	0.2444(12)	0.011(3)
H41	-0.0295	-0.1911	0.2576	0.013
H42	0.0425	-0.1774	0.1807	0.013
C40	0.1771(13)	-0.1244(3)	0.2827(11)	0.004(3)
C41	0.1952(15)	-0.0909(4)	0.2577(13)	0.014(4)
C42	0.2913(13)	-0.0330(3)	0.2130(11)	0.005(3)
C43	0.1792(14)	-0.0277(4)	0.2084(12)	0.011(3)
C44	0.2667(13)	0.0298(3)	0.1674(11)	0.005(3)
C45	0.2894(14)	0.0638(3)	0.1405(12)	0.007(3)
C46	0.4218(13)	0.1178(3)	0.0914(12)	0.008(3)
H43	0.4894	0.1289	0.1084	0.009
H44	0.4224	0.115	0.0277	0.009
C47	0.2221(12)	0.1287(3)	0.0878(11)	0.003(3)
H45	0.2205	0.1247	0.0245	0.004
H46	0.1699	0.1468	0.0996	0.004
C48	0.3325(12)	0.1425(3)	0.1124(11)	0.002(3)
H47	0.3442	0.1641	0.081	0.003

H48	0.3349	0.1476	0.1753	0.003
S1	0.0748(4)	-0.07442(9)	0.9813(3)	0.0126(9)
S2	0.3222(4)	-0.09019(10)	0.9864(3)	0.0160(9)
S3	0.1285(4)	0.00146(10)	0.9451(4)	0.0167(9)
S4	0.3653(4)	-0.01398(11)	0.9494(4)	0.0185(10)
S5	0.1747(4)	0.07475(10)	0.8778(3)	0.0164(9)
S6	0.4124(4)	0.05958(11)	0.8811(4)	0.0177(10)
S7	0.2192(4)	0.15257(11)	0.8363(4)	0.0185(10)
S8	0.4631(4)	0.13633(10)	0.8322(3)	0.0150(9)
S9	0.3216(4)	-0.09117(9)	0.4908(3)	0.0125(9)
S10	0.0752(4)	-0.07541(10)	0.4867(3)	0.0145(9)
S11	0.3659(3)	-0.01445(8)	0.4423(3)	0.0034(7)
S12	0.1289(3)	0.00118(8)	0.4402(3)	0.0062(7)
S13	0.4131(3)	0.05955(8)	0.3840(3)	0.0055(7)
S14	0.1748(3)	0.07467(8)	0.3777(3)	0.0062(8)
S15	0.4643(3)	0.13629(8)	0.3334(3)	0.0056(7)
S16	0.2209(3)	0.15306(8)	0.3352(3)	0.0041(7)
S17	0.1742(4)	0.09171(9)	0.6438(3)	0.0126(9)
S18	0.4224(4)	0.07700(9)	0.6440(3)	0.0123(8)
S19	0.1362(4)	0.01421(10)	0.6739(3)	0.0160(9)
S20	0.3735(4)	0.00027(9)	0.6799(3)	0.0112(8)
S21	0.0937(4)	-0.05897(10)	0.7454(3)	0.0166(9)
S22	0.3312(4)	-0.07316(10)	0.7469(3)	0.0162(9)
S23	0.0434(4)	-0.13667(10)	0.7897(3)	0.0163(9)
S24	0.2888(4)	-0.15099(11)	0.7958(4)	0.0182(10)

S25	0.2880(3)	-0.15149(8)	0.3034(3)	0.0024(7)
S26	0.0433(3)	-0.13704(8)	0.2963(3)	0.0051(7)
S27	0.3296(3)	-0.07460(8)	0.2512(3)	0.0060(7)
S28	0.0910(4)	-0.05995(9)	0.2466(3)	0.0091(8)
S29	0.3732(4)	-0.00060(9)	0.1888(3)	0.0081(8)
S30	0.1351(3)	0.01349(9)	0.1834(3)	0.0070(8)
S31	0.4226(4)	0.07558(10)	0.1388(3)	0.0141(9)
S32	0.1766(4)	0.09050(10)	0.1394(3)	0.0141(9)
Fe1	0.1123(2)	0.24858(5)	0.56202(18)	0.0104(6)
Fe2	0.1116(2)	0.24862(5)	1.06167(18)	0.0089(6)
Cl1	0.0183(4)	0.20979(9)	0.4878(3)	0.0133(8)
Cl2	0.2050(4)	0.22095(9)	0.6654(3)	0.0135(8)
Cl3	0.2221(3)	0.27584(9)	0.4746(3)	0.0101(8)
Cl4	0.0064(4)	0.28687(10)	0.6244(3)	0.0166(9)
Cl5	0.2229(4)	0.27562(10)	0.9726(3)	0.0160(9)
Cl6	0.0183(4)	0.21006(10)	0.9863(4)	0.0194(9)
Cl7	0.2068(4)	0.22134(9)	1.1638(3)	0.0118(8)
Cl8	0.0072(3)	0.28711(9)	1.1252(3)	0.0105(8)

TABLE S3-II. Atomic coordinates in β -(BDA-TTP)₂FeCl₄ under 3 kbar.

	x	y	z	$U_{\text{eq}} / \text{\AA}^2$
C1	0.1626(12)	-0.1392(8)	1.036(2)	0.033(5)
H1A	0.161	-0.141	0.9086	0.04
H1B	0.1486	-0.1622	1.0818	0.04
C2	0.2759(13)	-0.1289(9)	1.092(2)	0.031(5)
H2A	0.3253	-0.1477	1.0662	0.037
H2B	0.2778	-0.1254	1.2185	0.037
C3	0.0717(12)	-0.1163(9)	1.0878(19)	0.024(5)
H3A	0.0758	-0.1125	1.2137	0.029
H3B	0.0034	-0.1278	1.061	0.029
C4	0.2116(13)	-0.0622(8)	0.969(2)	0.027(5)
C5	0.2333(13)	-0.0299(9)	0.9259(19)	0.028(5)
C6	0.3259(13)	0.0276(8)	0.836(2)	0.028(5)
C7	0.2153(14)	0.0330(9)	0.8326(19)	0.031(5)
C8	0.3106(12)	0.0905(8)	0.7357(18)	0.020(5)
C9	0.3297(13)	0.1243(8)	0.7064(19)	0.021(5)
C10	0.4720(13)	0.1799(8)	0.762(2)	0.028(5)
H10A	0.4691	0.1779	0.889	0.033
H10B	0.5412	0.1903	0.7338	0.033
C11	0.2710(14)	0.1928(8)	0.764(2)	0.037(5)
H11A	0.2206	0.2113	0.7345	0.045
H11B	0.2733	0.1906	0.8909	0.045
C12	0.3846(15)	0.2030(10)	0.701(2)	0.052(6)
H12A	0.3836	0.2034	0.5739	0.063
H12B	0.4006	0.2263	0.7416	0.063
C13	0.1336(15)	-0.2026(10)	1.556(2)	0.054(6)
H13A	0.1207	-0.2261	1.516	0.065

H13B	0.1332	-0.203	1.6836	0.065
C14	0.2456(14)	-0.1919(8)	1.500(2)	0.036(5)
H14A	0.2458	-0.1895	1.3728	0.043
H14B	0.297	-0.2099	1.5318	0.043
C15	0.0412(14)	-0.1806(9)	1.493(2)	0.039(5)
H15A	-0.0263	-0.1917	1.5246	0.047
H15B	0.0429	-0.1792	1.3662	0.047
C16	0.1783(13)	-0.1242(8)	1.5518(19)	0.026(5)
C17	0.1976(12)	-0.0903(8)	1.5170(18)	0.019(5)
C18	0.2869(13)	-0.0324(8)	1.4242(19)	0.030(5)
C19	0.1792(13)	-0.0257(7)	1.4184(19)	0.022(5)
C20	0.2705(13)	0.0308(9)	1.326(2)	0.031(6)
C21	0.2876(14)	0.0632(9)	1.282(2)	0.030(6)
C22	0.4231(13)	0.1187(9)	1.170(2)	0.037(6)
H22A	0.4915	0.1299	1.1993	0.045
H22B	0.421	0.1152	1.0438	0.045
C23	0.2199(12)	0.1288(8)	1.1628(19)	0.027(5)
H23A	0.22	0.1238	1.038	0.032
H23B	0.1668	0.147	1.1809	0.032
C24	0.3326(13)	0.1430(8)	1.216(2)	0.042(5)
H24A	0.3438	0.165	1.1582	0.05
H24B	0.3346	0.1471	1.3421	0.05
S1	0.3217(4)	-0.0897(3)	0.9841(7)	0.044(4)
S2	0.0740(4)	-0.0739(2)	0.9743(6)	0.039(4)
S3	0.3657(3)	-0.0135(2)	0.8917(5)	0.030(3)
S4	0.1293(4)	0.0020(2)	0.8855(5)	0.030(3)
S5	0.4135(4)	0.0596(2)	0.7623(5)	0.031(3)
S6	0.1759(4)	0.0744(2)	0.7527(5)	0.031(3)

S7	0.4650(3)	0.1357(2)	0.6639(5)	0.032(3)
S8	0.2211(3)	0.1531(2)	0.6699(6)	0.038(3)
S9	0.2890(3)	-0.1513(2)	1.5994(6)	0.030(3)
S10	0.0425(3)	-0.1368(2)	1.5828(6)	0.030(3)
S11	0.3303(4)	-0.0737(2)	1.4983(6)	0.039(3)
S12	0.0920(4)	-0.0595(2)	1.4915(5)	0.031(3)
S13	0.3735(4)	-0.0004(2)	1.3672(6)	0.033(3)
S14	0.1357(4)	0.0134(2)	1.3556(5)	0.033(3)
S15	0.4224(4)	0.0758(2)	1.2768(6)	0.038(3)
S16	0.1759(4)	0.0907(2)	1.2765(6)	0.036(3)
Fe1	0.11084(18)	0.24899(12)	0.1185(3)	0.0307(17)
Cl1	0.2027(4)	0.2211(2)	0.3232(6)	0.049(3)
Cl2	0.0191(4)	0.2102(3)	-0.0325(7)	0.073(4)
Cl3	0.0050(4)	0.2869(2)	0.2414(6)	0.055(4)
Cl4	0.2224(4)	0.2755(3)	-0.0522(6)	0.058(4)

TABLE S3-III. Atomic coordinates in β -(BDA-TTP)₂FeCl₄ under 8 kbar.

	x	y	z	$U_{\text{eq}} / \text{\AA}^2$
C1	0.1609(10)	-0.1399(5)	1.0434(14)	0.024(3)
H1A	0.1594	-0.1429	0.9151	0.029
H1B	0.1459	-0.1624	1.0964	0.029
C2	0.2749(10)	-0.1286(5)	1.1007(14)	0.021(3)
H2A	0.3255	-0.1476	1.0782	0.025
H2B	0.2756	-0.1244	1.2281	0.025
C3	0.0713(10)	-0.1153(5)	1.0927(14)	0.022(3)
H3A	0.0763	-0.111	1.2199	0.026
H3B	0.0014	-0.1265	1.0685	0.026
C4	0.2149(10)	-0.0618(5)	0.9746(14)	0.019(3)
C5	0.2311(10)	-0.0285(5)	0.9285(14)	0.019(3)
C6	0.3249(10)	0.0274(5)	0.8323(13)	0.016(3)
C7	0.2184(10)	0.0339(5)	0.8263(14)	0.020(3)
C8	0.3105(10)	0.0918(5)	0.7339(14)	0.019(3)
C9	0.3322(10)	0.1246(5)	0.6997(14)	0.019(3)
C10	0.4754(11)	0.1792(5)	0.7594(14)	0.023(3)
H10A	0.4719	0.1764	0.8876	0.027
H10B	0.546	0.1893	0.7326	0.027
C11	0.2717(11)	0.1922(5)	0.7646(16)	0.035(4)
H11A	0.2192	0.2107	0.7424	0.042
H11B	0.2766	0.1887	0.8925	0.042
C12	0.3854(11)	0.2045(5)	0.6990(15)	0.029(4)
H12A	0.384	0.2059	0.5699	0.035
H12B	0.4012	0.2275	0.746	0.035
C13	0.1323(11)	-0.2049(6)	1.5611(16)	0.034(4)
H13A	0.1312	-0.2069	1.6899	0.041

H13B	0.1188	-0.2279	1.5112	0.041
C14	0.2446(11)	-0.1920(5)	1.5036(15)	0.029(4)
H14A	0.2429	-0.1888	1.3754	0.035
H14B	0.2984	-0.2099	1.5307	0.035
C15	0.0422(12)	-0.1798(6)	1.4975(17)	0.038(4)
H15A	-0.0281	-0.1905	1.5207	0.046
H15B	0.0477	-0.1773	1.3693	0.046
C16	0.1787(11)	-0.1240(6)	1.5603(15)	0.026(4)
C17	0.1969(10)	-0.0916(5)	1.5211(14)	0.018(3)
C18	0.2877(10)	-0.0332(5)	1.4241(14)	0.019(3)
C19	0.1796(10)	-0.0273(5)	1.4224(14)	0.016(3)
C20	0.2687(11)	0.0292(6)	1.3231(15)	0.026(4)
C21	0.2859(11)	0.0628(5)	1.2766(14)	0.023(3)
C22	0.4251(11)	0.1186(5)	1.1656(15)	0.027(4)
H22A	0.4935	0.1301	1.1975	0.032
H22B	0.424	0.1154	1.0374	0.032
C23	0.2178(10)	0.1286(5)	1.1581(14)	0.019(3)
H23A	0.2177	0.1234	1.0316	0.023
H23B	0.165	0.1471	1.1765	0.023
C24	0.3328(11)	0.1422(5)	1.2129(16)	0.031(4)
H24A	0.3442	0.1646	1.1563	0.037
H24B	0.3347	0.146	1.3408	0.037
S1	0.3229(3)	-0.09018(15)	0.9898(4)	0.0326(16)
S2	0.0724(3)	-0.07421(15)	0.9793(4)	0.0321(16)
S3	0.3675(3)	-0.01381(14)	0.8917(4)	0.0281(15)
S4	0.1281(3)	0.00172(14)	0.8857(4)	0.0242(15)
S5	0.4145(3)	0.05961(13)	0.7580(4)	0.0224(15)
S6	0.1744(3)	0.07478(14)	0.7484(4)	0.0275(14)

S7	0.4662(3)	0.13684(13)	0.6567(4)	0.0246(14)
S8	0.2205(3)	0.15357(14)	0.6654(4)	0.0275(16)
S9	0.2892(3)	-0.15174(14)	1.6071(4)	0.0255(16)
S10	0.0416(3)	-0.13743(13)	1.5922(4)	0.0275(14)
S11	0.3322(3)	-0.07387(13)	1.5036(4)	0.0257(14)
S12	0.0910(3)	-0.05954(14)	1.4969(4)	0.0254(15)
S13	0.3750(3)	-0.00015(14)	1.3661(4)	0.0246(14)
S14	0.1344(3)	0.01360(13)	1.3563(4)	0.0261(15)
S15	0.4239(3)	0.07613(14)	1.2699(4)	0.0310(16)
S16	0.1736(3)	0.09114(15)	1.2731(4)	0.0335(17)
Fe1	0.11104(15)	0.24854(7)	0.1155(2)	0.0255(9)
Cl1	0.2045(3)	0.22127(15)	0.3225(4)	0.0439(16)
Cl2	0.0192(3)	0.20982(16)	-0.0376(5)	0.058(2)
Cl3	0.0038(3)	0.28669(15)	0.2400(5)	0.0478(18)
Cl4	0.2247(3)	0.27596(14)	-0.0569(4)	0.0447(17)

TABLE S3-IV. Atomic coordinates in β -(BDA-TTP)₂FeCl₄ under 11 kbar.

	x	y	z	$U_{\text{eq}} / \text{\AA}^2$
C1	0.1604(11)	-0.1406(5)	1.0486(16)	0.025(4)
H1A	0.1578	-0.1442	0.9195	0.03
H1B	0.1454	-0.1629	1.1055	0.03
C2	0.2761(11)	-0.1289(6)	1.1032(15)	0.024(4)
H2A	0.3269	-0.1478	1.0791	0.029
H2B	0.2779	-0.1247	1.2319	0.029
C3	0.0714(10)	-0.1153(5)	1.0975(15)	0.017(3)
H3A	0.0771	-0.1107	1.2256	0.02
H3B	0.0006	-0.1264	1.0747	0.02
C4	0.2119(11)	-0.0622(6)	0.9758(15)	0.020(4)
C5	0.2314(10)	-0.0299(6)	0.9294(15)	0.019(4)
C6	0.3256(10)	0.0271(5)	0.8321(14)	0.015(3)
C7	0.2174(10)	0.0341(5)	0.8268(13)	0.011(3)
C8	0.3098(11)	0.0912(6)	0.7280(15)	0.019(4)
C9	0.3303(11)	0.1248(6)	0.6949(14)	0.014(3)
C10	0.4765(11)	0.1799(5)	0.7563(15)	0.021(3)
H10A	0.4759	0.1771	0.8859	0.026
H10B	0.5465	0.1903	0.7251	0.026
C11	0.2713(11)	0.1938(5)	0.7629(15)	0.023(4)
H11A	0.2204	0.2126	0.7342	0.027
H11B	0.273	0.191	0.8925	0.027
C12	0.3862(12)	0.2044(6)	0.7020(17)	0.034(4)
H12A	0.385	0.2063	0.572	0.04
H12B	0.403	0.2273	0.7505	0.04
C13	0.1344(11)	-0.2038(6)	1.5630(17)	0.032(4)
H13A	0.1338	-0.2045	1.6933	0.038

H13B	0.1226	-0.2275	1.52	0.038
C14	0.2461(11)	-0.1919(6)	1.5049(16)	0.029(4)
H14A	0.2446	-0.1885	1.3756	0.035
H14B	0.2994	-0.2101	1.5321	0.035
C15	0.0394(12)	-0.1813(6)	1.4978(16)	0.030(4)
H15A	-0.0294	-0.1927	1.5271	0.036
H15B	0.0423	-0.1792	1.368	0.036
C16	0.1782(11)	-0.1242(6)	1.5649(15)	0.020(4)
C17	0.1973(10)	-0.0906(5)	1.5274(14)	0.010(3)
C18	0.2879(10)	-0.0333(5)	1.4280(14)	0.012(3)
C19	0.1790(10)	-0.0270(5)	1.4254(14)	0.013(3)
C20	0.2671(10)	0.0299(6)	1.3225(14)	0.014(3)
C21	0.2878(11)	0.0627(5)	1.2750(14)	0.017(3)
C22	0.4234(10)	0.1180(5)	1.1598(14)	0.011(3)
H22A	0.4922	0.1298	1.1896	0.013
H22B	0.4211	0.1146	1.0307	0.013
C23	0.2160(11)	0.1286(5)	1.1536(15)	0.020(3)
H23A	0.2161	0.1234	1.026	0.024
H23B	0.163	0.1472	1.1724	0.024
C24	0.3295(11)	0.1416(6)	1.2100(16)	0.028(4)
H24A	0.3413	0.1643	1.156	0.033
H24B	0.3311	0.1447	1.3395	0.033
S1	0.3242(3)	-0.09050(15)	0.9931(4)	0.0261(16)
S2	0.0724(3)	-0.07431(14)	0.9825(4)	0.0234(16)
S3	0.3683(3)	-0.01380(14)	0.8922(4)	0.0236(16)
S4	0.1276(3)	0.00187(14)	0.8858(4)	0.0195(15)
S5	0.4157(3)	0.05991(14)	0.7548(4)	0.0178(15)
S6	0.1734(3)	0.07476(13)	0.7454(4)	0.0204(15)

S7	0.4666(3)	0.13720(13)	0.6530(4)	0.0211(15)
S8	0.2191(3)	0.15368(14)	0.6622(4)	0.0191(15)
S9	0.2904(3)	-0.15189(15)	1.6117(4)	0.0236(16)
S10	0.0410(3)	-0.13775(14)	1.5964(4)	0.0237(15)
S11	0.3328(3)	-0.07416(13)	1.5065(4)	0.0170(14)
S12	0.0909(3)	-0.05987(14)	1.5008(4)	0.0211(15)
S13	0.3758(3)	-0.00031(14)	1.3664(4)	0.0202(15)
S14	0.1334(3)	0.01351(14)	1.3565(4)	0.0228(16)
S15	0.4240(3)	0.07623(14)	1.2666(4)	0.0276(17)
S16	0.1724(3)	0.09111(15)	1.2706(4)	0.0259(16)
Fe1	0.11134(15)	0.24853(7)	0.1144(2)	0.0210(9)
Cl1	0.2055(3)	0.22117(15)	0.3220(4)	0.0363(16)
Cl2	0.0186(3)	0.20967(16)	-0.0407(5)	0.049(2)
Cl3	0.0026(3)	0.28677(15)	0.2391(5)	0.0408(18)
Cl4	0.2253(3)	0.27613(14)	-0.0591(4)	0.0381(17)

TABLE S3-V. Atomic coordinates in β -(BDA-TTP)₂FeCl₄ under 16 kbar.

	<i>x</i>	<i>y</i>	<i>z</i>	$U_{eq} / \text{\AA}^2$
C1	0.1620(11)	-0.1397(6)	1.0529(17)	0.022(4)
H1A	0.1599	-0.1427	0.9223	0.026
H1B	0.1466	-0.1624	1.1065	0.026
C2	0.2772(11)	-0.1293(6)	1.1078(16)	0.013(4)
H2A	0.3273	-0.1484	1.0805	0.016
H2B	0.2799	-0.1256	1.2379	0.016
C3	0.0712(12)	-0.1153(6)	1.1027(17)	0.022(4)
H3A	0.0762	-0.1108	1.232	0.027
H3B	0.0007	-0.1269	1.0788	0.027
C4	0.2111(12)	-0.0621(6)	0.9784(17)	0.017(4)
C5	0.2331(11)	-0.0282(6)	0.9307(15)	0.013(4)
C6	0.3254(10)	0.0276(5)	0.8313(15)	0.008(3)
C7	0.2178(11)	0.0345(6)	0.8245(16)	0.014(4)
C8	0.3092(11)	0.0918(6)	0.7249(15)	0.011(4)
C9	0.3294(11)	0.1254(6)	0.6930(15)	0.011(4)
C10	0.4755(11)	0.1794(6)	0.7521(16)	0.014(4)
H10A	0.4732	0.1762	0.8825	0.016
H10B	0.547	0.1896	0.7245	0.016
C11	0.2715(12)	0.1943(6)	0.7611(18)	0.026(4)
H11A	0.22	0.2132	0.734	0.031
H11B	0.2741	0.1914	0.8917	0.031
C12	0.3868(12)	0.2053(7)	0.6982(18)	0.030(4)
H12A	0.3854	0.2077	0.5673	0.035
H12B	0.405	0.228	0.7498	0.035
C13	0.1320(12)	-0.2045(7)	1.5675(19)	0.033(5)
H13A	0.1197	-0.2281	1.5221	0.04

H13B	0.1315	-0.2055	1.699	0.04
C14	0.2472(12)	-0.1915(6)	1.5053(17)	0.023(4)
H14A	0.2441	-0.1872	1.3757	0.028
H14B	0.3014	-0.2099	1.5276	0.028
C15	0.0401(12)	-0.1816(6)	1.5033(17)	0.020(4)
H15A	-0.0299	-0.1928	1.5305	0.024
H15B	0.0441	-0.1793	1.3725	0.024
C16	0.1777(12)	-0.1237(6)	1.5700(17)	0.019(4)
C17	0.1976(12)	-0.0903(6)	1.5299(17)	0.016(4)
C18	0.2878(11)	-0.0343(6)	1.4268(16)	0.014(4)
C19	0.1778(11)	-0.0269(6)	1.4265(16)	0.012(4)
C20	0.2672(12)	0.0301(7)	1.3207(17)	0.020(4)
C21	0.2884(12)	0.0629(6)	1.2731(17)	0.016(4)
C22	0.4249(11)	0.1191(6)	1.1559(16)	0.014(4)
H22A	0.4936	0.1309	1.1885	0.017
H22B	0.4242	0.1157	1.0254	0.017
C23	0.2164(12)	0.1291(6)	1.1487(16)	0.016(4)
H23A	0.2175	0.1237	1.0203	0.019
H23B	0.1622	0.1476	1.1655	0.019
C24	0.3286(11)	0.1429(6)	1.2046(17)	0.019(4)
H24A	0.3297	0.1465	1.3348	0.022
H24B	0.3395	0.1655	1.1478	0.022
S1	0.3253(3)	-0.09007(17)	0.9964(5)	0.0236(19)
S2	0.0713(3)	-0.07443(16)	0.9866(5)	0.0237(18)
S3	0.3691(3)	-0.01390(15)	0.8927(4)	0.0169(17)
S4	0.1264(3)	0.00185(16)	0.8862(5)	0.0188(18)
S5	0.4167(3)	0.06004(15)	0.7521(4)	0.0166(18)
S6	0.1720(3)	0.07492(15)	0.7426(4)	0.0184(17)

S7	0.4676(3)	0.13715(15)	0.6479(4)	0.0197(18)
S8	0.2181(3)	0.15412(16)	0.6591(4)	0.0190(18)
S9	0.2922(3)	-0.15232(16)	1.6181(4)	0.0192(18)
S10	0.0412(3)	-0.13799(15)	1.6030(5)	0.0220(19)
S11	0.3336(3)	-0.07410(15)	1.5094(5)	0.0205(17)
S12	0.0901(3)	-0.05997(16)	1.5043(5)	0.0182(17)
S13	0.3766(3)	-0.00053(16)	1.3665(4)	0.0168(17)
S14	0.1325(3)	0.01348(15)	1.3563(4)	0.0195(19)
S15	0.4247(3)	0.07627(16)	1.2633(5)	0.0262(19)
S16	0.1715(3)	0.09122(17)	1.2679(5)	0.0228(19)
Fe1	0.11112(17)	0.24871(9)	0.1119(2)	0.0183(11)
Cl1	0.2067(3)	0.22086(16)	0.3203(5)	0.0354(19)
Cl2	0.0181(3)	0.20999(19)	-0.0434(5)	0.050(2)
Cl3	0.0022(3)	0.28676(17)	0.2378(5)	0.0364(19)
Cl4	0.2260(3)	0.27633(16)	-0.0622(5)	0.037(2)

TABLE S3-VI. Atomic coordinates in β -(BDA-TTP)₂FeCl₄ under 21 kbar.

	x	y	z	$U_{\text{eq}} / \text{\AA}^2$
C1	0.1630(12)	-0.1416(7)	1.0603(18)	0.019(4)
H1A	0.1479	-0.164	1.1197	0.022
H1B	0.1616	-0.1457	0.929	0.022
C2	0.2773(12)	-0.1301(7)	1.1144(18)	0.017(4)
H2A	0.329	-0.1491	1.0883	0.02
H2B	0.2793	-0.1261	1.2459	0.02
C3	0.0680(12)	-0.1159(7)	1.1059(18)	0.017(4)
H3A	0.0701	-0.1115	1.237	0.02
H3B	-0.0025	-0.1275	1.0774	0.02
C4	0.2129(12)	-0.0628(7)	0.9844(17)	0.007(4)
C5	0.2318(13)	-0.0281(8)	0.9311(19)	0.019(4)
C6	0.3260(12)	0.0282(7)	0.8303(17)	0.012(4)
C7	0.2159(12)	0.0351(7)	0.8195(17)	0.013(4)
C8	0.3098(13)	0.0931(8)	0.7211(19)	0.020(5)
C9	0.3279(13)	0.1253(8)	0.6877(19)	0.019(5)
C10	0.4781(13)	0.1800(7)	0.7484(19)	0.022(4)
H10A	0.4779	0.1768	0.8804	0.027
H10B	0.5495	0.1903	0.7168	0.027
C11	0.2704(12)	0.1944(7)	0.7565(19)	0.027(4)
H11A	0.2188	0.2134	0.7269	0.032
H11B	0.2709	0.1916	0.8887	0.032
C12	0.3879(13)	0.2058(8)	0.698(2)	0.034(5)
H12A	0.3876	0.2091	0.5659	0.041
H12B	0.4053	0.2284	0.7541	0.041
C13	0.1338(13)	-0.2058(9)	1.571(2)	0.039(5)
H13A	0.1333	-0.2078	1.7032	0.047

H13B	0.1206	-0.2291	1.519	0.047
C14	0.2475(12)	-0.1919(6)	1.5086(19)	0.022(4)
H14A	0.2434	-0.1871	1.378	0.026
H14B	0.3029	-0.2103	1.5279	0.026
C15	0.0407(13)	-0.1803(7)	1.5062(19)	0.020(4)
H15A	-0.0308	-0.1915	1.5285	0.024
H15B	0.0469	-0.1772	1.3747	0.024
C16	0.1794(13)	-0.1256(7)	1.5789(18)	0.013(4)
C17	0.1966(13)	-0.0913(8)	1.5357(18)	0.018(4)
C18	0.2885(11)	-0.0347(7)	1.4317(16)	0.005(4)
C19	0.1763(12)	-0.0275(7)	1.4251(17)	0.013(4)
C20	0.2658(12)	0.0293(8)	1.3221(18)	0.014(4)
C21	0.2845(12)	0.0622(7)	1.2707(18)	0.009(4)
C22	0.4257(13)	0.1190(7)	1.1499(19)	0.022(4)
H22A	0.4949	0.131	1.182	0.026
H22B	0.4244	0.1157	1.018	0.026
C23	0.2182(12)	0.1294(7)	1.1462(18)	0.015(4)
H23A	0.2198	0.124	1.0163	0.018
H23B	0.1641	0.1482	1.163	0.018
C24	0.3281(11)	0.1427(7)	1.2017(17)	0.013(4)
H24A	0.3293	0.1459	1.3338	0.016
H24B	0.3389	0.1657	1.1464	0.016
S1	0.3258(3)	-0.09036(19)	1.0013(5)	0.022(2)
S2	0.0705(3)	-0.07472(19)	0.9910(5)	0.024(2)
S3	0.3701(3)	-0.01414(17)	0.8920(5)	0.0148(19)
S4	0.1258(3)	0.00174(18)	0.8871(5)	0.016(2)
S5	0.4175(3)	0.06003(18)	0.7501(5)	0.018(2)
S6	0.1718(3)	0.07506(17)	0.7391(5)	0.0154(19)

S7	0.4682(3)	0.13764(17)	0.6432(5)	0.017(2)
S8	0.2176(3)	0.15449(19)	0.6556(5)	0.019(2)
S9	0.2931(3)	-0.15299(18)	1.6240(5)	0.020(2)
S10	0.0402(3)	-0.13853(18)	1.6087(5)	0.022(2)
S11	0.3351(3)	-0.07425(17)	1.5128(5)	0.022(2)
S12	0.0895(3)	-0.05968(17)	1.5078(5)	0.019(2)
S13	0.3772(3)	-0.00061(17)	1.3658(5)	0.016(2)
S14	0.1313(3)	0.01324(17)	1.3561(5)	0.021(2)
S15	0.4255(3)	0.07644(18)	1.2587(5)	0.023(2)
S16	0.1706(3)	0.09123(19)	1.2650(5)	0.021(2)
Fe1	0.11094(16)	0.24862(9)	0.1094(3)	0.0178(12)
Cl1	0.2075(3)	0.22082(18)	0.3180(5)	0.033(2)
Cl2	0.0174(3)	0.2093(2)	-0.0461(6)	0.042(2)
Cl3	0.0010(3)	0.28688(18)	0.2380(5)	0.033(2)
Cl4	0.2275(3)	0.27600(18)	-0.0658(5)	0.034(2)

Chapter IV. Crystal Structural Change in [Cr(CN)₆][Mn((*R*)-pnH)(H₂O)](H₂O) under Pressure

4-1. INTRODUCTION

Molecule-based Magnetic Materials

The construction of molecule-based magnetic materials, which possess additional properties such as conductivity [1], photoreactivity [2], or optical properties [3-5], is currently a challenging target. The physical aspects of the current interest are centered on optical properties, particularly with respect to optical activity. When a magnet is characterized by optical transparency and chiral structure, there is a great possibility that the crystals have a chiral spin structure. These magnets display asymmetric magnetic anisotropy and magnetochiral dichroism (MChD) [4]. This category of materials is not only of academic interest; they also afford the potential of being used in new devices. When chiral molecule-based magnets are constructed, chirality must be controlled in the molecular structure as well as in the entire crystal structure. As a consequence of this difficulty, only few examples of this type of magnet exist. Most of the reported chiral magnets have low-dimensional magnetic structures, in which the magnetic ordering temperatures are below 10 K [5].

Recently, two-dimensional (2D) molecule-based chiral ferrimagnet, $[\text{Cr}(\text{CN})_6][\text{Mn}((R)\text{-pnH})(\text{H}_2\text{O})](\text{H}_2\text{O})$, [$(R)\text{-pn}$ = (R) -1,2-diaminopropane], that is called Green Needle [(R) -GN], was prepared [6] and the characteristic magnetic properties, such as giant nonlinear magnetic response, have been reported [7]. The magnetic transition temperature, $T_c = 38$ K, of the (R) -GN is relatively high among the known molecule-based magnets [Fig. 4-1(a)]. The crystal structures and crystallographic data for (R) -GN are shown in Fig. 4-1(b)-(d) and Table 4-I, respectively. The structure belongs to chiral space group $P2_12_12_1$ and forms a 2D chiral network. Four cyanide groups in the $[\text{Cr}(\text{CN})_6]^-$ ion are ligated to Mn^{2+} ions to form a bimetallic square, which is arranged almost perpendicular to the c -axis. Each unit has one chiral (R) -pn ligand and two water molecules between the sheets. The (R) -pn ligand and one of the water molecules coordinates to an Mn^{2+} ion and separates the sheets.

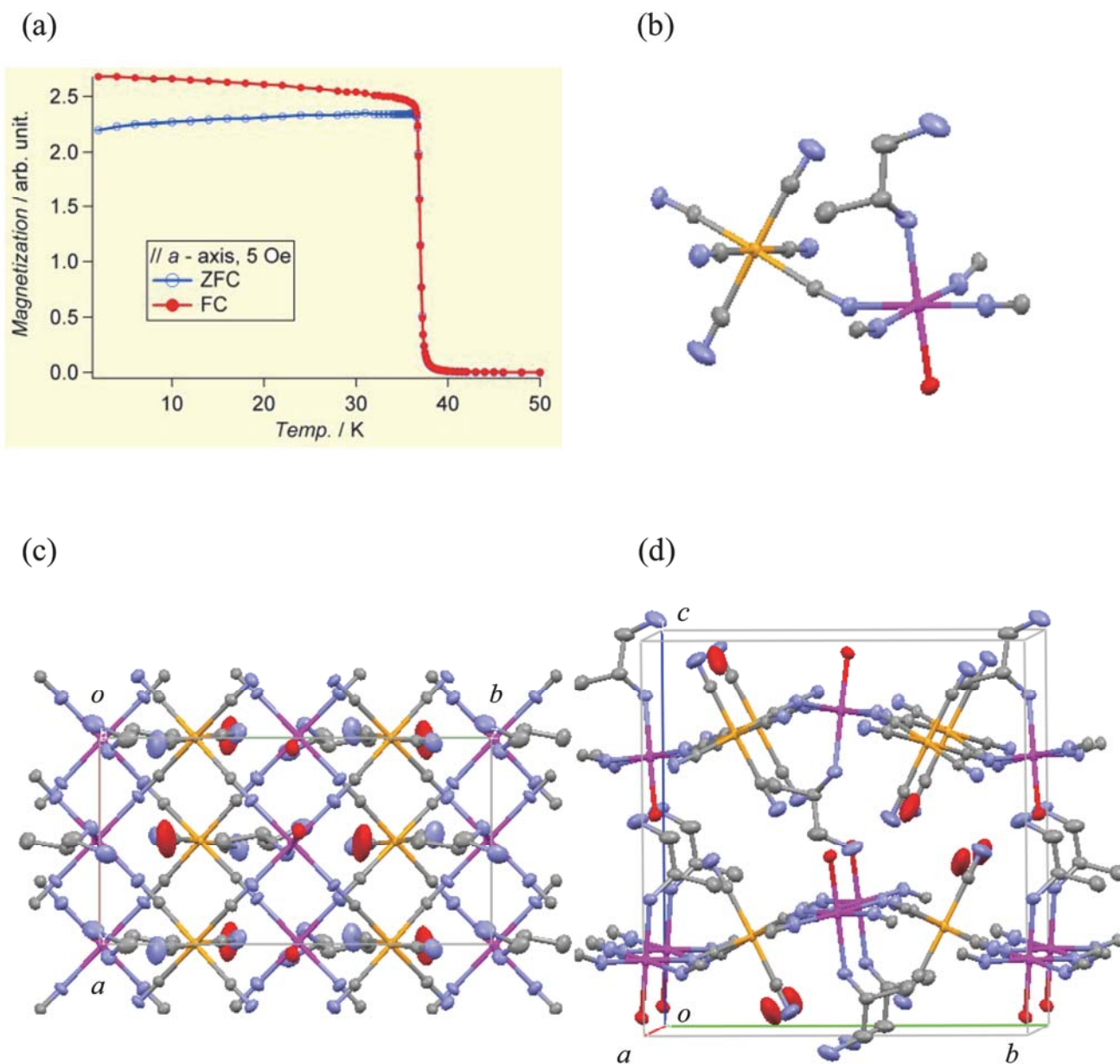


FIGURE 4-1. (a) Temperature dependence of the magnetization along *a*-axis for (R)-GN. (b) ORTEP drawing, crystal structure along (c) *c*-axis, and (d) *a*-axis for (R)-GN at room temperature and under ambient pressure (APRT Phase). Hydrogen atoms are omitted for clarify. orange: Cr, purple: Mn, gray: C, blue: N, and red: O.

Interestingly, the (R)-GN occurred structural phase transition and dehydration by heating [8]. If the crystal at room temperature and ambient pressure shown as Fig. 4-1, that is called APRT Phase, is heated gently, the crystal structure changes to high-temperature (HT) Phase at 320 K. The crystal structure and crystallographic data of the HT Phase are shown in Fig. 4-2 and Table 4-I, respectively. A different nitrogen atom of (R)-pn from APRT Phase is ligated to a Mn^{2+} ion in HT Phase. As a result, the (R)-pn seems to rotate in this structural phase transition. The space group of HT Phase belongs to $P2_12_12_1$ and also forms chiral 2D sheet network. If the HT Phase is heated under nitrogen atmosphere, dehydration occurs at 330 K. In this Dehydrated (DH) Phase, not only water molecules existed between 2D sheets but also ones ligated to Mn^{2+} ions are removed. Fig. 4-2 and Table 4-I also show the crystal structure and crystallographic data of the DH Phase, respectively. As a results, there-dimensional network thorough the cyanide-bridges between 2D sheets is formed in DH Phase. These structural phase transitions are reversible single-crystal to single-crystal transformation. The magnetic properties also changes with these structural change: magnetic ordering temperature rises slightly with 39K in HT Phase, and largely with 73 K by forming a 3D network in DH Phase.

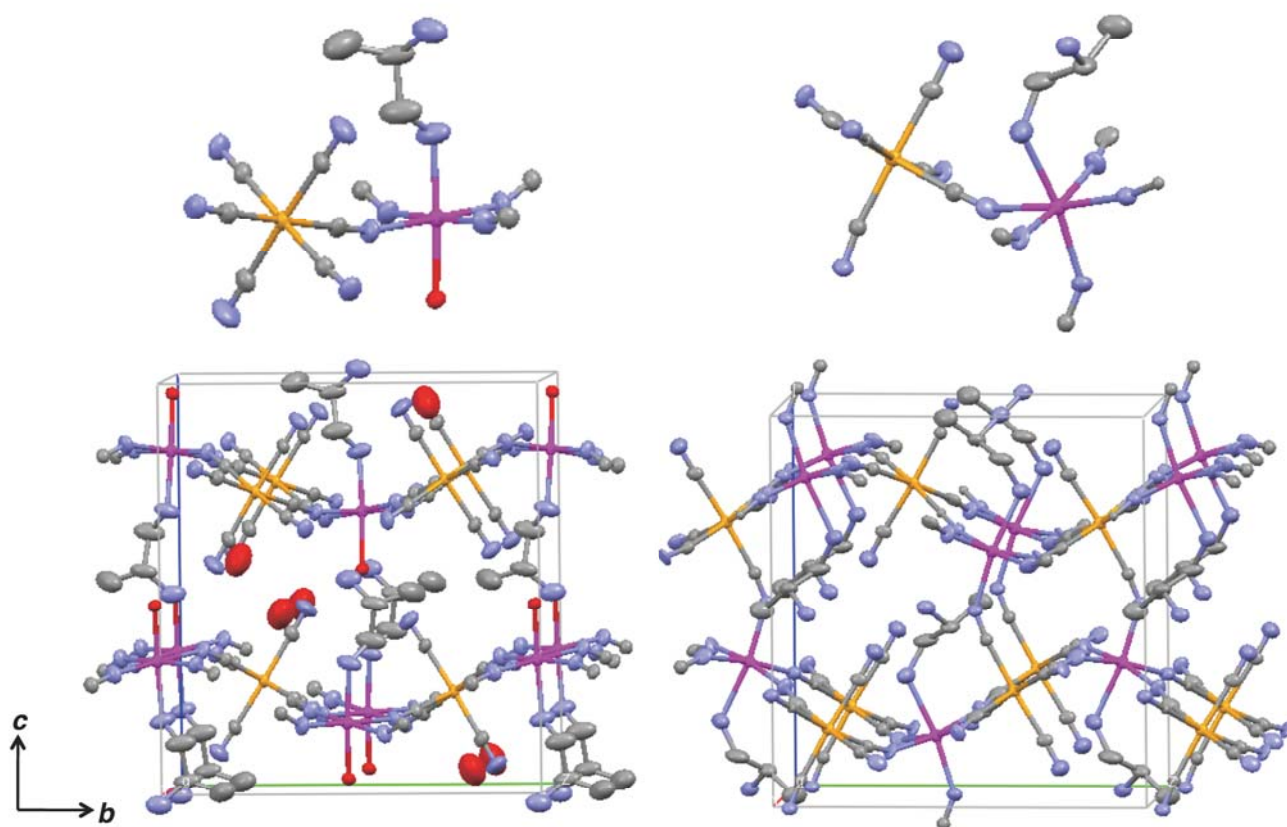


FIGURE 4-2. ORTEP drawing of crystallographically independent part (**upper**) and crystal structure along *a*-axis (**lower**) for high-temperature (HT) phase (**left**) and Dehydrated (DH) phase of (*R*)-GN.

TABLE 4-I. Crystallographic data for APRT, HT, and DH Phase of (*R*)-GN [8].

Phase	APRT	HT	DH
Formula	$\text{C}_9\text{H}_{15}\text{SCrMnN}_8\text{O}_2$		$\text{C}_9\text{H}_{11}\text{SCrMnN}_8$
F_w	374.23		338.20
Crystal shape, color, size / mm^3	block, yellow-green, $0.50 \times 0.20 \times 0.10$		
Crystal system, Space group	orthorhombic, $P2_12_12_1$		
$a / \text{\AA}$	7.6420(6)	7.4439(7)	7.712(2)
$b / \text{\AA}$	14.5365(12)	14.4725(8)	13.401(5)
$c / \text{\AA}$	14.9570(12)	15.6319(15)	14.058(5)
$V / \text{\AA}^3$	1661.5(2)	1684.1(3)	1452.8(9)
Z	4	4	4
$D_{\text{calcd.}} / \text{g cm}^{-3}$	1.496	1.476	1.546
μ / mm^{-1}	1.429	1.410	1.615
θ_{min} and $\theta_{\text{max}} / ^\circ$	2.722, 27.88	2.606, 27.72	3.040, 23.87
No. of observed [$I \geq 2\sigma(I)$]	2944	2923	1592
Parameters	205	200	174
GOF	0.982	0.963	1.136
R, wR	0.0309, 0.0725	0.0364, 0.0882	0.0707, 0.1594
Flack	-0.01(3)	-0.01(3)	0.14(12)
T / K	298	295	298

A structural change is expected also by pressure in (R)-GN. The change of diffraction pattern for (R)-GN by pressure was observed in the preliminary experiments using powder sample. Furthermore, when the sample was returned to ambient pressure after pressurizing to more than 26 kbar, the diffraction pattern that is different before pressuring was also observed. Although this structural change by pressure is interesting,

In this chapter, structural studies for (R)-GN under pressure using single crystal are described. The X-ray structural analysis using the single crystal of (R)-GN returned to ambient pressure after pressurizing to more than 25 kbar, was performed. As a result, the novel structure, which cannot be obtained at ambient pressure, High-Pressure (HP) Form, was found out. In order to clarify the mechanism of this structural change by pressure, the X-ray structural analysis under pressure were also carried out.

4-2. EXPERIMENTAL DETAILS

High Pressure Form

The crystal size used for X-ray diffraction measurements was $0.20 \times 0.10 \times 0.05 \text{ mm}^3$. Diamond anvil cell (DAC) was used for pressurizing the crystal. Daphne 7373 (Idemitsu Co. Ltd.) was employed as a pressure medium, and the value of pressure at room temperature was determined by the ruby fluorescence method [9]. Data were collected with a Bruker SMART-APEX three-circle diffractometer, equipped with a CCD area detector, graphite-monochromated MoK α radiation [$\lambda = 0.71073 \text{ \AA}$, ω -scan mode (0.3° step)], and nitrogen-flow cryostat (Japan Thermal Co. Ltd.) for temperature control. Structures were solved by direct methods and refined against F^2 by full-matrix least-squares method using the SHELEXS-97 program [10]. Hydrogen atoms are located in their calculated positions and all non-Hydrogen atoms were refined anisotropically.

X-ray Diffraction Measurement under Pressure

The crystal size used for X-ray diffraction measurements was $0.20 \times 0.10 \times 0.05 \text{ mm}^3$. A curved imaging plate (MACScience DIP320V) equipped with a 6 kW rotating-anode X-ray generator with a graphite monochromated $\text{MoK}\alpha$ radiation ($\lambda = 0.71073 \text{ \AA}$) was used for data collection. Oscillation photographs were taken with the angle of 3° for each exposure of 1 hour. The image data processing of IP digital data, cell refinements, and data reduction were performed using the *Denzo* and *Scalepack* programs [11].

The diffraction measurements under pressure were performed using a diamond anvil cell (DAC). Daphne 7373 (Idemitsu Co. LTd.) was employed as a pressure medium, and the value of pressure at room temperature was determined by the ruby fluorescence method [9]. The intensity data were corrected for the absorption of the incident and the diffraction beam through the DAC before the merging process. Detailed procedures and analysis under pressure is described in Chapter II.

Structures were solved by direct methods and refined against F^2 by full-matrix least-squares method using the SHELEXS-97 program [10]. Hydrogen atoms are located in their calculated positions. Although all non-Hydrogen atoms were refined anisotropically at 1 bar, Cr and Mn atoms were refined with the anisotropic temperature factor for structure analysis at 3 kbar.

4-3. RESULTS & DISCUSSION

4-3-1. High-Pressure Form

Space Group of High-Pressure Form

The space group of APRT phase for (*R*)-GN is $P2_12_12_1$, which possess extinction rules originated from 2-fold screw axes along each crystal axis. For this reason, the reflections that *h*, *k*, or *l* are odd about *h*00, 0*k*0, and 00*l*, respectively, could not be observed in APRT phase. On the other hand, the reflections that *h* is odd about *h*00, as shown in Fig. 4-3, were observed in HP Form. The diffraction intensity about *h*00, 0*k*0, and 00*l* are summarized in Table 4-II. The increase in the intensity about 0*k*0 and 00*l* was not observed in HP Form. It indicates that the extinction rule originated from only 2-fold screw axis along *a*-axis. As a result, the Space group of HP form changed from $P2_12_12_1$ to $P22_12_1$.

TABLE 4-II. Selected diffraction intensity for APRT phase and HP form of (*R*)-GN.

<i>hkl</i>	<i>I</i> (σ) in APRT	<i>I</i> (σ) in HP
300	−0.96 (2.75)	56.15 (3.78)
700	1.49 (3.33)	37.43 (6.98)
030	0.73 (1.89)	−0.12 (2.00)
003	−1.91 (0.85)	−1.16 (1.55)

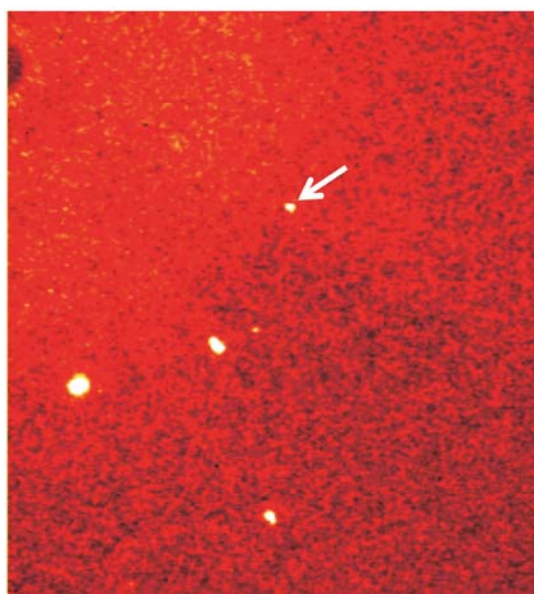


FIGURE 4-3. A diffraction photograph for HP Form of (*R*)-GN. The white arrow shows (3 0 0) reflection.

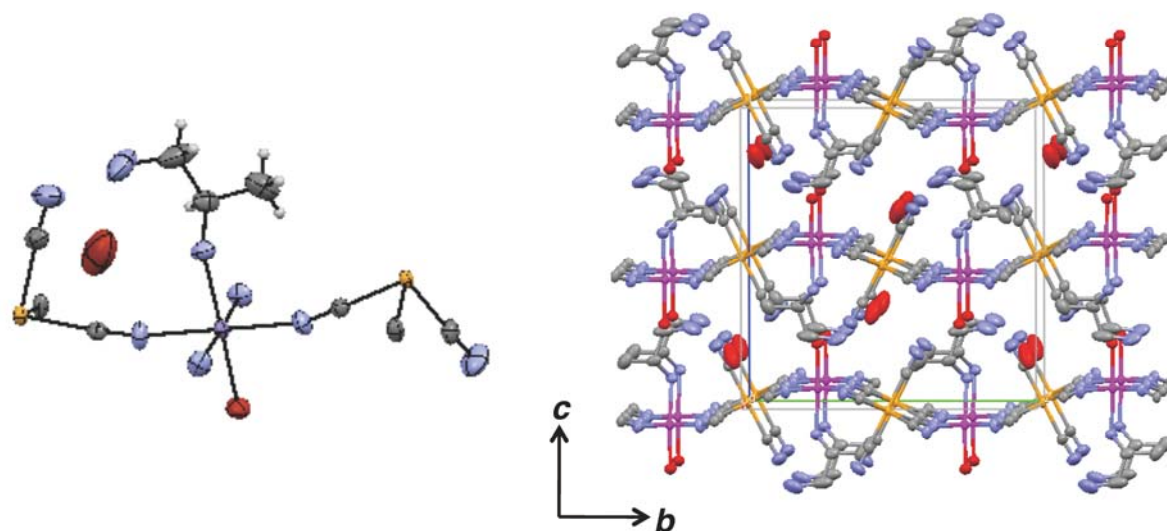


FIGURE 4-4. ORTEP drawing (**left**) and crystal structure along *a*-axis (**right**) for HP form of (*R*)-GN.

Crystal Structure of High-Pressure Form

The crystallographic data of HP form are shown in Table 4-III. Although the cell volume of the HP form was almost equal to that of APRT phase, *a* and *b*-axis, in which the metal ion are arranged, slightly expanded, whereas *c*-axis, which is the 2D sheet stacking direction, contracted. The crystal structures of HP form are shown in Fig. 4-4. One Mn atom and two half Cr atoms, which existed on 2-fold axis along *a*-axis, were crystallographically independent. Although the space group changed to $P2_212_1$, the 2D sheet structure was also formed in HP form. The details of this structural change are explained by compared the structure of HP form with APRT phase (Fig. 4-5). In HP form, the water molecules that existed between 2D sheets moved to different position from APRT phase. The arrangement of some (*R*)-pn in HP form also changed from APRT phase, that seemed to rotate 180° around the direction of a molecule long axis in HP form. This indicated that the movement of the water molecules and rotation of (*R*)-pn played the important role in the structural change by pressure.

TABLE 4-III. Crystallographic data of APRT Phase, High-Pressure (HP) Form, and Dehydrated (DH) Phase from HP Form for (*R*)-GN.

Phase / Form	APRT	HP	DH from HP
Formula	$\text{C}_9\text{H}_{15}\text{SCrMnN}_8\text{O}_2$		$\text{C}_9\text{H}_{11}\text{SCrMnN}_8$
F_w	374.23		338.20
Crystal shape, color size / mm ³	block, yellow-green, $0.20 \times 0.10 \times 0.05$		
Crystal system	orthorhombic		
Space group	$P2_12_12_1$	$P22_12_1$	$P2_12_12_1$
$a / \text{\AA}$	7.6381(4)	7.7077(4)	7.702(2)
$b / \text{\AA}$	14.5339(11)	14.5536(8)	13.465(4)
$c / \text{\AA}$	14.9634(9)	14.8204(8)	14.089(4)
$V / \text{\AA}^3$	1661.1(2)	1662.48(15)	1461.1(7)
Z	4	4	4
$D_{\text{calcd.}} / \text{g cm}^{-3}$	1.497	1.496	1.537
μ / mm^{-1}	1.429	1.428	1.606
Index range	$-8 \leq h \leq 7$	$-7 \leq h \leq 8$	$-8 \leq h \leq 8$
	$-16 \leq k \leq 13$	$-16 \leq k \leq 16$	$-13 \leq k \leq 14$
	$-16 \leq l \leq 15$	$-13 \leq l \leq 16$	$-15 \leq l \leq 14$
Reflections	2399	2403	2083
Parameters	194	195	176
GOF	1.161	1.109	1.083
R, wR	0.0329, 0.0984	0.0327, 0.0922	0.0680, 0.1531
Flack	0.02(6)	-0.02(6)	0.34(11)
T / K	295	295	295

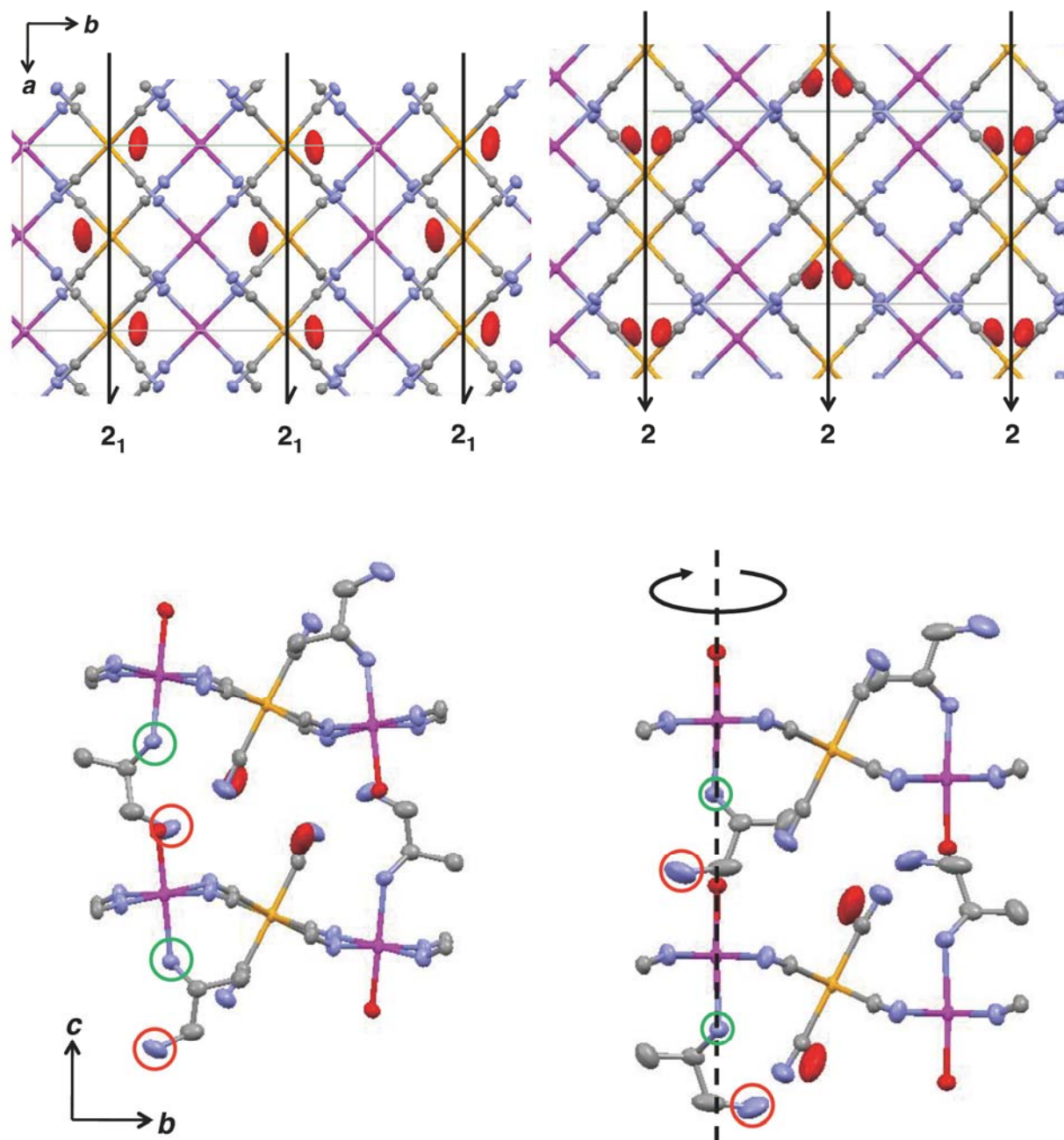


FIGURE 4-5. Crystal structure along *c*-axis (**upper**) and *a*-axis (**lower**) for APRT phase (**left**) and HP form (**right**). Oxygen atom of water molecule is red particle.

Dehydrated Phase from High-Pressure form

The HP form of (*R*)-GN also occurred dehydration at 350 K under nitrogen atmosphere by heating the single crystal. The space group returned to $P2_12_12_1$ from $P22_12_1$ by dehydration. The crystal structure and crystallographic data were shown in Fig. 4-6 and Table 4-III, respectively. The structure of dehydration from HP form was mostly in agreement with the DH phase obtained from APRT phase. It indicates that the two DH phases from which the routes differ are isostructural. The structural changes by temperature are reversible, whereas the structural change to HP Form by pressure, which was observed at ambient pressure after pressurized more than 25 kbar, is irreversible. It is suggested that it may be possible to return to APRT phase via DH phase from HP Form. However, if the single crystals of HP form after dehydration were cooling, the crystals broke down.

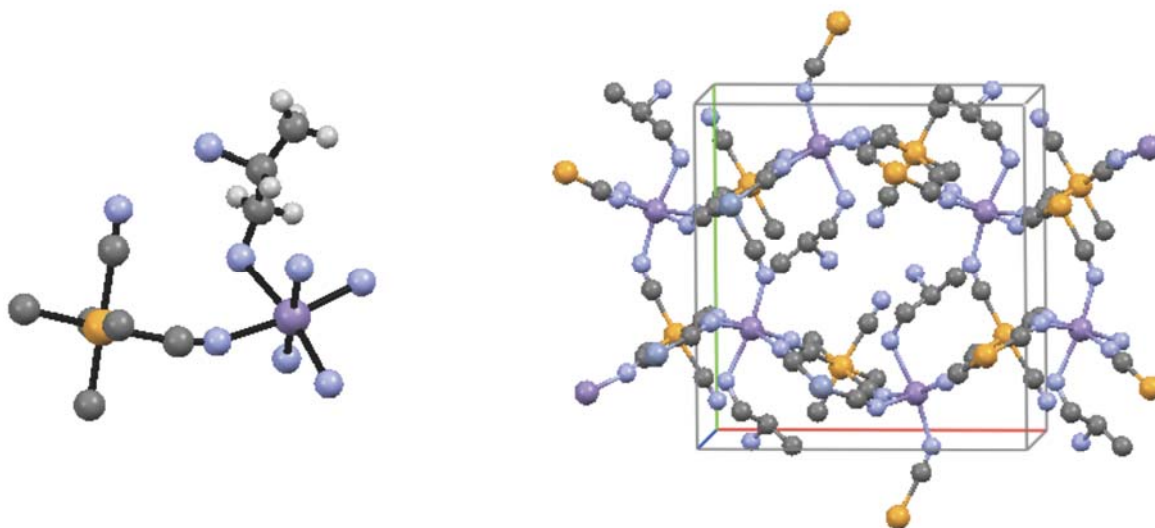


FIGURE 4-6. ORTEP drawing (**left**) and crystal structure along *a*-axis (**right**) of DH phase from HP form of (*R*)-GN.

4-3-2. Structures under Pressure

In order to clarify the mechanism for the structure change to High-Pressure form, X-ray studies under pressures were performed up to 27 kbar. The diffraction measurement for (*R*)-GN at 3, 9, 13, 21, and 27 kbar were performed. The crystal structure analysis for (*R*)-GN at 3 kbar was succeeded, whereas the only cell constants were calculated at 9 kbar and high pressures since the qualities of the crystal was reduced. Crystallographic data at 3 kbar are shown in Table 4-IV. Although each cell axis and volume was contracted, the structure is equivalent with the APRT Phase. The pressure dependence of the unit cell parameters is shown in Fig. 4-7. The change in the *c*-axis, which is the 2D sheet stacking direction, is largest.

The broadening of the diffraction spots was observed at 9 kbar and higher pressures as shown in Fig. 4-7. Each diffraction spot was broadened along *c**-axis direction in all photographs, indicating that the periodicity along *c*-axis direction in the crystal structure of the (*R*)-GN was getting worse more than 9 kbar. The author focuses on the diffraction intensity in reflections that *h* were odd about *h*00, which was different between APRT phase and HP form. The pressure dependence of the intensity in reflections that *h* were odd about *h*00 is shown in Fig. 4-9. The intensity of reflections about (3 0 0) and (5 0 0) had increased more than 9 kbar, suggesting that the structure of HP form together with some other structures, such as APRT phase, was formed in structure of (*R*)-GN more than 9 kbar. Furthermore, the broadening of the diffraction spots was not disappeared at 27 kbar, suggesting that a single High-Pressure Phase was not appeared more than 25 kbar and the structural change to HP form was occurred when the crystal of (*R*)-GN was depressurized and returned to ambient pressure.

TABLE 4-IV. Crystallographic data of (*R*)-GN at 1bar and 3 kbar.

<i>P</i> / kbar	1×10^{-3}	3
Formula, F_w	$C_9H_{15}SCrMnN_8O_2$, 374.23	
Crystal shape, color, size / mm ³	block, yellowish-green, $0.20 \times 0.10 \times 0.05$	
Crystal system, Space group	orthorhombic, $P2_12_12_1$	
<i>a</i> / Å	7.6370(4)	7.6050(8)
<i>b</i> / Å	14.5270(11)	14.519(5)
<i>c</i> / Å	14.9470(9)	14.790(3)
<i>V</i> / Å ³	1658.26(18)	1633.1(7)
<i>Z</i>	4	4
$D_{\text{calcd.}}$ / g cm ⁻³	1.499	1.522
μ / mm ⁻¹	1.432	1.454
Index range	$0 \leq h \leq 9$	$0 \leq h \leq 7$
	$0 \leq k \leq 19$	$0 \leq k \leq 11$
	$0 \leq l \leq 19$	$0 \leq l \leq 12$
Reflections	2141	501
Parameters	191	96
GOF	1.116	1.154
<i>R</i> , <i>wR</i>	0.0465, 0.1252	0.0643, 0.1564
Flack	0.42(6)	0.25(17)
<i>T</i> / K	295	295

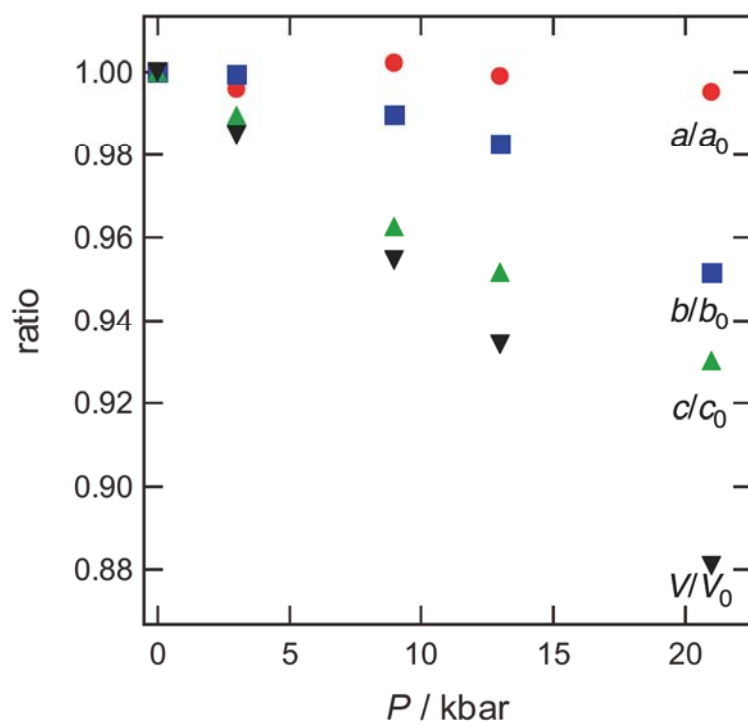


FIGURE 4-7. Pressure dependence of the unit cell parameters for (*R*)-GN.

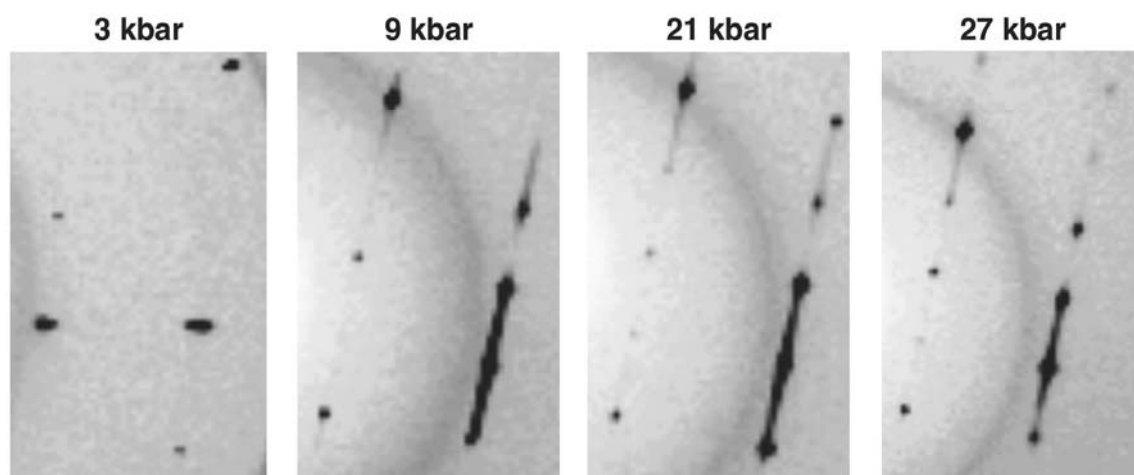


FIGURE 4-8. Diffraction photographs at 3, 9, 21, and 27 kbar for (*R*)-GN.

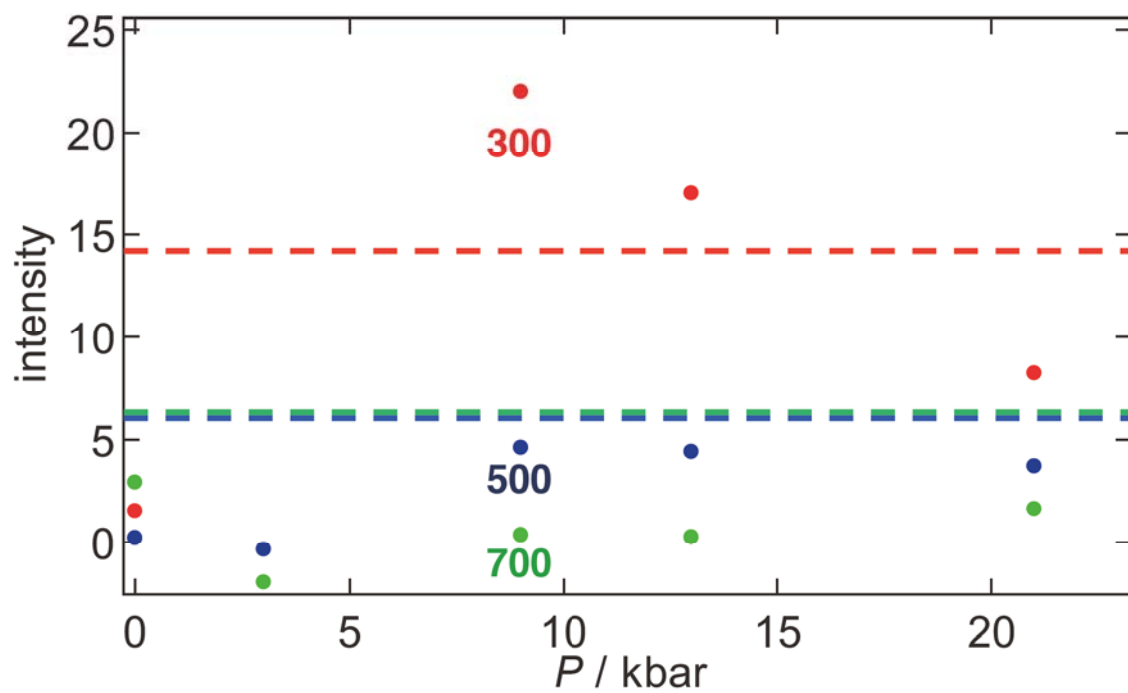


FIGURE 4-9. Pressure dependence of the diffraction intensity I/σ for (*R*)-GN. The intensities of each reflection in HP form are shown with dashed line.

4-4. CONCLUSION

The High-Pressure form of (*R*)-GN is found out when the single crystal of APRT phase was pressurize more than 25 kbar and then returned to ambient pressure. The space group of HP form changed to $P22_12_1$. In the structural change of (*R*)-GN by temperature and pressure, the rotation of (*R*)-pn ligands and movement of water molecules are considered to play the important role. The broadening of the diffraction spots and the reflections originated from HP form were observed under pressure. It indicates that the some structure including HP form exists under high pressure.

4-5. REFERENCES

- [1] a) M. Kurmoo, A. W. Graham, P. Day, S. J. Coles, M. B. Hursthouse, J. L. Caulfield, J. Singleton, F. L. Pratt, W. Hayes, L. Ducasse and P. Guionneau, *J. Am. Chem. Soc.* 117 (1995) 12209.
- b) L. Balicas, J. S. Brooks, K. Storr, S. Uji, M. Tokumoto, H. Tanaka, H. Kobayashi, A. Kobayashi, V. Barzykin and L. P. Gor'kov, *Phys. Rev. Lett.* 87 (2001) 067002.
- c) S. Uji, H. Shinagawa, T. Terashima, T. Yakabe, Y. Terai, M. Tokumoto, A. Kobayashi, H. Tanaka and H. Kobayashi, *Nature* 410 (2001) 908.
- d) E. Coronado, J. R. Galan-Mascaros, C. J. Gomez-Garcia and V. Laukhin, *Nature* 408 (2000) 447.
- [2] a) O. Sato, T. Iyoda, A. Fujishima and K. Hashimoto, *Science* 272 (1996) 704.
- b) S. Karasawa, H. Kumada, N. Koga and H. Iwamura, *J. Am. Chem. Soc.* 123 (2001) 9685.
- [3] a) C. Bellitto and P. Day, *J. Chem. Soc. Chem. Commun.* (1978) 511.
- P. Day, "Supramolecular Engineering of Synthetic Metallic Materials Conductors and Magnets": *NATO ASI Ser. Ser. C* 518 (1999) 253.
- [4] a) G. Wagniere and A. Mejer, *Chem. Phys. Lett.* 110 (1984) 546.
- b) G. L. J. A. Rikken and E. Raupach, *Nature* 390 (1997) 493.
- [5] a) A. Caneschi D. Gatteschi, P. Ray and R. Sessoli, *Inorg. Chem.* 30 (1991) 3936.
- b) M. Hernáez-Molina, F. Lloret, C. Ruiz-Pérez and M. Julve, *Inorg. Chem.* 37 (1998) 4131.
- c) H. Kumagai and K. Inoue, *Angew. Chem. Int. Ed.* 38 (1999) 1601.
- d) R. Andres, M. Brissard, M. Gruselle, C. Train, J. Vaissermann, B. Malezieux, J. P. Jamet and M. Verdaguer, *Inorg. Chem.* 40 (2001) 4633.
- e) E. Coronado, J. R. Galan-Mascaros, C. J. Gomez-Garcia and J. M. Martinez-Agudo, *Inorg. Chem.* 40 (2001), 40, 113.
- f) K. Inoue, H. Imai, P. S. Ghalsasi, K. Kikuchi, M. Ohba, H. Ôkawa and J. V. Yakhmi, *Angew. Chem. Int. Ed.* 40 (2001) 4242.

- [6] K. Inoue, K. Kikuchi, M. Ohba and H. Ôkawa, *Angew. Chem. Int. Ed.* 42 (2003) 4810.
- [7] a) A. Hoshikawa, T. Kamiyama, A. Purwanto, K. Ohishi, W. Higemoto, T. Ishigaki, H. Imai, and K. Inoue, *J. Phys. Soc. Jpn.* 73 (2004), 2597.
- b) K. Ohishi, W. Higemoto, A. Koda, S. R. Saha, R. Kadono, K. Inoue, H. Imai, and H. Higashikawa, *J. Phys. Soc. Jpn.* 75 (2006), 063705.
- c) Y. Yoshida, K. Inoue, and M. Kurmoo, *Chem. Lett.* 37 (2008), 586.
- d) J. Kishine, K. Inoue, and Y. Yoshida, *Prog. Theor. Phys.* 159 (2005), 82.
- e) M. Mito, K. Iriguchi, H. Deguchi, J. Kishine, K. Kikuchi, H. Ohsumi, Y. Yoshida, and K. Inoue, *Phys. Rev. B* 79 (2009) 012406.
- [8] Y. Yoshida, Doctor thesis, Hiroshima University (2008).
- [9] G. J. Piermarini, S. Block, J. D. Barnett, and R. A. Forman, *J. Appl. Phys.* 46 (1975) 2774.
- [10] G. M. Sheldrick, SHELX-97, University of Göttingen, Germany (1997).
- [11] Z. Otwinowski and W. Minor, *Methods Enzymology, Macromolecular Crystallography, part A* (Eds.: C. W. Carter Jr. and R. M. Sweet) Academic Press, New York 276 (1997) 307.

4-6. APPENDIX

TABLE S4-I. Atomic coordinates in the high-pressure form of (*R*)-GN.

atom	<i>x</i>	<i>y</i>	<i>z</i>	$U_{\text{eq}} / \text{\AA}^2$
C1	0.8704(8)	0.9079(5)	-0.0399(5)	0.0290(19)
C2	0.6782(11)	1.0649(4)	-0.1234(4)	0.0377(16)
C3	0.4884(8)	0.9084(5)	-0.0410(5)	0.0261(19)
C4	0.2705(7)	0.6989(4)	0.1548(3)	0.0420(13)
H4	0.389(7)	0.701(3)	0.131(4)	0.05
C5	0.2117(8)	0.5990(4)	0.1533(4)	0.0640(18)
H5A	0.0942	0.595	0.1744	0.096
H5B	0.2856	0.5632	0.1918	0.096
H5C	0.2184	0.5759	0.0927	0.096
C6	0.2757(8)	0.7334(6)	0.2530(4)	0.073(2)
H6A	0.1599	0.7291	0.2782	0.087
H6B	0.3503	0.693	0.2877	0.087
C7	-0.1258(8)	0.5903(5)	-0.0434(5)	0.0276(18)
C8	-0.5059(8)	0.5922(5)	-0.0398(6)	0.031(2)
C9	-0.3096(10)	0.4365(4)	-0.1247(4)	0.0328(15)
Cr1	0.6793(2)	1	0	0.0214(3)
Cr2	-0.3161(2)	0.5	0	0.0201(3)
Mn1	0.18014(7)	0.74857(6)	-0.06117(3)	0.02201(19)
N1	0.6784(12)	1.1061(4)	-0.1894(4)	0.0705(19)
N2	0.3824(7)	0.8559(4)	-0.0573(5)	0.0393(16)

N3	0.3903(7)	0.6437(4)	-0.0605(5)	0.0359(16)
N4	-0.0241(7)	0.8580(4)	-0.0605(5)	0.0371(16)
N5	0.1574(5)	0.7555(4)	0.0949(2)	0.0383(9)
N6	0.3381(8)	0.8285(4)	0.2635(4)	0.0805(18)
N7	-0.0226(7)	0.6431(4)	-0.0642(5)	0.0381(16)
N8	-0.3031(11)	0.3995(4)	-0.1931(4)	0.0654(18)
O1	0.1799(4)	0.7509(3)	-0.20947(17)	0.0410(7)
O2	0.1499(9)	0.9580(4)	0.1680(5)	0.130(3)

TABLE S4-II. Atomic coordinates in dehydrated phase from high-pressure form of (*R*)-GN.

atom	<i>x</i>	<i>y</i>	<i>z</i>	$U_{eq} / \text{\AA}^2$
Cr2	-0.09947(11)	0.29604(11)	0.3779(6)	0.0319(5)
Mn1	0.15830(11)	0.34309(11)	0.8779(5)	0.0325(5)
C7	-0.0039(18)	0.3401(19)	0.209(3)	0.064(9)
C8	-0.1961(17)	0.2331(16)	0.194(2)	0.037(6)
C9	-0.1721(7)	0.4261(8)	0.376(4)	0.034(3)
C10	-0.0171(9)	0.1708(10)	0.354(3)	0.048(5)
C11	-0.0064(14)	0.3490(13)	0.5780(19)	0.016(4)
C12	0.1310(16)	0.1070(14)	0.943(2)	0.098(8)
H12A	0.081	0.0603	0.9729	0.118
H12B	0.1667	0.1229	1.0481	0.118
C13	0.2020(16)	0.0624(14)	0.819(2)	0.073(6)
H13	0.233(13)	0.115(13)	0.75(2)	0.088
C14	0.2811(15)	0.0042(12)	0.873(5)	0.140(10)
H14A	0.2598	-0.0347	0.9685	0.21
H14B	0.3358	0.0432	0.9095	0.21
H14C	0.3016	-0.0355	0.7785	0.21
C16	-0.1830(13)	0.2416(16)	0.579(2)	0.026(5)
N7	0.0457(12)	0.3630(12)	0.6784(15)	0.037(5)
N8	0.0496(14)	0.3721(15)	1.093(3)	0.065(7)
N10	0.2607(15)	0.2972(16)	1.093(2)	0.042(5)
N11	0.0812(8)	0.1911(7)	0.882(4)	0.077(5)
N12	0.0229(10)	0.1037(10)	0.344(4)	0.127(10)
N13	0.2028(6)	0.4978(7)	0.864(3)	0.038(3)
N14	0.1448(9)	0.0043(10)	0.6843(18)	0.068(4)
N15	0.2685(15)	0.2978(17)	0.689(2)	0.045(5)

TABLE S4-III. Atomic coordinates in (*R*)-GN under 3 kbar.

	<i>x</i>	<i>y</i>	<i>z</i>	$U_{eq} / \text{\AA}^2$
C1	0.694(2)	0.3357(16)	0.2913(16)	0.019(5)
C2	0.6821(19)	0.1514(16)	0.2165(16)	0.015(5)
C3	0.3175(19)	0.3324(16)	0.3157(16)	0.019(5)
C4	0.517(3)	0.187(2)	0.3853(16)	0.040(6)
C5	0.485(2)	0.3101(16)	0.1388(14)	0.026(5)
C6	0.298(2)	0.1516(17)	0.2336(16)	0.022(5)
C7	0.0362(18)	-0.0851(17)	0.4003(14)	0.020(5)
H7A	0.1608	-0.0711	0.3905	0.024
C8	0.006(3)	-0.1884(17)	0.3814(14)	0.035(5)
H8A	-0.1056	-0.2067	0.4057	0.053
H8B	0.0978	-0.2237	0.4094	0.053
H8C	0.0072	-0.199	0.3173	0.053
C9	-0.007(3)	-0.071(2)	0.5027(15)	0.044(5)
H9A	-0.1341	-0.0703	0.5089	0.053
H9B	0.0348	-0.1253	0.5349	0.053
Cr1	0.4977(5)	0.2428(2)	0.2625(2)	0.0135(11)
Mn1	-0.0095(2)	-0.0081(2)	0.19260(18)	0.0145(10)
N1	0.536(3)	0.144(2)	0.4513(18)	0.076(7)
N2	0.475(2)	0.3495(15)	0.0737(14)	0.043(5)
N3	0.1932(17)	0.0962(16)	0.2182(14)	0.031(4)
N4	0.1970(18)	-0.1145(15)	0.1874(14)	0.025(4)
N5	-0.2193(16)	0.0926(15)	0.1957(14)	0.025(4)
N6	-0.2153(18)	-0.1132(16)	0.1649(14)	0.032(5)
N7	-0.0680(15)	-0.0217(15)	0.3480(13)	0.029(4)
N8	0.0629(18)	0.010(2)	0.5483(15)	0.048(5)
O1	0.0544(11)	0.0106(13)	0.0471(10)	0.027(3)
O2	-0.008(3)	0.165(2)	0.4313(19)	0.124(8)

Chapter V. Preparation, Crystal Structure, and Magnetic Properties of a New Dithiolene Ligand, 1,3,2-Dithiazole-4-thione-5-thiolate and its Metal Complex

5-1. INTRODUCTION

Metal Dithiolene Complex

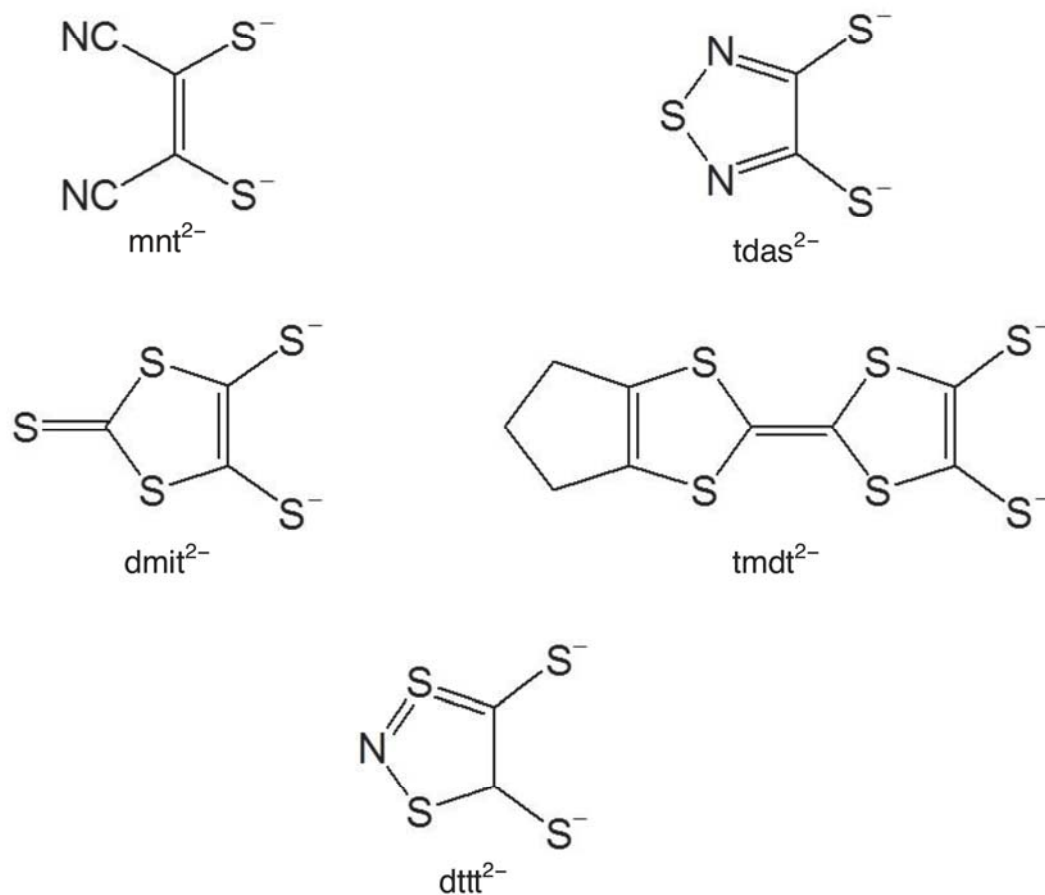
Metal 1,2-dithiolene complexes have attracted a great deal of interest as precursors for functional molecular materials [1]. The central metal atom, its oxidation state, counter-cation, and organic components of the ligand leads can be appropriately selected to result in a variety of physical properties. For example, $\text{NH}_4[\text{Ni}(\text{mnt})_2] \cdot \text{H}_2\text{O}$ [mnt = 1,2-maleonitrile-1,2-dithiolate] becomes an insulating ferromagnet below 4.5 K [2], while $(\text{Me}_4\text{N})[\text{Ni}(\text{dmit})_2]_2$ [dmit = 1,3-dithiolene-2-thione-4,5-dithiolate] shows superconducting properties below 5 K under 7 kbar [3]. The first single-component molecular conductor, $\text{Ni}(\text{tmdt})_2$ [tmdt = trimethylenetetrafulvalenedithiolate], was recently discovered [4]. It was also reported that $\text{Pd}(\text{dmit})_2$ derivatives with geometrical frustration displayed new quantum phenomena [5]. Strong intermolecular interactions may impart interesting physical properties in these materials.

Sulfur-Nitrogen (S-N) Ring

Sulfur-nitrogen (S–N) rings enhance strong intermolecular interactions in the solid state because of their characteristic intermolecular S···N and/or S···S contacts [6]. For example, organic compounds with the S–N ring moieties are very attractive as building blocks in molecule-based magnets and conductors [7-11]. In 1990, Underhill et al. synthesized metal dithiolene complexes with 1,2,5-thiadiazole rings, $[M(\text{tdas})_2]^{n-}$ [tdas = 1,2,5-thiazole-3,4-dithiolate], where $M = \text{Ni}^{\text{II}}, \text{Pd}^{\text{II}}, \text{Pt}^{\text{II}}$ and Cu^{II} ($n = 2$) and $M = \text{Fe}^{\text{III}}$ ($n = 1$) [12]. Subsequently, crystal structures of tetraalkylammonium and tetrabutylphosphonium salts of $\text{Ni}(\text{tdas})_2$ and $\text{Fe}(\text{tdas})_2$ were reported [13, 14]. It is also noteworthy that $(\text{Bu}_4\text{N})[\text{Fe}(\text{tdas})_2]$ showed a peculiar phase transition with reentrant magnetism [14]. Furthermore, the unique pressure effect, such as that was investigated in $\text{BBDTA} \cdot \text{InCl}_4$ [15], is also expected in organic thiazyl radicals.

This Work

In this work, the author focuses on the preparation of a new dithiolene ligand with a S–N ring, 1,3,2-dithiazole-4-thione-5-thiolate (dttt^-) (Scheme 5-1). The preparation, molecular structure and properties of a 1:1 salt of the ligand with a tetrabutylammonium cation (TBA^+), $\text{TBA} \cdot \text{dttt}$ (**1**), and the crystal structure and magnetic properties of its chromium complex $\text{Cr}(\text{dttt})_3 \cdot \text{CS}_2$ (**2**) is reported in this Chapter.

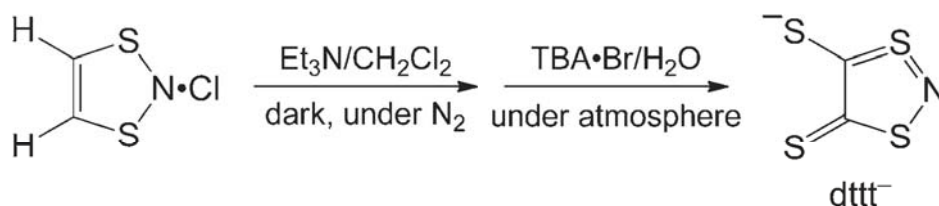


SCHEME 5-1. Chemical structures of a new dithiolene ligand, 1,3,2-dithiazole-4-thione-5-thiolate (dttt⁻) and some known dithiolene ligands, where mnt²⁻ is 1,2-maleonitrile-1,2-dithiolate, tdas²⁻ is 1,2,5-thiazole-3,4-dithiolate, dmit²⁻ is 1,3-dithiolene-2-thione-4,5-dithiolate, and tmdt²⁻ is trimethylenetetraathiafulvalenedithiolate.

5-2. EXPERIMENTAL DETAILS

Preparation Methods of 1 and 2

Compound **1** was obtained through a synthetic method using 1,3,2-dithiazole-4-thione [16], with a minor modification as described in Scheme 5-2. The counteraction of dttt^- may be altered; for instance, a dttt^- salt with a tetraphenylphosphonium cation (TPP^+) was obtained when $\text{TPP}\cdot\text{Cl}$ was used instead of $\text{TBA}\cdot\text{Br}$ in the last step of Scheme 5-2. In this reaction, 5-ethyl-1,3,2-dithiazole-4-thione and triethylammonium chloride were identified as byproducts. The details of preparation method are shown below.



SCHEME 5-2. Synthetic procedure for dttt^- .

Trimethylsilylazide and tetrabutylammonium bromide were purchased from Tokyo Kasei Chemicals Co. Ltd. and other chemicals were purchased from Wako Chemicals Co. Ltd. NMR spectra were recorded on JEOL EX 270 (270 MHz ^1H NMR) spectrometers using tetramethylsilane as the internal standard. Element analyses were carried out by using CE-440F (EAI Co. Ltd.).

1: Triethylamine (24 mL, 0.17 mol) was added to a suspension of 1,3,2-dithiazolium chloride [17] (11.7 g, 0.084 mol) in dichloromethane (300 mL) under N₂ and protected from light. The color of the solution immediately changed to deep violet. The reaction mixture was stirred for 16 h at room temperature. After filtration of the reaction mixture and, evaporation of the solvent and residual Et₃N under atmospheric conditions, the resultant residual black solid was dissolved in water (200 mL), and TBA•Br (10 g) was added. The resultant black precipitate of **1** was filtered, and dried under vacuum (yield: 1.6 g; 5.0 %). Single crystals of **1** were obtained as dark purple blocks with metallic luster, by layering diethylether over an acetone solution of **1**.

¹H NMR (CDCl₃, 270 MHz): d (ppm) 3.25 (*t*, *J* = 8.1 Hz, 8 H), 1.65-1.57 (m, 8H), 1.50-1.30 (m, 8H), 0.99 (*t*, *J* = 8.1 Hz, 12 H).

Anal. Calcd. for C₁₈H₃₆N₂S₄: C, 52.88; H, 8.88; N, 6.85 Found C, 52.60; H, 8.86; N, 6.67.

2: CrCl₃•6H₂O (0.13 g, 0.49 mmol) and **1** (0.61 g, 1.35 mmol) were mixed in EtOH (100 mL) at room temperature to form a black precipitate, **2** (yield: 0.20 g; 75 %). The crude product was dissolved in CS₂ and slow evaporation of the solvent gave black block crystals.

Anal. Calcd. for C₇CrN₃S₈: C, 13.41; H, 0.00; N, 6.70. Found C, 14.00; H, 0.14; N, 6.83.

Molecular orbital calculations for dttt^- were carried out using Gaussian 09 program [18].

TABLE 5-I. Cartesian coordinate of input geometry of dttt^- and key words.

b3lyp/6-31+g(d) geom=connectivity					
spin multiplicity = 1, charge = -1					
Center Number	Atomic Number	Atomic Type	Coordinates / Å		
			X	Y	Z
1	6	0	-0.330827	-0.730515	-0.000025
2	6	0	-0.330824	0.730517	0.000015
3	7	0	2.261140	-0.000006	0.000024
4	16	0	-1.666075	-1.765211	-0.000067
5	16	0	-1.666067	1.765219	0.000031
6	16	0	1.295511	1.360054	0.000053
7	16	0	1.295502	-1.360060	-0.000024

UV-Vis Spectrum of 1

UV-Vis absorption spectroscopy in solution of **1** was recorded on a Shimadzu UV-160 Spectrophotometer. A solution (9.64×10^{-4} M) of **1** in a 1 cm quartz cell in dry acetonitrile under atmosphere was used for the measurement.

ESR Spectrum of 1

ESR spectroscopy in single crystals of **1** was recorded on a Bruker EMX Spectrophotometer (X-band). Measurement conditions were as follows; Power 0.1 mW, Modulation 1 G, Field 3146.2 to 3646 G, Time constant 0.01 s. No signal was observed in the measurement range at room temperature.

X-ray Measurements and Analyses of 1 and 2

X-ray diffraction data were collected with graphite-monochromated Mo-K α ($\lambda = 0.71073$ Å) radiation on a RIGAKU Mercury CCD diffractometer. All structures were solved by a direct method using the SHELXS-90 program [19] and refined by successive differential Fourier syntheses and a full-matrix least-squares procedure using the SHELXL-97 program [20]. Anisotropic thermal factors were applied to all non-hydrogen atoms.

Magnetic Susceptibility Measurements of 1 and M-H Curve Measurement of 2

Magnetic measurements of **1** and **2** were carried out for a powder sample on a SQUID (Quantum Design MPMS XL) magnetometer in a cooling mode with a cooling rate of -5 K min $^{-1}$. Temperature dependence of the dc susceptibility was measured under 500 and 1000 Oe for **1** and **2**, respectively.

The χ_p values were obtained from the dc susceptibility, subtracting the diamagnetic susceptibility including a sample holder, -0.000346 and -0.000759 emu K mol $^{-1}$ for **1** and **2**, respectively, evaluated by assuming that χ_p follows the Curie-Weiss law within the temperature range of 10 – 300 K [21]. Field dependence of magnetization of **2** was carried out at 2 K.

5-3. RESULTS & DISCUSSION

5-3-1. Crystal Structure and Physical Properties of TBA·dttt (1)

Crystal Structure of 1

The chemical formula and structure of **1** were determined by single-crystal X-ray structure analysis, elemental analysis, and NMR spectroscopy. Crystallographic data of **1** is shown in Table 5-II. The obtained crystal was found to include dttt units and TBA units at a molar ratio of 1:1. Although almost all dithiolene ligands are divalent anions [1], this dttt unit is a monovalent anion. Fig. 5-1 shows the crystal structure of **1**, which crystallized in the monoclinic $P2_1$ space group with two dttt[−] anions and two TBA⁺ cations that are crystallographically independent. Fig. 5-1(a) shows the molecular alignment of **1**. There were no intermolecular short contacts between the dttt[−] anions because the bulky TBA fragment prevented the dttt[−] anions to interact with each other. The dttt[−] anion was found to possess a planar molecular structure. The bond lengths and bond angles in independent dttt[−] anions are shown in Table 5-III and 5-IV, respectively.

TABLE 5-II. Crystallographic data of **1**.

Formula, F_w	$C_{18}H_{36}N_2S_4$, 408.76	$D_{\text{calcd.}} / \text{g cm}^{-3}$	1.199
Crystal shape, color	block, purple	μ / mm^{-1}	0.424
Crystal system	monoclinic	Index range	$-10 \leq h \leq 9$
Space group	$P2_1$		$-16 \leq k \leq 16$
$a / \text{\AA}$	8.5728(13)		$-27 \leq l \leq 27$
$b / \text{\AA}$	12.9355(13)	Reflection collected	8342
$c / \text{\AA}$	21.224(3)	GOF	1.000
$\beta / ^\circ$	106.298(7)	R	0.0527
$V / \text{\AA}^3$	2259.0(5)	wR	0.0921
Z	4	T / K	120

Table 5-III. Bond lengths in independent dtt^- anions of **1**.

atom	atom	distance / \AA	atom	atom	distance / \AA
S1	C17	1.682(3)	S3	N4	1.632(3)
S2	N1	1.640(3)	S3	C21	1.711(3)
S2	C18	1.713(3)	S6	C20	1.681(3)
S4	N1	1.635(3)	S7	C21	1.675(3)
S4	C17	1.715(3)	S8	N4	1.633(3)
S5	C18	1.689(3)	S8	C20	1.713(3)
C17	C18	1.436(4)	C20	C21	1.445(4)

Table 5-IV. Bond angles in independent dttt^- anions of **1**.

atom	atom	atom	angle / °	atom	atom	atom	angle / °
N1	S2	C18	103.89(15)	N4	S3	C21	104.57(16)
N1	S4	C17	104.40(15)	N4	S8	C20	103.95(15)
C18	C17	S1	128.1(2)	C21	C20	S6	126.9(2)
C18	C17	S4	110.7(2)	C21	C20	S8	111.4(2)
S1	C17	S4	121.17(18)	S6	C20	S8	121.75(19)
C17	C18	S5	126.9(2)	C20	C21	S7	127.3(2)
C17	C18	S2	111.6(2)	C20	C21	S3	110.5(2)
S5	C18	S2	121.53(18)	S7	C21	S3	122.20(19)
S4	N1	S2	109.41(16)	S3	N4	S8	109.62(16)

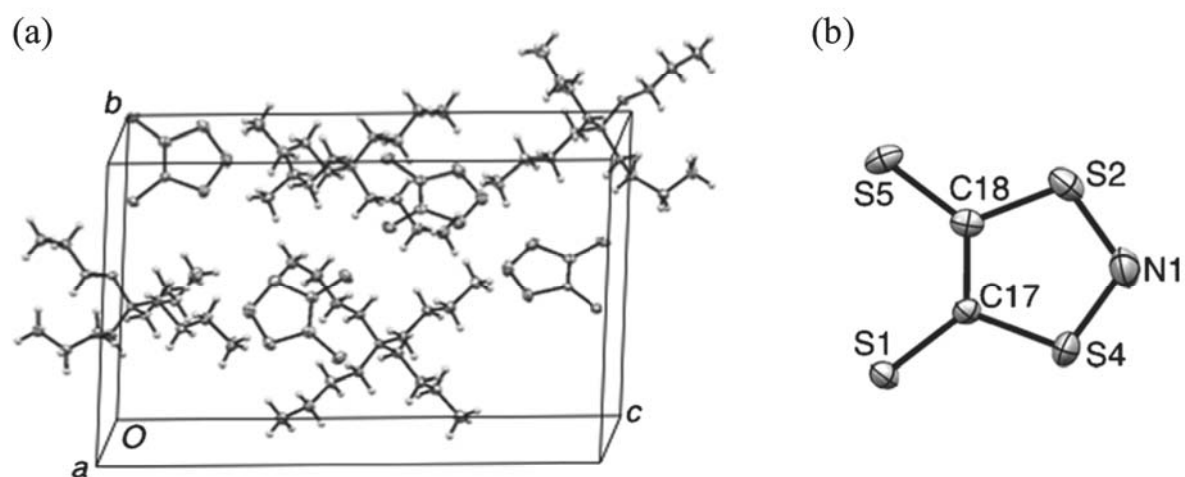


FIGURE 5-1. Crystal structure of **1**. Thermal ellipsoids are drawn at the 50 % probability level; hydrogen atoms are shown as spheres of an arbitrary size. **(a)** Molecular alignment and **(b)** molecular structure of dttt^- .

Physical Properties of **1**

The mechanism of the reaction in Scheme 5-2 is yet to be elucidated and requires further investigation; however, it is known that this reaction is initiated by Et₃N abstracting a proton from 1,3,2-dithiazolium chloride and that the exocyclic sulfur atoms of dttt⁻ must originate from another 1,3,2-dithiazolium cation.

Compound **1** was found to be stable in its crystalline state and in solution in solvents such as water, methanol, acetone, acetonitrile, and dichloromethane under atmospheric conditions. Stable 1,3,2-dithizole derivatives are usually neutral or positively charged [22]. Therefore, **1** is a rare anion example, which contains a closed-shell electron configuration, as inferred by molecular orbital calculations (Fig. 5-2), ESR spectroscopy, and magnetic measurements (Fig. 5-3). UV-Vis spectrum in solution of **1** is shown in Fig. 5-4. Solutions of **1** were deep purple or blue ($\lambda_{\text{max}} = 587 \text{ nm}$, $\epsilon = 475 \text{ dm}^3\text{mol}^{-1}\text{cm}^{-1}$ in acetonitrile).

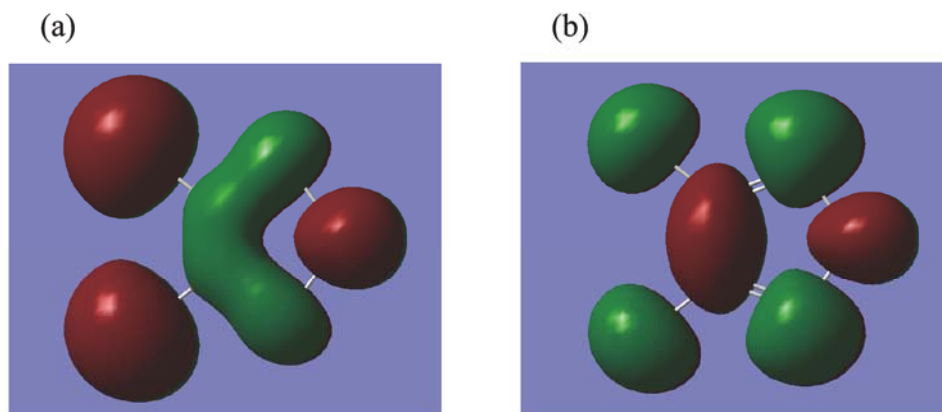


FIGURE 5-2. (a) HOMO and (b) LUMO of dttt⁻. The eigenvalues are -0.05007 Hartree and 0.03436 Hartree, respectively.

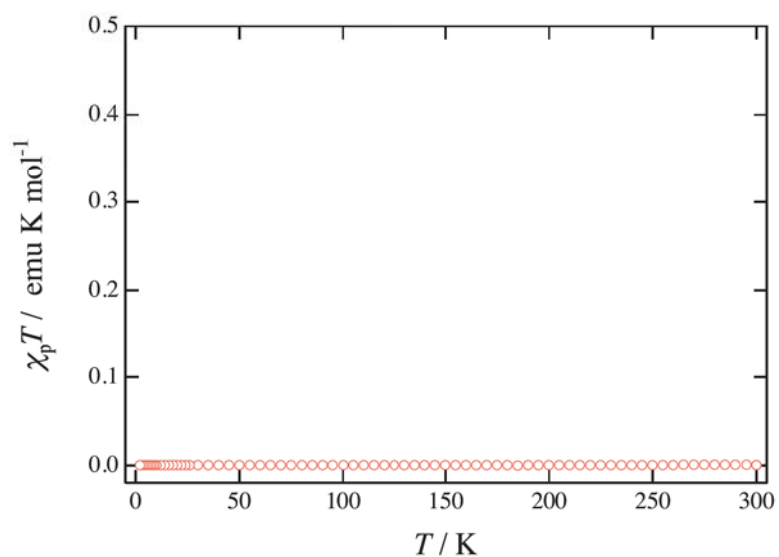


FIGURE 5-3. Temperature dependence of $\chi_p T$ of **1**.

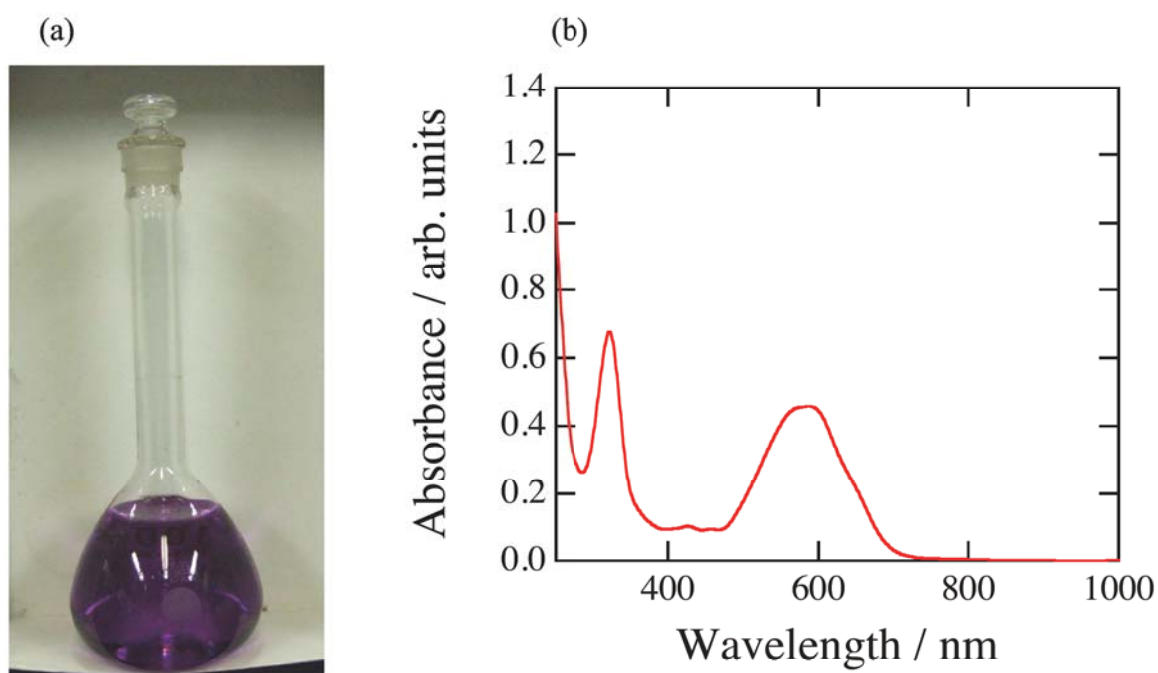


FIGURE 5-4. (a) The photo and (b) UV-Vis spectrum of an acetonitrile solution of **1**.

5-3-2. Crystal Structure and Magnetic Property of $\text{Cr}(\text{dttt})_3 \cdot \text{CS}_2$ (**2**)

Crystal Structure of 2

The author successfully prepared the chromium complex of dttt^- , **2**, and its composition and structure were determined by X-ray structure and elemental analyses. Crystallographic data of **2** is shown in Table 5-V. The crystals included Cr^{III} , dttt^- , and CS_2 as the crystal solvent at a molar ratio of 1:3:1. Fig. 5-5 shows the structure of **2**, which crystallized in the monoclinic $P2_1/c$ space group with one Cr^{III} ion, three dttt^- anions, and one CS_2 molecule that were crystallographically independent. Fig. 5-5(a) shows the molecular structure of **2**. The dttt^- ligand was found to coordinate with the chromium ion, and the complex exhibited an octahedral geometry with the chromium ion surrounded by six exocyclic sulfur atoms from the three dttt^- anions. Fig. 5-4(b) shows two adjacent molecules in this crystal. Between the two molecules, there were three $\text{S} \cdots \text{S}$ and two $\text{S} \cdots \text{C}$ interatomic contacts that were found to be shorter than the sums of the van der Waals radii, 3.60 and 3.50 Å, for interatomic $\text{S} \cdots \text{S}$ and $\text{S} \cdots \text{C}$ distances, respectively [23]. The interatomic $\text{S} \cdots \text{S}$ distances were 3.3654(17), 3.3654(17) and 3.3786(13) Å and the $\text{S} \cdots \text{C}$ distances were 3.466(3) and 3.466(3) Å. The short interatomic contacts indicate that a dimer may have formed. Additionally, many intermolecular interatomic $\text{S} \cdots \text{S}$, $\text{S} \cdots \text{C}$ or $\text{S} \cdots \text{N}$ contacts were found to surround the dimer in the bc plane. The intermolecular distances of **2** are summarized in Table 5-VI. The average values of these interatomic distances were 3.45, 3.43 and 3.27 Å for twenty-two $\text{S} \cdots \text{S}$, four $\text{S} \cdots \text{C}$ and four $\text{S} \cdots \text{N}$ contacts, respectively (the sum of the van der Waals radii was 3.35 Å for the $\text{S} \cdots \text{N}$ distance) [23]. These interdimer contacts seem to construct a multidimensional magnetic network, although the interdimer interactions are weaker than the intradimer interaction. Moreover, an exchange magnetic interaction is expected between the molecules.

Table 5-V. Crystallographic data of **2**.

Formula, F_w	$C_7CrN_3S_8$	$D_{\text{calcd.}} / \text{g cm}^{-3}$	2.065
Crystal shape, color	block, black	μ / mm^{-1}	2.017
Crystal system	monoclinic	Index range	$-17 \leq h \leq 16$
Space group	$P2_1/c$		$-14 \leq k \leq 14$
$a / \text{\AA}$	13.167(4)		$-17 \leq l \leq 17$
$b / \text{\AA}$	11.287(3)	Reflection collected	14755
$c / \text{\AA}$	14.273(5)	GOF	1.101
$\beta / ^\circ$	108.090(4)	R	0.0410
$V / \text{\AA}^3$	2016.3(11)	wR	0.0919
Z	4	T / K	173

Table 5-VI. Intermolecular distances of **2**.

atom	atom	distance / \AA	atom	atom	distance / \AA
S2	S5 ¹	3.4345(9)	S3	S3 ²	3.3766(8)
S3	S5 ³	3.4102(8)	S3	S11 ²	3.3624(10)
S3	N26 ³	3.5258(19)	S4	S15 ⁴	3.4988(10)
S5	S2 ⁵	3.4345(9)	S5	S3 ⁶	3.4102(8)
S5	S7 ⁶	3.3846(8)	S5	C21 ⁵	3.592(3)
S5	C23 ⁵	3.425(3)	S6	S7 ⁶	3.5302(9)
S6	S8 ⁵	3.4169(9)	S7	S5 ³	3.3846(8)
S7	S6 ³	3.5302(9)	S8	S6 ¹	3.4169(9)
S9	S11 ⁶	3.5444(10)	S9	S14 ⁶	3.4521(10)
S10	N18 ⁷	3.379(2)	S10	N26 ¹	3.269(3)

S10	C25 ⁸	3.496(4)	S11	S3 ²	3.3624(10)
S11	S9 ³	3.5444(10)	S11	C17 ²	3.463(2)
S11	C20 ²	3.563(2)	S12	N22 ⁹	3.452(3)
S13	N18 ⁶	3.543(3)	S13	N26 ¹	3.398(2)
S13	C25 ¹⁰	3.587(3)	S14	S9 ³	3.4521(10)
S14	N22 ⁸	3.573(3)	S15	S4 ¹⁰	3.4988(10)
N18	S10 ⁹	3.379(2)	N18	S13 ³	3.543(3)
N22	S12 ⁷	3.452(3)	N22	S14 ⁸	3.573(3)
N22	N26 ¹	3.245(4)	N26	S3 ⁶	3.5258(19)
N26	S10 ⁵	3.269(3)	N26	S13 ⁵	3.398(2)
N26	N22 ⁵	3.245(4)	N26	C21 ⁵	3.458(3)
N26	C23 ⁵	3.396(3)	C17	S11 ²	3.463(2)
C20	S11 ²	3.563(2)	C21	S5 ¹	3.592(3)
C21	N26 ¹	3.458(3)	C23	S5 ¹	3.425(3)
C23	N26 ¹	3.396(3)	C25	S10 ⁸	3.496(4)
C25	S13 ⁴	3.587(3)			

Symmetry Operators:

- | | |
|-----------------------------|------------------------------|
| (1) $-X+1, Y+1/2-1, -Z+1/2$ | (2) $-X+1, -Y+1, -Z$ |
| (3) $X, -Y+1/2, Z+1/2-1$ | (4) $-X+2, Y+1/2, -Z+1/2$ |
| (5) $-X+1, Y+1/2, -Z+1/2$ | (6) $X, -Y+1/2, Z+1/2$ |
| (7) $X, Y-1, Z$ | (8) $-X+2, -Y, -Z$ |
| (9) $X, Y+1, Z$ | (10) $-X+2, Y+1/2-1, -Z+1/2$ |

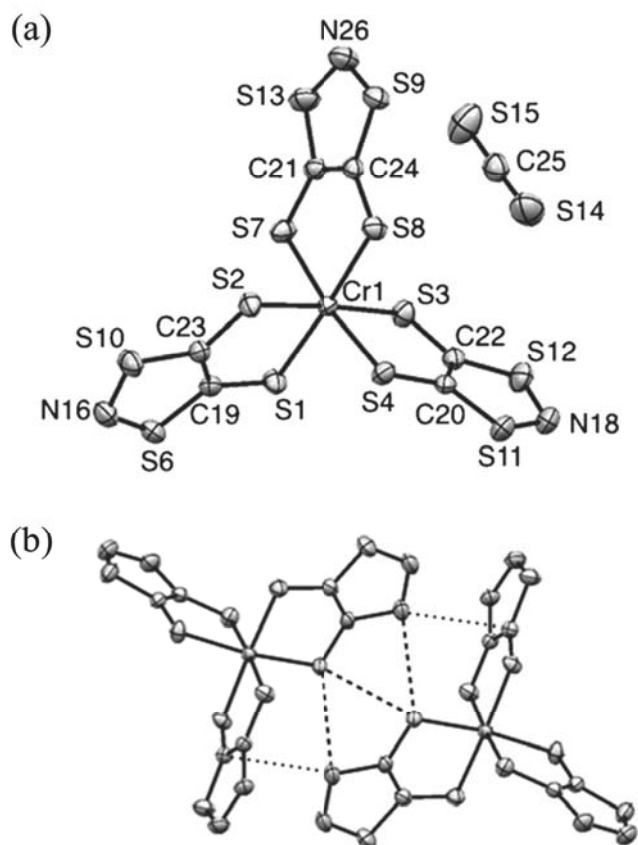


FIGURE 5-5. Crystal structure of the chromium complex **2**. **(a)** Molecular structure. **(b)** Molecular orientation and intermolecular interatomic short contacts of the dimer. Broken and dashed lines represent short interatomic S \cdots S and S \cdots C contacts, respectively. Thermal ellipsoids are drawn at the 50% probability level.

Figure 5-6(a) shows the temperature dependence of the product of the paramagnetic susceptibility χ_p and temperature T in **2**. The $\chi_p T$ value increases with a decrease in temperature down to approximately 5 K but subsequently decreases with a further decrease in temperature. This observation suggests the dominance of ferromagnetic interactions in the dimer and weak antiferromagnetic interactions between the dimers. The Curie and Weiss constants [24] were 2.006 emu K mol⁻¹ and +1.8 K, respectively, thus suggesting that the complex has a spin value $S = 3/2$ and a g -factor of $g = 2.069$; these values are typical for octahedral Cr^{III} complexes [25]. Field dependence of magnetization of **2** at 2 K is shown in Fig. 5-6(b). The value of magnetization at 2 K under 70 kOe was 16638 erg Oe⁻¹ mol⁻¹, which corresponds to the theoretical value of saturation magnetization for the aforementioned S and g values. A Cr^{III} compound in an octahedral environment has a small zero-field splitting of $|D|/k_B < 1$ K; this effect is negligible and can be ignored under these experimental conditions. Based on the structure, we interpreted the magnetic data using an $S = 3/2$ dimer model [26], modified by the addition of a simple mean-field approximation [27] to account for weak interdimer magnetic interactions, as follows:

$$\chi_p = \frac{\chi_{\text{dimer}}}{1 - \frac{2zJ'}{Ng^2\mu_B^2}\chi_{\text{dimer}}} \quad (1),$$

where

$$\chi_{\text{dimer}} = \frac{Ng^2\mu_B^2}{k_B T} \frac{14 + 5 \exp(6y) + \exp(10y)}{7 + 5 \exp(6y) + 3 \exp(10y) + \exp(12y)} \quad (2)$$

and

$$y = -\frac{J}{k_B T} \quad (3)$$

in which J and J' are the intradimer and the interdimer magnetic coupling constants, respectively, z is the number of the nearest neighbors, N is the Avogadro constant, k_B is the Boltzmann constant, and m_B is the Bohr magneton. The solid curve in Figure 5-6(a) is the theoretical best-fit with the parameters $J/k_B = +1.2$ K and $zJ'/k_B = -0.5$ K ($z = 8$). The result agrees with the structure. However, the magnetic interactions in this material were found to be very weak despite the short intermolecular S \cdots S, S \cdots C and S \cdots N contacts. Hence, this chromium complex may exhibit a lower spin delocalization from the metal atom to the ligands.

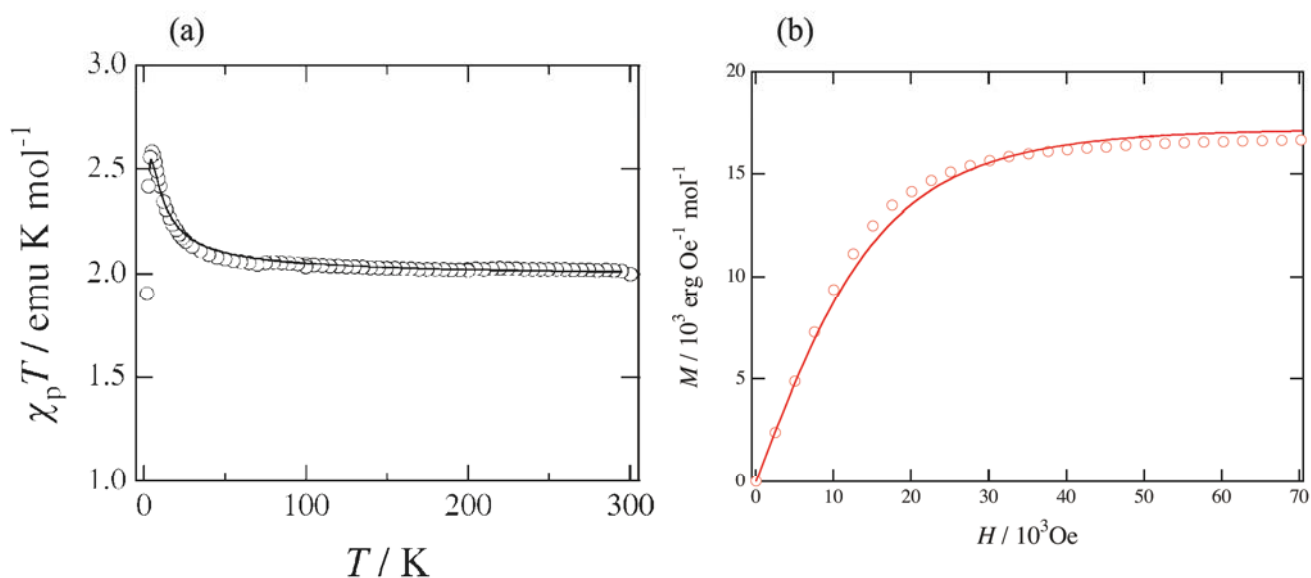


FIGURE 5-6. (a) Temperature dependence of the product of the paramagnetic susceptibilities and temperature, $\chi_p T$, of **2**. The solid line shows the theoretical best-fit of the $S = 3/2$ dimer model modified by a molecular field correlation. (b) Field dependence of magnetization of **2** at 2 K. the solid line shows the theoretical value for $S = 3/2$ and $g = 2.069$.

5-4. CONCLUSION

The author studied the preparation, crystal structure, and magnetic properties of the new dithiolene ligand **1** and its chromium tris(dithiolene) complex **2**. The author believes that dithiolene complexes of the new ligand will lead to an available functionality. Further investigations on preparing complexes of dttt^- including other metal ions and their partially oxidized compounds are currently in progress. Furthermore, the author also plans to the magnetic measurement and crystal structural analysis under pressure for complex **2**.

5-5. REFERENCES

- [1] *Dithiolene Chemistry: Synthesis, Properties, Applications: Prog. Inorg. Chem. Vol. 52* (Ed.: E. I. Stiefel), Wiley, NJ, (2004).
- [2] A. T. Coomber, D. Beljonne, R. H. Friend, J. L. Brédas, A. Charlton, N. Robertson, A. E. Underbill, M. Kurmoo and P. Day, *Nature* 380 (1996) 144.
- [3] A. Kobayashi, H. Kim, Y. Sasaki, R. Kato, H. Kobayashi, S. Moriyama, Y. Nishio, K. Kajita and W. Sasaki, *Chem. Lett.* (1987) 1819.
- [4] H. Tanaka, Y. Okano, H. Kobayashi, W. Suzuki and A. Kobayashi, *Science* 291 (2001) 285.
- [5] a) T. Itou, A. Oyamada, S. Maegawa and R. Kato, *Nat. Phys.* 6 (2010) 673.
b) M. Yamashita, N. Nakata, Y. Senshu, M. Nagata, H. M. Yamamoto, R. Kato, T. Shibauchi and Y. Matsuda, *Science* 328 (2010) 1246.
c) S. Yamashita, T. Yamamoto, Y. Nakazawa, M. Tamura and R. Kato, *Nat. Commun.* 2 (2011) 275.
d) D. Watanabe, M. Yamashita, S. Tonegawa, Y. Oshima, H. M. Yamamoto, R. Kato, I. Sheikin, K. Behnia, T. Terashima, S. Uji, T. Shibauchi and Y. Matsuda, *Nat. Commun.* 3 (2012) 1090.
- [6] J. M. Rawson, A. J. Banister and I. Lavender, *Adv. Heterocycl. Chem.* 62 (1995) 137.
- [7] a) C. D. Bryan, A. W. Cordes, R. M. Fleming, N. A. George, S. H. Glarum, R. C. Haddon, R. T. Oakley, T. T. M. Palstra, A. S. Perel, L. F. Schneemeyer and J. V. Waszczak, *Nature* 365 (1993) 821.
b) C. M. Robertson, A. A. Leitch, K. Cvrkalj, D. J. T. Myles, R. W. Reed, P. A. Dube and R. T. Oakley, *J. Am. Chem. Soc.* 130 (2008) 14791.
c) K. Lakin, S. M. Winter, L. E. Downie, X. Bao, J. S. Tse, S. Desgreniers, R. A. Secco, P. A. Dube and R. T. Oakley, *J. Am. Chem. Soc.* 132 (2010) 16212.

- d) A. A. Leitch, K. Lakin, S. M. Winter, L. E. Downie, H. Tsuruda, J. S. Tse, M. Mito, S. Desgreniers, P. A. Dube, S. Zhang, Q. Liu, C. Jin, Y. Ohishi and R. T. Oakley, *J. Am. Chem. Soc.* **133** (2011) 6051.
- [8] a) G. Wolmershäuser, M. Schnauber and T. Wilhelm, *J. Chem. Soc. Chem. Commun.* (1984) 573.
 b) G. Wolmershäuser, G. Wortman and M. Schnauber, *J. Chem. Res. Synop.* (1988) 358.
 c) G. Wolmershäuser and R. Johann, *Angew. Chem Int. Ed.* **28** (1989) 920.
- [9] J. M. Rawson, A. Alberola and A. Whalley, *J. Mater. Chem.* **16** (2006) 2560.
- [10] S. Brownridge, H. Du, S. A. Fairhurst, R. C. Haddon, H. Oberhammer, S. Parsons, J. Passmore, M. J. Schriver, L. H. Sutcliffe and N. P. C. Westwood, *Dalton Trans.* (2000) 3365.
- [11] a) W. Fujita and K. Awaga, *Science* **286** (1999) 261.
 b) W. Fujita and K. Awaga, *J. Am. Chem. Soc.* **123** (2001) 3601.
 c) H. Matsuzaki, W. Fujita, K. Awaga and H. Okamoto, *Phys. Rev. Lett.* **91** (2003) 017403.
 d) W. Fujita and K. Awaga, *Chem. Phys. Lett.* **388** (2004) 186.
 e) W. Fujita, R. Kondo, S. Kagoshima and K. Awaga, *J. Am. Chem. Soc.* **128** (2006) 6016.
 f) W. Fujita, K. Kikuchi and K. Awaga, *Angew. Chem. Int. Ed.* **47** (2008) 9480.
 g) W. Fujita and K. Kikuchi, *Chem. Asian J.* **4** (2009) 400.
 h) K. Suzuki, T. Kodama, K. Kikuchi and W. Fujita, *Chem. Lett.* **39** (2010) 1096.
 i) W. Fujita, K. Takahashi and H. Kobayashi, *Cryst. Growth Des.* **11** (2011) 575.
- [12] I. Hawkins and A. E. Underhill, *J. Chem. Soc. Chem. Commun.* (1990) 1593.
- [13] a) O. A. Dyachenko, S. V. Konovalikhin, A. I. Kotov, G. V. Shilov, E. B. Yabuskii, C. Faulmann and P. Cassoux, *J. Chem. Soc. Chem. Commun.* (1993) 508.
 b) S. Schenk, I. Hawkins, S. B. Wilkes, A. E. Underhill and A. Kobayashi, *J. Chem. Soc. Chem. Commun.* (1993) 1648.
- [14] K. Awaga, T. Okuno, Y. Maruyama, A. Kobayashi, H. Kobayashi, S. Schenk and A. E. Underhill, *Inorg. Chem.* **33** (1994) 5598.

- [15] M. Mito, S. Kawagoe, H. Deguchi, S. Takagi, W. Fujita, K. Awaga, R. Kondo, and S. Kagoshima, *J. Phys. Soc. Jpn* 78 (2009) 124705.
- [16] M. A. Gray and C. W. Rees, *J. Chem. Soc. Perkin Trans. I* (1993) 3077.
- [17] J. L. Morris and C. W. Rees, *J. Chem. Soc. Perkin Trans. I* (1987) 211.
- [18] Gaussian 09, Revision A.02, M. J. Frisch, G. W. Trucks, H. B. Schlegel, G. E. Scuseria, M. A. Robb, J. R. Cheeseman, G. Scalmani, V. Barone, B. Mennucci, G. A. Petersson, H. Nakatsuji, M. Caricato, X. Li, H. P. Hratchian, A. F. Izmaylov, J. Bloino, G. Zheng, J. L. Sonnenberg, M. Hada, M. Ehara, K. Toyota, R. Fukuda, J. Hasegawa, M. Ishida, T. Nakajima, Y. Honda, O. Kitao, H. Nakai, T. Vreven, J. A. Montgomery, Jr., J. E. Peralta, F. Ogliaro, M. Bearpark, J. J. Heyd, E. Brothers, K. N. Kudin, V. N. Staroverov, R. Kobayashi, J. Normand, K. Raghavachari, A. Rendell, J. C. Burant, S. S. Iyengar, J. Tomasi, M. Cossi, N. Rega, J. M. Millam, M. Klene, J. E. Knox, J. B. Cross, V. Bakken, C. Adamo, J. Jaramillo, R. Gomperts, R. E. Stratmann, O. Yazyev, A. J. Austin, R. Cammi, C. Pomelli, J. W. Ochterski, R. L. Martin, K. Morokuma, V. G. Zakrzewski, G. A. Voth, P. Salvador, J. J. Dannenberg, S. Dapprich, A. D. Daniels, O. Farkas, J. B. Foresman, J. V. Ortiz, J. Cioslowski and D. J. Fox, Gaussian, Inc., Wallingford CT, (2009).
- [19] G. M. Sheldrick, *Acta Crystallogr. A* 46 (1990) 467.
- [20] G. M. Sheldrick, SHELEXS-97, University of Göttingen, Germany (1997).
- [21] R. L. Carlin, *Magnetochemistry*, Springer-Verlag, New York, (1985).
- [22] R. T. Boéré and T. L. Roemmele, *Coord. Chem. Rev.* 210 (2000) 369.
- [23] J. E. Huheey, E. A. Keiter and R. L. Keiter, *Inorganic Chemistry 4th Ed.*, HarperCollins College Publishers, New York (1993).
- [24] R. L. Carlin, *Magnetochemistry*, Springer, New York (1985).
- [25] S. F. A. Kettle, *Physical Inorganic Chemistry*, Oxford University Press, Oxford (1998).
- [26] J. T. Veal, W. E. Hatfield, D. Y. Jeter, J. C. Hempel and D. J. Hodgson, *Inorg. Chem.* 12 (1973) 342.

[27] O. Kahn, *Molecular Magnetism*, Wiley-VCH, New York (1993).

5-6. APPENDIX

TABLE S5-I. Atomic coordinates in **1**.

atom	<i>x</i>	<i>y</i>	<i>z</i>	$U_{\text{eq}} / \text{\AA}^2$
S1	0.92006(9)	0.86433(6)	0.04931(4)	0.02259(16)
S2	0.83746(10)	1.09380(6)	0.18027(4)	0.0318(2)
S4	0.96582(11)	0.90409(7)	0.19066(4)	0.0333(2)
S5	0.75703(9)	1.11315(6)	0.03529(4)	0.02674(18)
C17	0.9018(3)	0.9425(2)	0.11014(14)	0.0190(6)
C18	0.8338(3)	1.0447(2)	0.10488(15)	0.0208(6)
N1	0.9219(4)	1.0016(3)	0.23161(14)	0.0397(8)
S3	0.05351(11)	0.46215(7)	0.30509(4)	0.0339(2)
S6	0.28803(10)	0.24010(7)	0.44734(4)	0.0334(2)
S7	0.14092(12)	0.48957(7)	0.44944(4)	0.0353(2)
S8	0.17298(11)	0.27209(7)	0.30332(4)	0.0323(2)
N2	1.2615(3)	-0.01107(19)	0.95274(11)	0.0142(5)
N3	0.7794(3)	0.3636(2)	0.54508(11)	0.0173(5)
C2	1.3104(3)	0.0853(2)	0.99568(13)	0.0163(6)
C24	0.9544(3)	0.3597(2)	0.58783(13)	0.0195(6)
H1	0.9786	0.4247	0.6113	0.023
H2	1.0246	0.3548	0.5592	0.023
C3	1.3608(3)	-0.0087(2)	0.90401(13)	0.0170(6)
H25	1.4749	-0.0088	0.9284	0.02
H26	1.3389	0.056	0.8801	0.02
C25	0.6593(3)	0.3670(2)	0.58640(13)	0.0179(6)

H3	0.5501	0.3705	0.5569	0.021
H4	0.6682	0.3027	0.6107	0.021
C4	1.0180(3)	0.0804(2)	0.87452(14)	0.0202(6)
H27	1.0639	0.0797	0.8376	0.024
H28	1.0511	0.144	0.8988	0.024
C5	1.0806(3)	-0.0116(2)	0.91865(13)	0.0167(6)
H69	1.0547	-0.0741	0.8925	0.02
H70	1.0228	-0.0146	0.9519	0.02
C26	0.7656(4)	0.4591(2)	0.50256(14)	0.0206(6)
H5	0.8512	0.4566	0.4809	0.025
H6	0.7854	0.5192	0.531	0.025
C6	1.2095(3)	0.1057(2)	1.04361(13)	0.0170(6)
H29	1.0997	0.1251	1.0195	0.02
H30	1.2041	0.0435	1.0684	0.02
C20	0.1994(4)	0.3144(2)	0.38213(15)	0.0233(7)
C7	1.1860(4)	0.2242(3)	1.13563(15)	0.0259(7)
H45	1.0783	0.2418	1.1097	0.039
H46	1.2348	0.2829	1.1613	0.039
H47	1.1806	0.1677	1.1643	0.039
C27	0.8338(4)	0.2479(3)	0.45423(15)	0.0246(7)
H7	0.9448	0.2295	0.4773	0.029
H8	0.8359	0.3104	0.4292	0.029
C28	0.6814(4)	0.4564(2)	0.63486(14)	0.0217(6)
H9	0.6669	0.5215	0.6113	0.026
H10	0.7905	0.4549	0.6645	0.026

C29	0.9982(3)	0.2727(2)	0.63747(14)	0.0209(6)
H11	0.9735	0.2067	0.6152	0.025
H12	0.9346	0.2786	0.6686	0.025
C8	1.2886(4)	0.1926(2)	1.09024(14)	0.0220(7)
H31	1.3038	0.2521	1.0648	0.026
H32	1.3949	0.1702	1.1166	0.026
C30	1.1786(3)	0.2779(2)	0.67376(15)	0.0243(7)
H13	1.2034	0.3454	0.694	0.029
H14	1.2415	0.2697	0.6425	0.029
C31	0.8481(4)	0.1334(3)	0.35923(16)	0.0309(8)
H48	0.8461	0.1912	0.3307	0.046
H49	0.7987	0.0747	0.3337	0.046
H50	0.9586	0.1173	0.3825	0.046
C32	0.7370(4)	0.2664(2)	0.50310(14)	0.0212(6)
H15	0.7516	0.2072	0.5322	0.025
H16	0.6227	0.2695	0.4791	0.025
C9	0.8330(3)	0.0758(2)	0.84961(14)	0.0224(7)
H33	0.8012	0.0142	0.8231	0.027
H34	0.7886	0.0708	0.8868	0.027
C10	1.2958(3)	-0.1092(2)	0.99392(13)	0.0171(6)
H35	1.247	-0.1671	0.9663	0.021
H36	1.2426	-0.1036	1.0285	0.021
C11	1.3319(3)	-0.0965(2)	0.85440(14)	0.0202(6)
H37	1.3551	-0.1622	0.8772	0.024
H38	1.2189	-0.0968	0.8285	0.024

C21	0.1365(4)	0.4178(2)	0.38327(15)	0.0227(6)
N4	0.0821(4)	0.3685(3)	0.25804(13)	0.0373(7)
C12	1.4410(4)	-0.0829(3)	0.80951(15)	0.0261(7)
H39	1.5536	-0.0876	0.8355	0.031
H40	1.424	-0.0144	0.7901	0.031
C13	1.5018(4)	-0.1917(2)	1.09023(14)	0.0219(6)
H41	1.4262	-0.2492	1.0838	0.026
H42	1.611	-0.2199	1.1029	0.026
C33	0.5768(4)	0.5332(3)	0.72482(16)	0.0319(8)
H51	0.6828	0.5289	0.7555	0.048
H52	0.4956	0.5258	0.7478	0.048
H53	0.5643	0.5991	0.7032	0.048
C34	0.4625(4)	0.5888(3)	0.35472(15)	0.0345(8)
H54	0.4395	0.5313	0.325	0.052
H55	0.4761	0.6501	0.3314	0.052
H56	0.3739	0.5983	0.3735	0.052
C35	0.7544(4)	0.1604(3)	0.40809(15)	0.0296(8)
H17	0.6447	0.1806	0.3843	0.036
H18	0.7473	0.0996	0.4339	0.036
C36	0.5569(4)	0.4474(3)	0.67403(15)	0.0281(7)
H19	0.4482	0.4504	0.6441	0.034
H20	0.5695	0.3809	0.6961	0.034
C37	0.6173(4)	0.5677(3)	0.40892(16)	0.0319(8)
H21	0.7057	0.5568	0.3894	0.038
H22	0.6436	0.628	0.437	0.038

C38	0.6048(4)	0.4745(3)	0.45050(15)	0.0261(7)
H23	0.5788	0.4134	0.423	0.031
H24	0.5187	0.4851	0.4713	0.031
C39	1.2282(4)	0.1945(3)	0.72657(16)	0.0296(7)
H57	1.1688	0.2038	0.7583	0.044
H58	1.3426	0.1997	0.7479	0.044
H59	1.2044	0.1276	0.7067	0.044
C14	0.7619(4)	0.1704(3)	0.80895(17)	0.0348(8)
H60	0.7939	0.2316	0.8349	0.052
H61	0.6455	0.1654	0.7954	0.052
H62	0.8014	0.1737	0.7709	0.052
C15	1.4748(3)	-0.1333(2)	1.02515(14)	0.0212(6)
H43	1.536	-0.0692	1.0329	0.025
H44	1.5153	-0.1748	0.995	0.025
C16	1.4093(4)	-0.1635(3)	0.75463(16)	0.0348(8)
H63	1.4231	-0.2315	0.7734	0.052
H64	1.4847	-0.1535	0.7292	0.052
H65	1.3003	-0.156	0.7268	0.052
C40	1.4790(4)	-0.1238(2)	1.14546(14)	0.0277(7)
H66	1.5474	-0.0639	1.1498	0.042
H67	1.5078	-0.162	1.1858	0.042
H68	1.3675	-0.1025	1.1356	0.042

TABLE S5-II. Atomic coordinates in **2**.

atom	<i>x</i>	<i>y</i>	<i>z</i>	$U_{\text{eq}} / \text{\AA}^2$
Cr1	0.65836(4)	0.24447(4)	0.15822(4)	0.02388(13)
S2	0.49256(7)	0.14358(7)	0.14001(6)	0.0321(2)
S3	0.81889(6)	0.35646(7)	0.17923(6)	0.0329(2)
S4	0.57156(6)	0.37315(7)	0.02324(6)	0.03032(19)
S5	0.62058(7)	0.36645(7)	0.27967(6)	0.0323(2)
S6	0.44300(7)	0.34992(7)	0.37079(6)	0.0337(2)
S7	0.76345(7)	0.11347(7)	0.28431(6)	0.0340(2)
S8	0.68771(7)	0.11359(7)	0.03877(6)	0.03208(19)
S9	0.82368(8)	-0.10382(8)	0.06483(7)	0.0410(3)
S10	0.34788(7)	0.15925(8)	0.26624(7)	0.0412(3)
S11	0.66162(8)	0.57292(8)	-0.06583(7)	0.0406(3)
S12	0.86280(8)	0.55428(8)	0.05624(8)	0.0457(3)
S13	0.88800(7)	-0.10311(8)	0.26249(7)	0.0426(3)
S14	0.93370(10)	0.23486(12)	-0.01899(9)	0.0671(4)
S15	1.06500(10)	0.08378(11)	0.15521(9)	0.0681(4)
N16	0.3464(3)	0.2556(3)	0.3503(3)	0.0401(8)
N18	0.7825(3)	0.6233(3)	-0.0374(3)	0.0457(8)
N26	0.8959(3)	-0.1687(3)	0.1642(3)	0.0464(8)
C19	0.5064(3)	0.3033(3)	0.2902(3)	0.0274(7)
C20	0.6747(3)	0.4627(3)	0.0180(3)	0.0271(7)
C21	0.8041(3)	0.0113(3)	0.2150(3)	0.0291(7)
C22	0.7792(3)	0.4542(3)	0.0833(3)	0.0300(7)
C23	0.4545(3)	0.2058(3)	0.2331(3)	0.0280(7)
C24	0.7707(3)	0.0115(3)	0.1107(3)	0.0273(7)
C25	0.9990(3)	0.1604(4)	0.0689(3)	0.0422(9)

TABLE S5-III. Bond lengths in **2**.

atom	atom	distance / Å
Cr1	S2	2.4037(12)
Cr1	S3	2.4004(11)
Cr1	S4	2.4000(11)
Cr1	S5	2.3840(12)
Cr1	S7	2.4069(10)
Cr1	S8	2.3764(12)
S2	C23	1.710(4)
S3	C22	1.709(4)
S4	C20	1.713(4)
S5	C19	1.712(4)
S6	N16	1.615(3)
S6	C19	1.701(4)
S7	C21	1.711(4)
S8	C24	1.697(3)
S9	N26	1.617(3)
S9	C24	1.701(4)
S10	N16	1.624(4)
S10	C23	1.698(4)
S11	N18	1.619(4)
S11	C20	1.698(4)
S12	N18	1.623(3)
S12	C22	1.703(4)
S13	N26	1.618(4)

S13	C21	1.697(3)
S14	C25	1.533(4)
S15	C25	1.535(4)
C19	C23	1.413(4)
C20	C22	1.405(5)
C21	C24	1.414(5)

TABLE S5-IV. Bond angles in **2**.

atom	atom	atom	angle / °
S2	Cr1	S3	176.32(4)
S2	Cr1	S4	90.56(4)
S2	Cr1	S5	87.97(4)
S2	Cr1	S7	94.69(4)
S2	Cr1	S8	88.42(4)
S3	Cr1	S4	87.88(4)
S3	Cr1	S5	88.83(4)
S3	Cr1	S7	87.17(4)
S3	Cr1	S8	94.81(4)
S4	Cr1	S5	94.55(4)
S4	Cr1	S7	172.70(5)
S4	Cr1	S8	86.75(5)
S5	Cr1	S7	90.71(5)
S5	Cr1	S8	176.18(4)
S7	Cr1	S8	88.32(4)

Cr1	S2	C23	101.36(11)
Cr1	S3	C22	101.61(12)
Cr1	S4	C20	101.87(10)
Cr1	S5	C19	102.17(12)
N16	S6	C19	101.42(16)
Cr1	S7	C21	101.08(11)
Cr1	S8	C24	101.85(13)
N26	S9	C24	102.05(17)
N16	S10	C23	101.50(16)
N18	S11	C20	101.78(16)
N18	S12	C22	101.73(17)
N26	S13	C21	102.14(17)
S6	N16	S10	112.7(3)
S11	N18	S12	112.1(2)
S9	N26	S13	112.0(2)
S5	C19	S6	124.02(18)
S5	C19	C23	123.7(3)
S6	C19	C23	112.3(3)
S4	C20	S11	123.71(18)
S4	C20	C22	123.9(3)
S11	C20	C22	112.4(3)
S7	C21	S13	124.3(2)
S7	C21	C24	123.8(3)
S13	C21	C24	111.9(3)
S3	C22	S12	123.44(18)

S3	C22	C20	124.6(3)
S12	C22	C20	111.9(3)
S2	C23	S10	123.82(18)
S2	C23	C19	124.2(3)
S10	C23	C19	112.0(3)
S8	C24	S9	123.4(2)
S8	C24	C21	124.7(3)
S9	C24	C21	111.9(3)
S14	C25	S15	178.6(4)

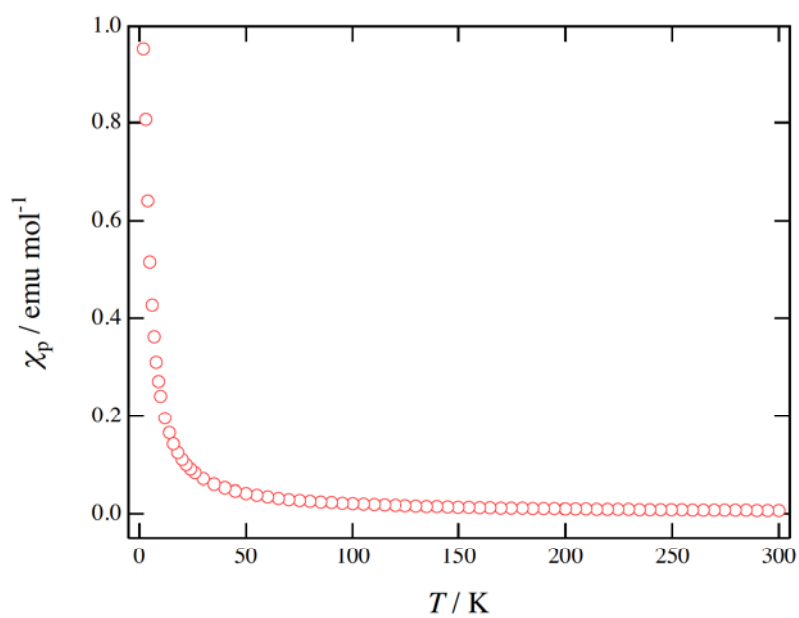


FIGURE S5-1. Temperature dependence of χ_p of **2**.

Chapter VI. Summary

In this work, structural studies of molecule-based materials under pressure are described. The author succeeded in developing the method of single crystal X-ray structural analysis under pressure using diamond anvil cell (DAC). The diffraction spots observed by overlapping with the diffraction from DAC, such as the halo pattern from Be backing-disks and gasket, and strong spots from diamond anvils, were deleted, and the program of the absorption correction for DAC was developed.

The studies in the crystal and electronic structures of pressure-induced molecule-based superconductor β -(BDA-TTP)₂FeCl₄ induced by lowering temperature and by increasing pressure is described. The author succeeded in providing structural evidence for the 2-fold structure and charge separation causing the metal-insulator (MI) transition in β -(BDA-TTP)₂FeCl₄ by X-ray structure analysis below $T_{\text{MI}} = 113$ K. The author also found that the application of pressures causes variations in the conformation of donor molecule and the donor arrangement, which are responsible for almost uniform interaction in the donor stacking and for an increase in bandwidth (W) as a result, the suppression of MI transition and subsequent occurrence of superconductivity would be observed in β -(BDA-TTP)₂FeCl₄ increasing pressure.

The structural change of the molecule-based chiral ferrimagnet (*R*)-GN under pressure is described. The novel structure that cannot be obtained under ambient pressure, High-Pressure Form, was found out by applying pressure.

The preparation, crystal structure, and magnetic properties of new dithiolene ligand dttt^- and its chromium tris(dithiolene) complex, $\text{Cr}(\text{dttt})_3 \cdot \text{CS}_2$ are described. The crystal structure and magnetic properties of $\text{Cr}(\text{dttt})_3 \cdot \text{CS}_2$ are expected to change under pressure.

The method of the structure analysis under pressure, established in this work, is very useful to the structural analysis for other various molecule-based materials under pressure, and wide application for this method are expected.

List of Publications

[1] “Preparation, Crystal Structure, and Magnetic Properties of a New Dithiolene Ligand, 1,3,2-Dithiazole-4-thione-5-thiolate, and its Metal Complex”

T. Nakamura, K. Sasamori, T. Kodama, K. Kikuchi and W. Fujita

Chemistry An Asian Journal 8 (2013) 348.

[2] “Charge-Ordered State with a Two-Fold Crystal Structure in the Pressure-Induced Organic Superconductor β -(BDA-TTP)₂FeCl₄”

K. Sasamori, K. Takahashi, T. Kodama, W. Fujita, K. Kikuchi, and J. Yamada, to be submitted.

[3] “Hydrogen Bonded Anion Ribbons, Networks and Clusters and Sulfur-Anion Interactions in Novel Radical Cation Salts of BEDT-TTF with Sulfamate, Pentaborate and Bromide”

A. C. Brooks, L. Martin, P. Day, E. B. Lopes, M. Almeida, K. Kikuchi, W. Fujita, K. Sasamori, and J. D. Wallis, to be submitted.

[4] “Crystal Structure of High-Pressure Form for Molecule-based Magnet [Cr(CN)₆][Mn((*R*)-pnH)(H₂O)] (H₂O)”

K. Sasamori, T. Kodama, W. Fujita, K. Kikuchi, and K. Inoue, in preparation.

Acknowledgement

The author is sincerely grateful to Prof. Koichi Kikuchi (Department of Chemistry, Graduate School of Science and Engineering, Tokyo Metropolitan University), for his kind instruction and valuable suggestions throughout this work. Great appreciation is also made to Associate Prof. Wataru Fujita and Dr. Takeshi Kodama (Department of Chemistry, Graduate School of Science and Engineering, Tokyo Metropolitan University), for their kind, useful, strict advice and helpful encouragement. The author acknowledges Prof. Tadashi Kato (Department of Chemistry, Graduate School of Science and Engineering, Tokyo Metropolitan University), for helpful advice and valuable suggestion. Great thanks are offered to Associate Prof. Jun-ichi Yamada (Department of Material Science, Graduate School of Material Science, University of Hyogo), for offering the crystals of β -(BDA-TTP)₂FeCl₄, and to Prof. Katsuya Inoue (Department of Chemistry, Faculty of Science, Hiroshima University), for offering the crystals of Green Needle. Grateful thank is also made to Prof. Yoji Achiba, Prof. Haruo Shiromaru and the members of the Laboratory of Physical Chemistry of Molecular Structure and Reaction (Department of Chemistry, Graduate School of Science and Engineering, Tokyo Metropolitan University), for ruby fluorescence measurement. The author would like to appreciate to former and current members of Physical Chemistry of Advanced Materials Laboratory (Department of Chemistry, Graduate School of Science and Engineering, Tokyo Metropolitan University), for their hearty encouragement and friendship. Finally, the author sincerely thanks to his mother, grandparents, and other family members for their constant encouragement and affectionate assistance.

Tokyo Metropolitan University

2013, March.

Kota Sasamori